Maritime controls on coastal East Asian climate during the Holocene: evidence from the sediments of Lake Motosu, Japan

Thesis submitted in accordance with the requirements of the University of Adelaide for an Honours Degree in Environmental Geoscience

Sarah Alexandra McDonald

November 2018

THE UNIVERSITY of ADELAIDE

MARITIME CONTROLS ON COASTAL EAST ASIAN CLIMATE DURING THE HOLOCENE: EVIDENCE FROM THE SEDIMENTS OF LAKE MOTOSU, JAPAN

LAKE MOTOSU PALAEOCLIMATE

ABSTRACT

The East Asian Summer Monsoon controls the timing and amount of rainfall for around a third of the world's population. An understanding of past changes in monsoon strength is crucial for placing current events in context and characterising future climate risk. Despite numerous studies focusing on the East Asian Summer Monsoon, debates remain surrounding the timing, spatial patterns, and drivers of Holocene monsoon variability. This thesis presents a well-dated, 8000-year lacustrine sedimentary sequence recovered from Lake Motosu, central Japan. Variations in the amount and isotopic composition of carbon and nitrogen in bulk organic matter suggest strong monsoon conditions between 8-6 ka, with sedimentation after 3 ka influenced by local volcanic activity. This record is then used to increase the spatial coverage of a multi-proxy synthesis of 18 hydroclimate records from East Asia. Two peaks in monsoon strength are identified centred on ~6.5 ka and ~4.5 ka. Spatial heterogeneity in this analysis suggests that sites in coastal East Asia are more sensitive to changes in Pacific Ocean conditions than sites in continental Asia. This record has the potential to improve understanding of the drivers of monsoon variability through the Holocene in this socially and economically important region.

KEYWORDS

Lake Motosu, Japan, EASM, Holocene, isotopes, palaeoclimate, palaeolimnology

TABLE OF CONTENTS

Maritime controls on coastal East Asian climate during the Holocene: evidence from the sediments of Lake Motosu, Japan i
Lake Motosu palaeoclimate i
Abstract i
Keywords i
List of figures 3
List of tables 4
Introduction 5
Study site 8
Methods 11
Geochemical analyses 11
Bulk organic matter 11
Sedimentary cellulose 11
FTIRS analysis 12
Statistical analyses 12
Regional synthesis 13
Results 16
Geochemical analyses 16
FTIRS analysis 21
Statistical analyses 22
Regional synthesis 22
Discussion 26
Palaeohydrology of Lake Motosu 26
Sources of organic matter 26
Environmental influence on Lake Motosu 28
Volcanic influence on Lake Motosu 32
Holocene palaeoclimate of Lake Motosu 33
Regional monsoon variability 36
Implications for the East Asian Monsoon 40
Conclusions 41
Acknowledgments 43
References 43
Appendix A: Modern climatology 50
Appendix B: Age model 51

Appendix C: Cellulose extraction method..... 52
Appendix D: Carbon and nitrogen isotope data 54
Appendix E: Sedimentary cellulose oxygen isotope data 68
Appendix F: Location of proposed turbidites..... 69
Appendix G: Spectral analysis 70
Appendix H: Wavelet analysis 71
Appendix I: Cross-wavelet analysis 74
Appendix J: Original datasets included in multi-proxy synthesis 76
Appendix K: Correlation between Lake Motosu and regional climate 77
Appendix L: Excluded turbidites..... 78

LIST OF FIGURES

Figure 1: Location of the study site. Left: Topographic map of Japan showing the location of the study region (red box). Middle: Map of the Mt Fuji region showing the location of major lakes (blue shading) including Lake Motosu (red box). The Aokigahara lava flow (red shading) divided a pre-existing larger lake to form Lake Motosu in ~864 CE. Right: Bathymetric map of Lake Motosu courtesy of the Geospatial Information Authority of Japan. The collection site for core MOT15-2 is indicated (white cross). Figure adapted from Obrochta et al. (2018). 9
Figure 2: Location of sites included a multi-proxy synthesis of East Asian Summer Monsoon records. Numbers refer to sites listed north to south in Table 1. Symbols refer to archive type. The dashed line indicates the modern monsoon limit following Yihui & Chan (2005) and Wang et al. (2010). 14
Figure 3: Lake Motosu elemental and isotopic data. Horizontal lines indicate mean values. Grey shading represents the period inferred as strong monsoon conditions in Lake Motosu. Black vertical lines represent major catchment changes (changes in sedimentation patterns at 8 ka and 2 ka following Lamair et al. (2018); the emergence of the Omuro Scoria Cone at 3.26-3.06 ka; deposition of the Aokigahara Lava Flow at ~864 CE). Arrows indicate periods of higher $\delta^{13}C$ associated with possible turbidite deposits. 18
Figure 4: Generalised additive models fitted to elemental and isotopic data from Lake Motosu. Dots indicate original data, solid lines indicate mean model values and shading represents 95% confidence intervals. Grey shading represents the period inferred as strong monsoon conditions in Lake Motosu. Black vertical lines represent major catchment changes (changes in sedimentation patterns at 8 ka and 2 ka following Lamair et al. (2018); the emergence of the Omuro Scoria Cone at 3.26-3.06 ka; deposition of the Aokigahara Lava Flow at ~864 CE). 19
Figure 5: Scatter plots of compositional variables in Lake Motosu. Dots are coloured based on sediment type. Black indicates scoria layers; grey indicates samples which may contain some scoria; green indicates turbidites proposed by Lamair et al. (2018); light brown indicates background sedimentation. Lines represent a linear model fitted to each data set with the R^2 value given in the top righthand corner. 20
Figure 6: Example FTIRS spectra. For clarity, curves have been vertically offset. Upper: Example FTIRS spectra for a subset of bulk sediment samples. Absorbance peaks associated with carbonates are indicated in grey following Rosén et al. (2011). Lower: Example FTIRS spectra for a subset of cellulose samples extracted from the Lake Motosu sediments. Absorbance peaks associated with pure cellulose are indicated in grey following Larkin (2011). 21
Figure 7: Percent variance explained for an increasing number of principal components. Principal components are calculated for 10,000 age model iterations for 18 East Asian Summer Monsoon sites. Principal component (PCA) axes are shown by black dots (mean value), solid lines (68% confidence) and dashed lines (90% confidence). Confidence intervals are also shown for 1,000 iterations of white noise (blue) and red noise (orange). 23
Figure 8: Time-series expansions of the first (PCA1) and second (PCA2) principal components extracted from an MCEOF analysis of 18 East Asian Summer Monsoon records. Confidence intervals are shown by solid lines (mean), dark bands (68%) and light bands (90%). Axes are orientated so that wetter conditions plot upwards. 24
Figure 9: Map of the study region showing the principal component loadings for each site for the first principal component (PCA1; top) and second principal component (PCA2; bottom) of an MCEOF analysis of 18 East Asian Summer Monsoon records. Warm colours (positive loadings) represent sites with patterns which strongly (larger dots) reflect the regional trend. Cool colours (negative loadings) represent sites with patterns which strongly (larger dots) reflect the inverse of the regional trend. Symbols represent archive type. 25
Figure 10: Source of organic matter to the Lake Motosu sediments. Shading represents regions associated with major sources of organic carbon to lake sediments. Figure adapted from Meyers & Lallier-Vergés (1999). 28
Figure 11: Comparison plot of selected Japanese palaeoclimate records and possible climate drivers. From top: C/N ratio of bulk organic matter in Lake Motosu (this study); total organic carbon in Lake Aoki, Japan (Adhikari et al., 2002); speleothem $\delta^{18}O$ from Ohtaki Cave, Japan (Mori et al., 2018); carbon productivity in Lake Biwa (Ishiwatari et al., 2009); the second principal component (PCA2) of climate in the East Asian Monsoon region (this study); total solar insolation (pale purple) fitted with a 20-point running mean (dark purple; Steinhilber et al., 2012); reconstructed sea surface temperatures in the West Pacific Warm Pool (light red) from core MD81 fitted with a 10-point running mean (dark red; Stott et al.,

2004). Axes are oriented such that wet/strong monsoon conditions plot upwards. Grey shading indicates maximum warm and/or wet conditions inferred from each record. 35
Figure 12: Comparison plot of selected regional trends in the East Asian Summer Monsoon and possible climate drivers. From top: global sea level (yellow; Yokoyama et al., 2007); orbital insolation (red; Berger & Loutre, 1991); $\delta^{18}O$ in Dongge Cave as a proxy for Indian Monsoon intensity (light green) fitted with a 20-point running mean (dark green; Wang et al., 2005); two major trends in East Asian monsoon climate (PCA1; PCA2; this study), total solar insolation (light purple) fitted with a 20-point running mean (dark purple; Steinhilber et al., 2012); reconstructed sea surface temperatures in the West Pacific Warm Pool (light red) from core MB81 fitted with a 10-point running mean (dark red; Stott et al., 2004). 38

LIST OF TABLES

Table 1: Lake Motosu hydrology 10
Table 2: Sites included in a multi-proxy synthesis of East Asian Summer Monsoon records listed north to south. 15

INTRODUCTION

Around a third of the world's population live in areas influenced by the East Asian Summer Monsoon (EASM) system (An et al., 2015; Chen et al., 2015; Liu et al., 2013; Wang, 2006; Zheng et al., 2014). This densely populated region relies on monsoon rainfall to sustain agriculture and is heavily impacted by floods and droughts caused by anomalous monsoon activity. An understanding of how the monsoon may evolve in response to recent climate changes, therefore, has important social and economic implications (Corlett et al., 2014). Modelling future monsoon variability relies on an understanding of how the monsoon has varied in the past. In the absence of long instrumental records, natural archives can provide insight into past monsoon changes and improve our understanding of monsoon processes and variability (e.g. Chen et al., 2015; Liu et al., 2015; van Soelen et al., 2016; Wang et al., 2008, 2001).

Monsoon variability during the Holocene (11-0 ka) is of particular interest, as it occurred under modern sea level and tectonic boundary conditions (Chen et al., 2015; Wu et al., 2018). The most widely cited records of Holocene EASM variability are well-dated, high-resolution speleothem records from southern China (Dong et al., 2010; Dykoski et al., 2005; Wang et al., 2001, 2005). The oxygen isotopic composition of these speleothems is interpreted to show a strong EASM interval from 9-7 ka, followed by a weakening of the monsoon through the Holocene in response to a decline in external orbital forcing (Wang et al., 2005). However, the interpretation of these records has been questioned (Clemens et al., 2010; Maher, 2008; Pausata et al., 2011; Thomas et al., 2016), and the extent to which records from southern China are representative of changes across the whole of the EASM region is unclear (Chen et al., 2008; Hong et al., 2005; Liu et al., 2015; Park et al., 2018). An improved understanding of EASM

mechanisms thus requires palaeoclimate records from across the East Asia region, to assess whether the patterns identified in southern China are regionally applicable. There is a requirement for more high-resolution, Holocene, EASM records, particularly from regions with a paucity of records, such as Japan.

Japan is located at the north-easternmost edge of the EASM and thus is well-situated to provide complementary records to those from continental Asia (Schöne et al., 2004; van Soelen et al., 2016). Existing studies of monsoon variability in Japan have predominantly focused on glacial-interglacial variability (Ishiwatari et al., 2009; Mori et al., 2018; Shen et al., 2010), with studies on shorter timescales focussing either on the East Asian Winter Monsoon (Sone et al., 2013) or on shorter periods within the Holocene (Sakashita et al., 2017; van Soelen et al., 2016). The few studies which do extend through the Holocene suggest a mid-Holocene (8-6 ka) moisture optimum, although the timing and amplitude of this event remain debated (Adhikari et al., 2002; Schöne et al., 2004). There is thus the potential for the development of high-resolution, Holocene, EASM records from Japan to expand our knowledge of EASM variability and identify underlying climate drivers.

Lake sediments can provide high-resolution, continuous records of past climate (Leng et al., 2006; Meyers & Lallier-Vergés, 1999). Lake sediments contain a wide array of materials that can be used as proxies to infer past changes in rainfall, including plant, algal and faunal microfossils (Battarbee, 2000), sedimentology (Oldfield et al., 1983), and isotope geochemistry (Leng et al., 2006). In particular, the oxygen isotopic composition of sedimentary cellulose ($\delta^{18}O$) in lake sediments is strongly linked to

changes in regional hydroclimate (Wissel et al., 2008; Wolfe et al., 2007) and hence can be used to reconstruct EASM strength.

The interpretation of cellulose $\delta^{18}O$ assumes sedimented organic matter is of algal origin (Wolfe et al., 2001, 2007). Therefore, contributions from terrestrial sources can act to contaminate the record (Sauer et al., 2001). Total organic carbon to nitrogen ratios (C/N) can be used to differentiate between algal (C/N < 10) and terrestrial (C/N >20) organic matter contributions to lake sediments (Meyers & Lallier-Vergés, 1999). Furthermore, changes in the isotopic ratios of sedimentary carbon ($\delta^{13}C$) and nitrogen ($\delta^{15}N$) can be used to infer past lake ecosystem dynamics, which are often related to climate variability. The $\delta^{13}C$ composition of aquatic organic matter is sensitive both to changes in productivity and the isotopic composition of dissolved inorganic carbon in the water column (Leng et al., 2006; Moschen et al., 2009). $\delta^{15}N$ can provide information about changes in nitrogen cycling within the lake, which is influenced by the dominance of algal species capable of fixing atmospheric nitrogen (Talbot, 2002). Lake productivity and nitrogen cycling within lake systems are sensitive to climate, and so the elemental and isotopic composition of bulk organic matter can be used in addition to cellulose $\delta^{18}O$ to infer changes in monsoon strength.

Whilst the composition of lake sediments is strongly linked to climate, their interpretation can be confounded by limitations associated with individual archives and site-specific idiosyncrasies. For example, records in the Mt Fuji region, Japan, are impacted both by regional climate and by volcanic and seismic activity (Lamair et al., 2018; Obrochta et al., 2018; Yamamoto et al., 2018). Problems related to site-specific effects can be addressed in part by objectively combining multiple records across a

region in order to identify the coherent, common patterns of regional climate change (Anchukaitis & Tierney, 2013; Falster et al., 2018; Field et al., 2018; Tyler et al., 2015). In the EASM region, patterns of change which are consistent across sites and between different archive types can be interpreted to reflect regional patterns of monsoon strength. Existing syntheses of EASM records have identified two major patterns of hydroclimate change (Herzschuh, 2006; Wang et al., 2010). However, the numerical approaches behind these syntheses do not accommodate the inherent chronological uncertainty associated with all palaeoclimate records. The studies to date are also confined to continental Asia due to a paucity of records from coastal regions including Japan, Korea, Taiwan and eastern China.

This thesis presents a high-resolution, multi-proxy study of an 8,000-year lacustrine sedimentary sequence from Lake Motosu, Mt Fuji, central Japan. Variations in bulk organic sediment composition are interpreted to be sensitive to regional changes in monsoon strength, prior to marked volcanic influences after 3.5 ka. This record is then used to increase the spatial coverage of a regional analysis of 18 EASM records. This analysis identifies possible differences between coastal and continental Asia, with spatial variations in the relative dominance of orbital and Pacific Ocean conditions as major climate drivers across the EASM region.

STUDY SITE

Lake Motosu (35°27′50″ N, 138°35′10″ E, 900 m.a.s.l.) is one of five volcanically dammed lakes located at the northern foot of Mt. Fuji, central Japan (Figure 1). These lakes are located at the present north-easternmost boundary of the EASM and so are well-suited to investigate monsoon variability. The lake was formed by the division of

an existing larger lake by the Aokigahara Lava Flow (868-854 CE) which formed Lake Motosu, Lake Shoji and Lake Sai (Hamada et al., 2012). Average rainfall for the period 1933-2017 at the nearest meteorological station (Kawaguchiko, 18 km ENE) was 1573 mm, a third of which fell during the summer monsoon season in June-July-August (Appendix A; Japan Meteorological Agency, 2018). Precipitation is predominately sourced from Sagami and Suruga Bay to the South East (Adhikari, 2014).

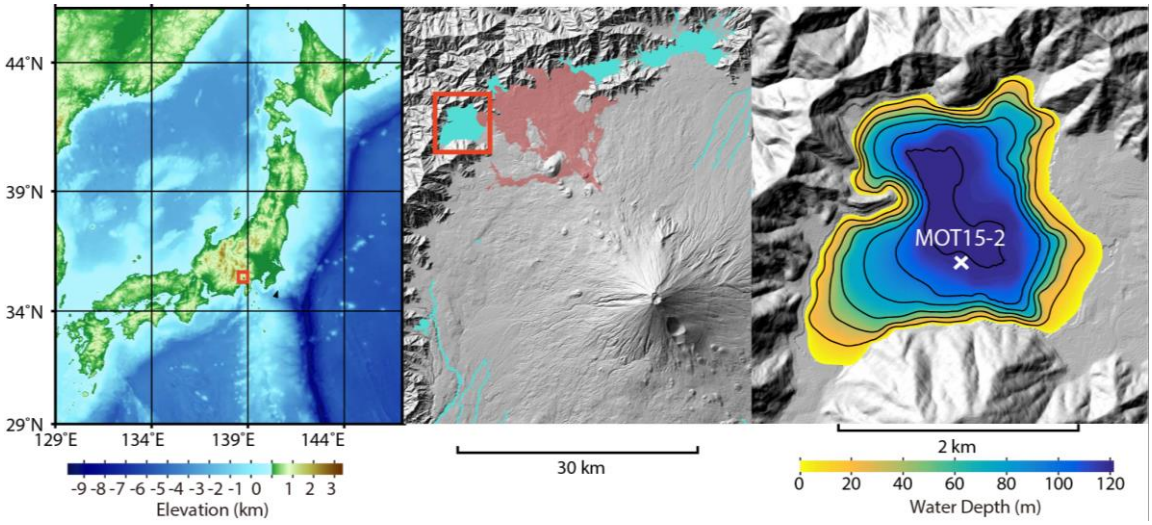

Figure 1: Location of the study site. Left: Topographic map of Japan showing the location of the study region (red box). Middle: Map of the Mt Fuji region showing the location of major lakes (blue shading) including Lake Motosu (red box). The Aokigahara lava flow (red shading) divided a pre-existing larger lake to form Lake Motosu in ~864 CE. Right: Bathymetric map of Lake Motosu courtesy of the Geospatial Information Authority of Japan. The collection site for core MOT15-2 is indicated (white cross). Figure adapted from Obrochta et al. (2018).

Lake Motosu is oligotrophic and seasonally stratified from late March to late January (Table 1; Hamada et al., 2012). The lake has no major inflows or outflows, with the exception of a modern withdrawal for power generation (Hamada et al., 2012). Whilst ephemeral streams may flow into the lake during heavy rainfall events (Adhikari, 2014), catchment runoff is minimal as precipitation rapidly enters underground aquifers through permeable lava flow deposits, and enters the lake as groundwater (Hamada et al., 2012). Several existing studies have aimed to constrain groundwater flow regimes in

the Mt. Fuji area (Koshimizu & Tomura, 2000; Yasuhara et al., 2007). However, calculations of groundwater contributions to Lake Motosu are contradictory, and range from minimal (Koshimizu & Tomura, 2000) to a third of lake input (Hamada et al., 2012). Water loss is through surface evaporation (35%) and groundwater outflow (65%), with lake levels varying annually up to 2 m (Hamada et al., 2012; Takeuchi et al., 1995).

Table 1: Lake Motosu hydrology

Maximum depth	121.6 m [a]
Shoreline	11.6 km [a]
Volume	0.33 km^3 [a]
Surface area	4.7 km^2 [a]
Catchment area	24.6 km^2 [a]
Residence time	7.9 years [b]

[a] (Hamada et al., 2012)

[b] (Yoshizawa, 2009)

Lake Motosu was cored in 2015 as part of a project to investigate the tectonic and climatic history of central Japan. A series of gravity and piston cores were collected and subsequently used to investigate the seismic and volcanic history of the lake and influences on sedimentation patterns (Lamair et al., 2018; Obrochta et al., 2018). As part of this study, three overlapping 2 m piston cores and a 1 m gravity core were collected using a UWITEC Platform and spliced to form a 3.67 m composite core which covers the period 8-0.5 ka (MOT15-2; Obrochta et al., 2018). The core consists primarily of fine-grained, siliceous muds with coarser turbidite and scoria layers. The age of the core is constrained by a Bayesian age model based on 27 bulk organic radiocarbon dates, four macrofossil radiocarbon dates and two regional tephra layers (Appendix B; Obrochta et al., 2018).

METHODS

Geochemical analyses

BULK ORGANIC MATTER

The bulk organic composition of lake sediments records changes in the source of organic matter, catchment processes and regional climate. To measure changes in the amount and isotopic composition of carbon and nitrogen preserved in Lake Motosu, a 3.67 m sediment core (MOT15-2; Obrochta et al., 2018) was subsampled contiguously at 5 mm intervals and then further subsampled for isotopic analysis. The carbon (TC) and nitrogen (TN) concentrations and the isotopic ratios of $^{13}C/^{12}C$ and $^{15}N/^{14}N$ in the bulk sediment were measured at 2 cm resolution (~45 years) by combustion in a Eurovector Elemental Analyser coupled to a Nu-Horizon Isotope Ratio Mass Spectrometer. Standardisation was achieved using in-house glycine, glutamic acid and triphenylamine standards which had been calibrated against international standards. Analyses included at least 10% replicate samples. Following convention, isotopic compositions are reported in standard delta notation as per mil (‰) deviations relative to Vienna Pee Dee Belemnite (VPDB) for $\delta^{13}C$ and atmospheric nitrogen (AIR) for $\delta^{15}N$ where

$$\delta = \left(\frac{R_{sample}}{R_{standard}}\right) - 1 \text{ x } 1000$$

and R is the ratio of $^{13}C/^{12}C$ and $^{15}N/^{14}N$.

SEDIMENTARY CELLULOSE

Prior to oxygen isotope analysis, cellulose was extracted from bulk sediments following the dissolution-precipitation method of Wissel et al. (2008; Appendix C). This method

produces a purer cellulose product compared to methods which sequentially remove non-cellulose material (e.g. Wolfe et al., 2007). Due to the low cellulose content of the samples, sixteen adjacent samples were combined to give a resolution of 8 cm (~190 years). ~0.3 mg of cellulose was weighed into silver capsules and crimped. Re-precipitated cellulose is hygroscopic and so samples were stored for at least three weeks in an ~45°C oven, prior to pyrolysis and subsequent isotopic analysis by combustion in an Elementar high-temperature pyrolysis device coupled to a Nu-Horizon Isotope Ratio Mass Spectrometer. Standardisation to Vienna Standard Mean Ocean Water (VSMOW) was achieved using international standards USGS KHS Keratin, USGS CBS Keratin and IAEA-NO-3.

FTIRS analysis

Fourier transform infrared spectroscopy (FTIRS) can be used both to quantify the composition of lake sediments and assess the purity of chemical compounds. To confirm the absence of carbonate in the Lake Motosu sediments, a subset of bulk sediment samples was analysed using a PerkinElmer Spectrum 100 FTIR transmission spectrometer at a 1 cm^{-1} resolution between 4000 cm^{-1} and 450 cm^{-1}. The spectra were then compared to spectral peaks known to be associated with carbonate. To confirm the purity of the extracted sedimentary cellulose, a subset of cellulose samples was also analysed alongside a cellulose standard following the same procedure.

Statistical analyses

Sedimentation in Lake Motosu is impacted by turbidite and scoria deposits which do not reflect background environmental change. Samples containing scoria and anomalous

samples associated with turbidite deposits were removed from the dataset prior to statistical analysis following Lamair et al. (2018) and Obrochta et al. (2018).

Generalised additive models (GAMs) can be used to identify complex non-linear trends in unequally-sampled data. To separate significant trends from noise, GAMs were fitted to each of the proxy time series using the mgcv package in R (Wood, 2017). Models were fitted with a Gaussian model with 290 basis dimensions for bulk organic matter and 25 basis dimensions for sedimentary cellulose.

Periodicities in palaeoclimate time series can be used to identify possible drivers of environmental change. To identify possible periodicities in the Lake Motosu time series, periodograms were computed for each dataset fitted with a Welch window using the REDFIT function in PAST (Hammer et al., 2001). Periodicities are often non-stationary and so wavelet transforms were also computed using the unequal wavelet function in PAST (Hammer et al., 2001). Cross-wavelet analysis can be used to identify common periodicities between datasets. To assess the influence of solar insolation and Pacific Ocean sea surface temperatures on the Lake Motosu record, cross-wavelets were computed against solar insolation (Steinhilber et al., 2012) and sea surface temperatures in the West Pacific Warm Pool (Stott et al., 2004) using the biwavelet package in R (Gouhier et al., 2018). Due to low sample resolution, spectral analyses were not applied to $\delta^{18}O$.

Regional synthesis

The identification of climate signals in individual sites is confounded by site-specific idiosyncrasies. Identification of trends which are consistent between various archives and across regional areas can isolate coherent patterns of climatic change from site-

specific variability. To identify patterns of monsoon change in East Asia, a set of existing palaeoclimate records were synthesised (Figure 2; Table 1). Palaeoclimate records were selected from the EASM region (Yihui & Chan, 2005) based on a set of criteria adapted from Wang et al. (2010). Records were selected which spanned the majority of the Holocene (11-0 ka); reflected moisture or precipitation changes; had a temporal resolution of at least 200 years per sample and at least four age-control points during the Holocene. For sites with multiple records, the most recent, quantitative moisture reconstruction which fit the criteria and for which data was available was selected. To reduce bias, in all cases palaeoclimate interpretations respect those of the original authors.

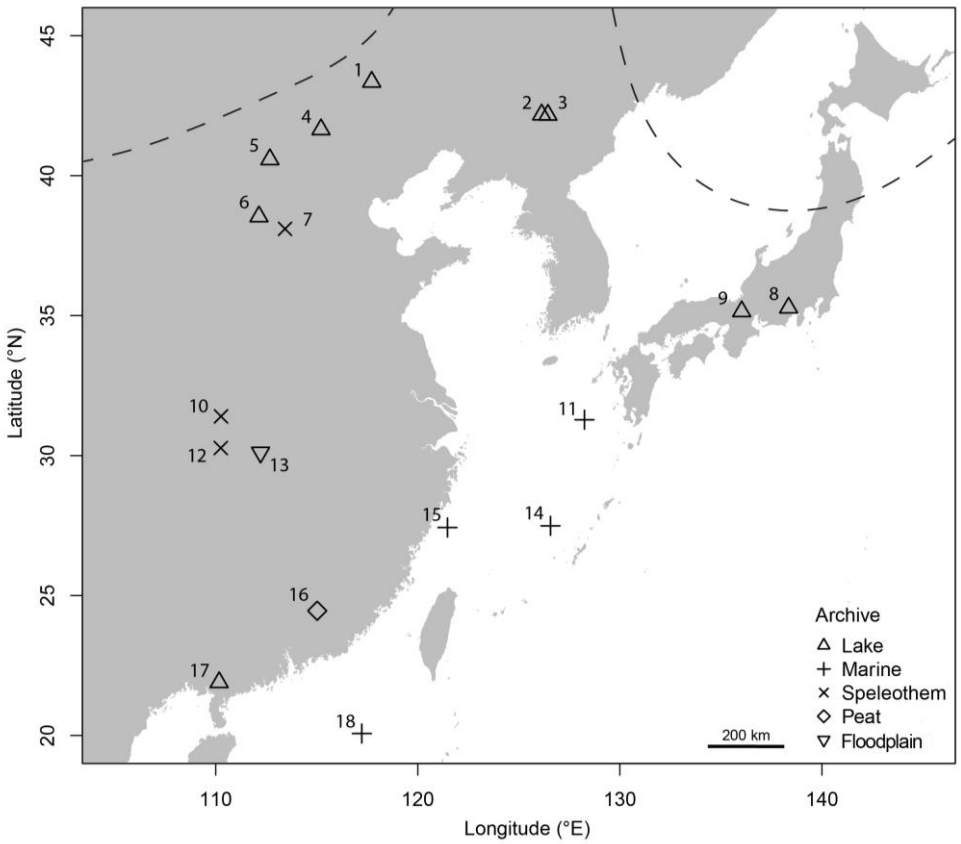

Figure 2: Location of sites included a multi-proxy synthesis of East Asian Summer Monsoon records. Numbers refer to sites listed north to south in Table 1. Symbols refer to archive type. The dashed line indicates the modern monsoon limit following Yihui & Chan (2005) and Wang et al. (2010).

Table 2: Sites included in a multi-proxy synthesis of East Asian Summer Monsoon records listed north to south.

No.	Site	Latitude (°N)	Longitude (°E)	Elevation (m.a.s.l.)	Archive	Proxy	Reference
1	Dali Lake	43.35	117.22	1226	Lake	TOC	Xiao et al., 2008
2	Xiaolongwan Lake	42.18	126.21	655	Lake	$\delta^{13}C_{(27\text{-}31)}$	Chu et al., 2014
3	Sihailongwan Lake	42.17	126.36	797	Lake	Pollen (P_{ann})	Stebich et al., 2015
4	Bayanchagan Lake	41.65	115.21	1355	Lake	Pollen (P_{ann})	Jiang et al., 2006
5	Daihai Lake	40.58	112.68	1221	Lake	Pollen (P_{ann})	Xu et al., 2010
6	Gonghai Lake	38.54	112.14	1860	Lake	$\delta^{13}C$	Rao et al., 2016
7	Lianhua Cave	38.1	113.43	1200	Speleothem	$\delta^{18}O$	Dong et al., 2015
8	Motosu Lake	35.28	138.35	900	Lake	C/N	This study
9	Biwa Lake	35.15	136.03	86	Lake	TOC	Ishiwatari et al., 2009
10	Sanbao Cave	31.4	110.26	1900	Speleothem	$\delta^{18}O$	Dong et al., 2010
11	East China Sea	31.28	128.25	-590	Marine	C/N	Chang et al., 2015
12	Heshang Cave	30.27	110.25	294	Speleothem	$\delta^{18}O$	Cheng et al., 2007
13	Jianghan Plain	30.11	112.22	42	Floodplain	Rb/Sr	Li et al., 2014
14	Okinawa Trough	27.49	126.57	-1264	Marine	$\delta^{18}O_{residual}$	Sun et al., 2005
15	East China Sea	27.43	121.47	-47	Marine	Fine silt modal grain size	Wang et al., 2014
16	Dahu Peat	24.45	115.02	250	Peat	Humidification degree	Zhong et al., 2011
17	Huguangyan Lake	21.9	110.17	23	Lake	$\delta^{13}C_{(31\text{-}29)}$	Jia et al., 2015
18	South China Sea	20.07	117.23	-1727	Marine	$\delta^{18}O$	Wang et al., 1999

Age uncertainties associated with radiocarbon dating complicate the objective comparison of palaeoclimate records. To accommodate these chronological uncertainties, regional patterns of change were extracted using the Monte Carlo Empirical Orthogonal Function (MCEOF) approach of Anchukaitis and Tierney (2013), using code modified from Tyler et al. (2015) and Field et al. (2018). For consistency, Bayesian age-depth models were developed using 'Bacon' software in R (Blaauw & Christen, 2011) with radiocarbon reservoir corrections following those of the original authors. Radiocarbon ages were calibrated using IntCal13 or MarineCal as appropriate (Reimer et al., 2013). Non-radiocarbon errors were assumed to be Gaussian. 10,000 age model iterations were extracted for each site, linearly interpolated, resampled at a resolution of 200 years and trimmed to the period 9-0 ka. Principal component analysis (PCA) was then performed for each age iteration using the vegan package in R (Oksanen et al., 2018). The number of significant components was estimated using two 'rule N' tests following the approach of Anchukaitis & Tierney (2013) using code adapted from Falster et al. (2018).

RESULTS

Geochemical analyses

In total, 361 samples at 1 cm resolution were analysed for isotopic and elemental carbon and nitrogen concentrations, with a subset of 291 samples interpreted as reflecting background sedimentation (Appendix D). Cellulose was successfully extracted and analysed from 32 samples at ~8 cm resolution (Appendix E). Analytical errors on 10% replicate samples as a percentage of mean values were 4.1% for TC, 11.2% for TN, 0.4% for $\delta^{13}C$, 3.4% for $\delta^{15}N$ and 1.8% for $\delta^{18}O$.

Isotopic and elemental analysis of the Lake Motosu sediments showed both short-term variability and long-term trends (Figures 3, 4). Mean TC for the core was 3.63% (σ = 0.46%). TC subtly increased towards the present with a marked increase in variability following 2 ka. A GAM fitted to TC also identified a possible increasing trend through the Holocene. TN increased between 8-6 ka, before fluctuating around a mean value of 0.34% (σ = 0.0036%) and then rapidly increasing to ~0.5% at 0.6 ka. Modelled TN also showed an increase between 8-6 ka but did not identify the rapid shift at 0.6 ka. C/N fluctuated around a mean of 12.74 (σ = 3.07%). The modelled trend showed decreasing values to a minimum of ~11 at 5 ka, before increasing to a peak of ~16 at 2 ka. Following this, values were stable around the mean before decreasing after 1 ka.

$\delta^{13}C$ fluctuated around the mean (μ = -26.33‰, σ = 0.56‰), except for a period of low (~-28‰) and fluctuating values between 6-4.5 ka. A GAM identified a minor increase in $\delta^{13}C$ to -25‰ at ~7 ka before a drop centred at ~5 ka. Following this, values fluctuated stably around the mean. $\delta^{15}N$ varied around a mean of 2.68‰ (σ = 0.34‰). The GAM showed variable values with minima at ~7.5 ka, ~4.5 ka, ~3.5 ka, and ~1.5 ka. $\delta^{18}O$ varied around a mean of 22.87‰ (σ = 0.80‰) with a singular low value of 20‰ at 5.3 ka. A GAM identified a possible increasing trend in $\delta^{18}O$ but with a poor fit to the data. The oxygen content of extracted cellulose varied from 30-47% (μ = 40%, σ = 4%), lower than the theoretical value of 49% (Heyng et al., 2015).

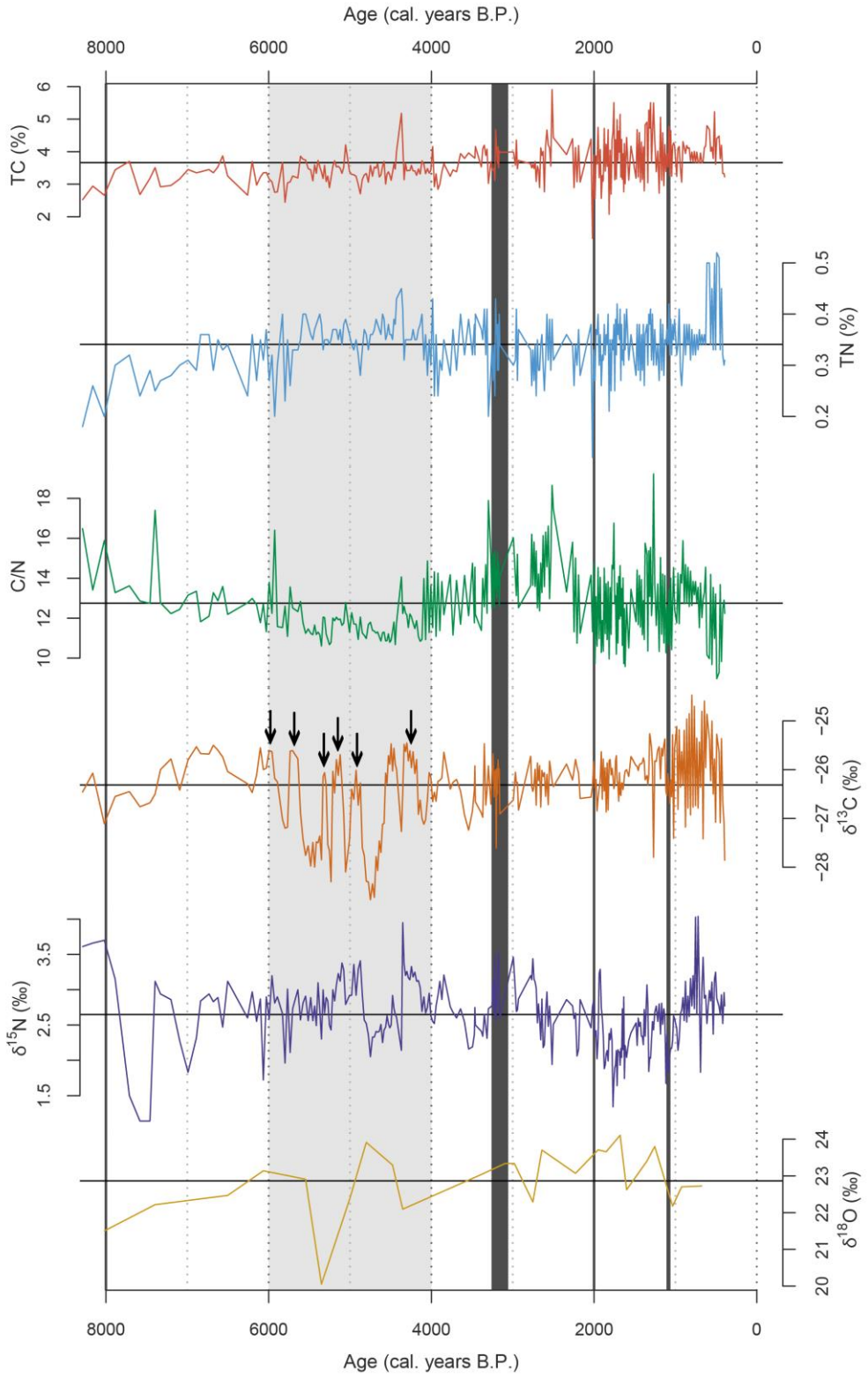

Figure 3: Lake Motosu elemental and isotopic data. Horizontal lines indicate mean values. Grey shading represents the period inferred as strong monsoon conditions in Lake Motosu. Black vertical lines represent major catchment changes (changes in sedimentation patterns at 8 ka and 2 ka following Lamair et al. (2018); the emergence of the Omuro Scoria Cone at 3.26-3.06 ka; deposition of the Aokigahara Lava Flow at ~864 CE). Arrows indicate periods of higher $\delta^{13}C$ associated with possible turbidite deposits.

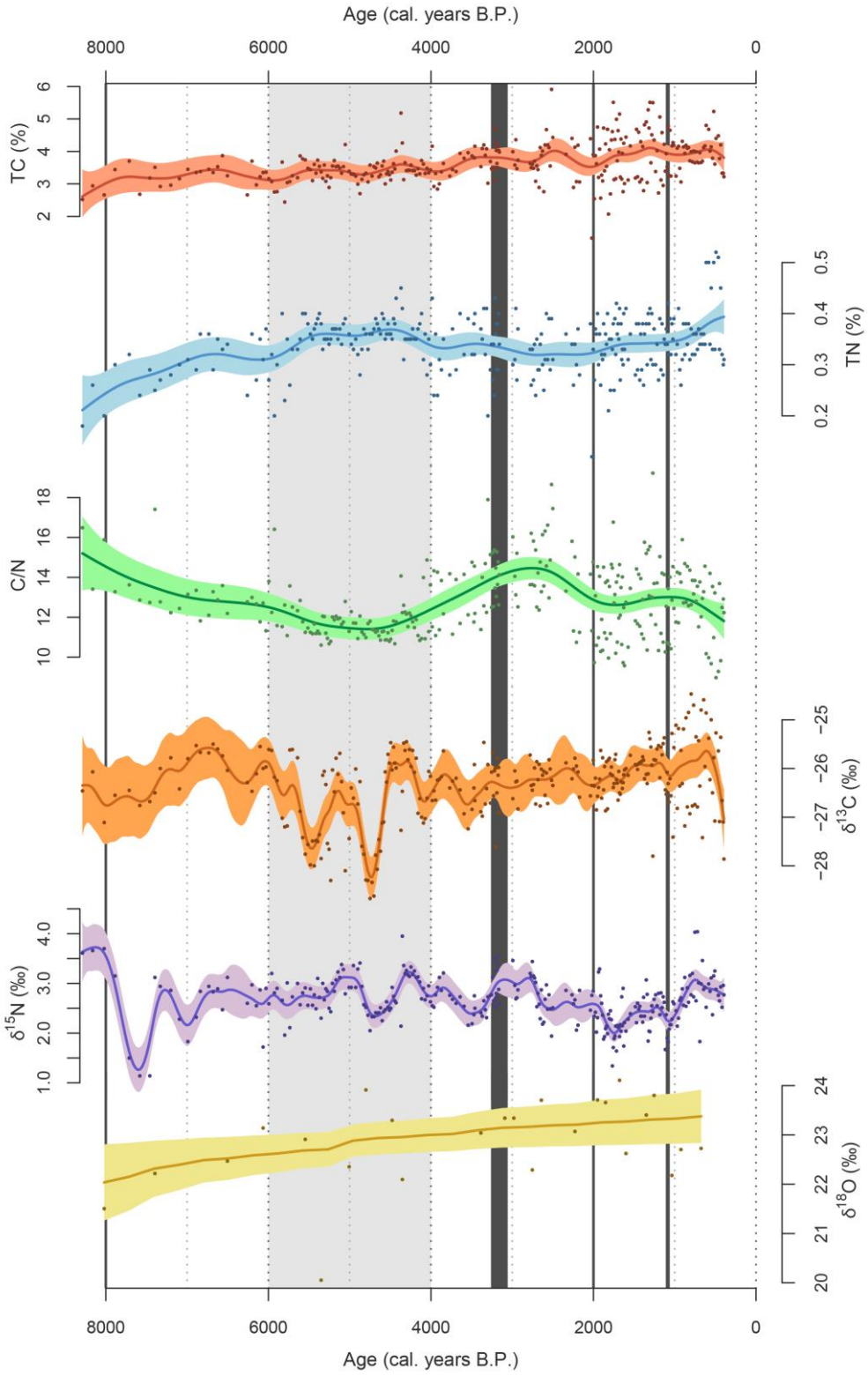

Figure 4: Generalised additive models fitted to elemental and isotopic data from Lake Motosu. Dots indicate original data, solid lines indicate mean model values and shading represents 95% confidence intervals. Grey shading represents the period inferred as strong monsoon conditions in Lake Motosu. Black vertical lines represent major catchment changes (changes in sedimentation patterns at 8 ka and 2 ka following Lamair et al. (2018); the emergence of the Omuro Scoria Cone at 3.26-3.06 ka; deposition of the Aokigahara Lava Flow at ~864 CE).

Prior to ~4 ka, turbidite layers proposed by Lamair et al. (2018) were associated with marked shifts towards higher $\delta^{13}C$ (Figure 3). Following ~4 ka there were no consistent variations in composition associated with proposed turbidite layers (Appendix F). Scatter plots of geochemical data show some turbidite layers with higher TC, C/N or $\delta^{15}N$; however, the majority plot in the same space as non-turbidite layers (Figure 5). Scoria layers generally have lower TC and TN but there is some overlap.

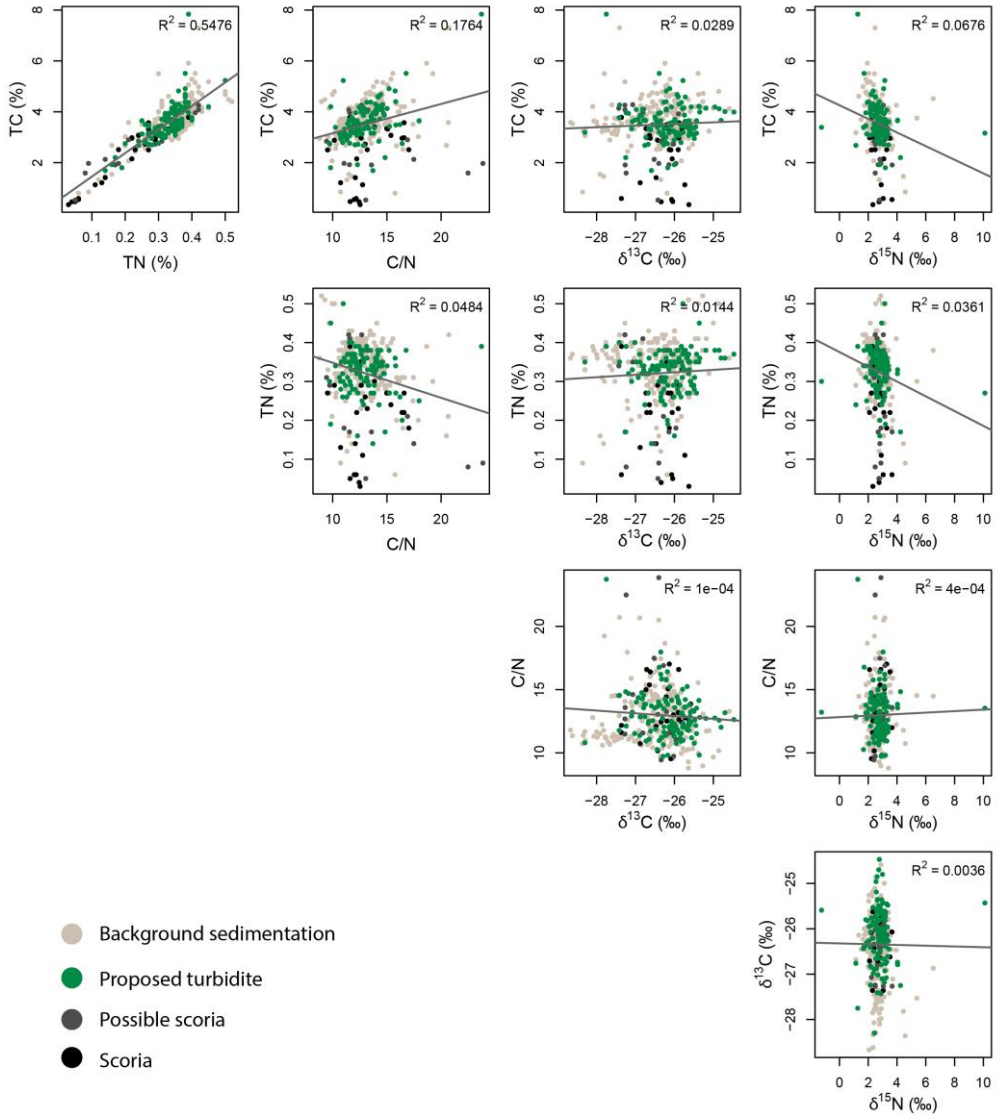

Figure 5: Scatter plots of compositional variables in Lake Motosu. Dots are coloured based on sediment type. Black indicates scoria layers; grey indicates samples which may contain some scoria; green indicates turbidites proposed by Lamair et al. (2018); light brown indicates background sedimentation. Lines represent a linear model fitted to each data set with the R^2 value given in the top righthand corner.

FTIRS analysis

FTIRS analysis of a subset of bulk sediment samples showed a broad peak centred around 1000 cm^{-1}, the height of which varied between samples (Figure 6). No peaks were observed at wavelengths associated with carbonate, namely 1460, 1795 and 2515 cm^{-1}. Analysis of cellulose samples purified from Lake Motosu sediment showed peaks at 670, 900, 1000, 1160, 1320, 1380, 1650, and 2900 cm^{-1} (Figure 6). Identical peaks were observed for a cellulose standard and cellulose extracted from leaves.

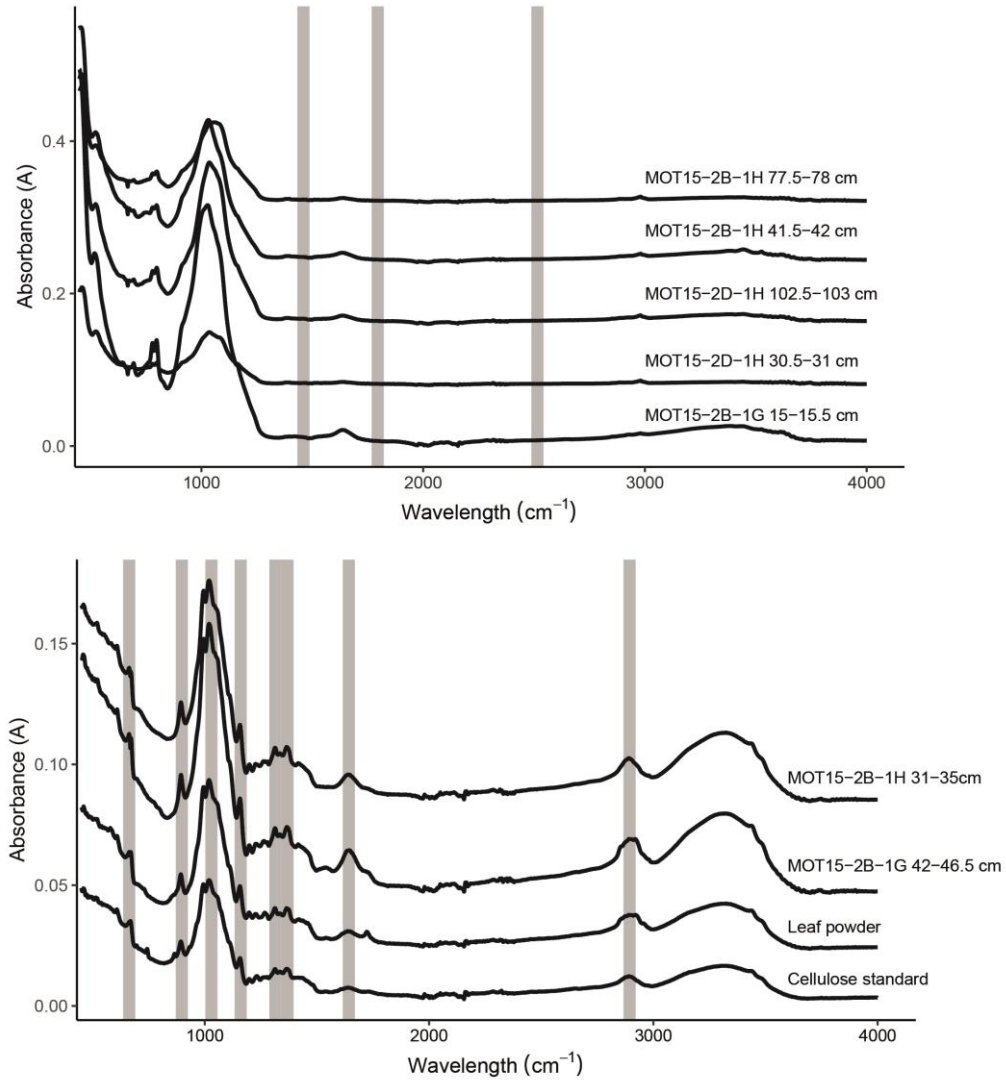

Figure 6: Example FTIRS spectra. For clarity, curves have been vertically offset. Upper: Example FTIRS spectra for a subset of bulk sediment samples. Absorbance peaks associated with carbonates are indicated in grey following Rosén et al. (2011). Lower: Example FTIRS spectra for a subset of cellulose samples extracted from the Lake Motosu sediments. Absorbance peaks associated with pure cellulose are indicated in grey following Larkin (2011).

Statistical analyses

For the period prior to major volcanic influences on Lake Motosu (8-3 ka), spectral analysis identified no statistically significant periodicities in TC, C/N or $\delta^{13}C$. At the critical chi2 99% level, significant periodicities were identified in $\delta^{15}N$ at ~735 years and in TN at ~1065 years (Appendix G). Wavelet analysis identified a possible periodicity at ~1000 years prior to 3 ka in all records (Appendix H). Cross-wavelet analysis identified no significant common periodicities between any of the records and either total solar insolation (Steinhilber et al., 2012) or sea surface temperature in the West Pacific Warm Pool (Appendix I; Stott et al., 2004).

Regional synthesis

Including Lake Motosu, 18 EASM records were identified which fit the selection criteria (Figure 2; Table 1; Appendix J). Of these, the majority were lake sediment records (n = 8). The remaining records came from marine sediment (n = 4), speleothem (n = 3), peat (n = 1) and floodplain (n = 1) archives. Past moisture conditions were inferred from bulk isotopes, compound-specific isotopes, bulk organic matter concentrations, pollen-based precipitation reconstructions and sedimentological features.

MCEOF analysis identified two statistically significant patterns of regional hydroclimate change (Figures 7, 8). The first component (PCA1; 35 ± 3.0% explained variance) showed high values in the early Holocene (9-6.5 ka) before declining steadily towards the present. The second component (PCA2; 21 ± 2.3% explained variance) increased to a peak at ~4.5 ka before declining into the present. Principal component loadings represent the degree to which each pattern is present in each record. Most

continental sites loaded strongly on PCA1, excluding those in Japan and northeast China which had either weak positive or negative loadings (Figure 9). Marine records did not show a consistent spatial trend. PCA2 was more variable; however, most lake sites loaded positively, particularly in northeast China and Japan. Similar to PCA1, marine sites did not show a consistent signal. Lake Motosu had a weak negative loading on the PCA1 and a weak positive loading on PCA2. However, when the volcano affected sediments from 3-0 ka were excluded, C/N from Lake Motosu correlated strongly and negatively to PCA2 (Appendix K).

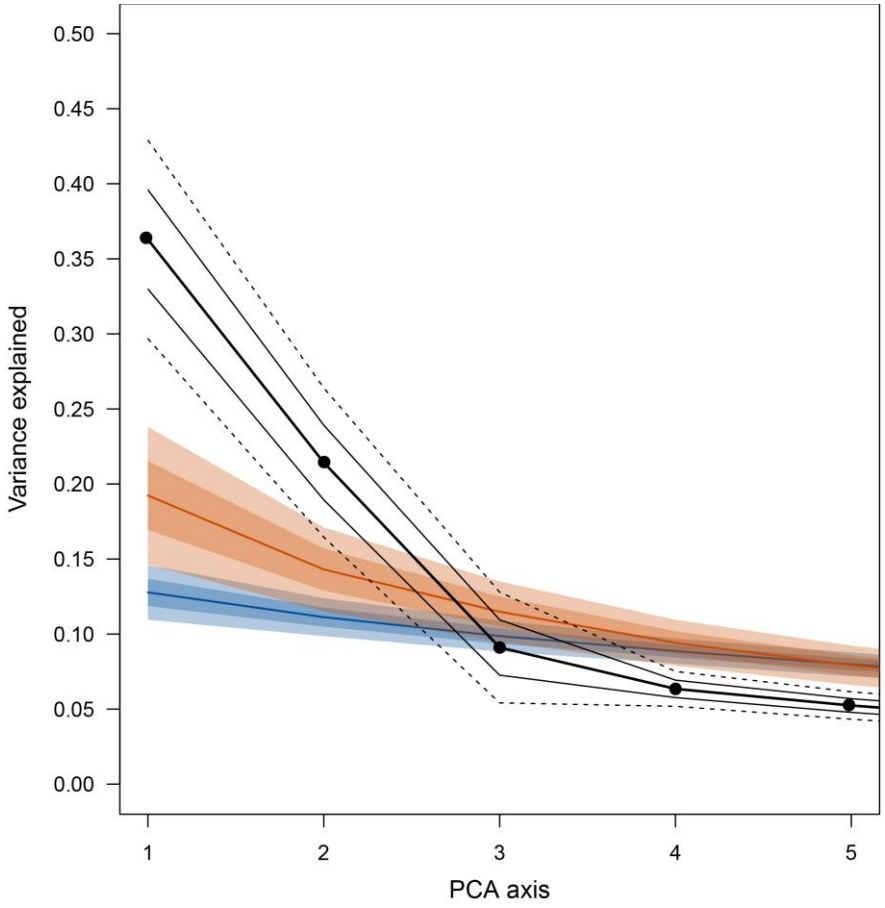

Figure 7: Percent variance explained for an increasing number of principal components. Principal components are calculated for 10,000 age model iterations for 18 East Asian Summer Monsoon sites. Principal component (PCA) axes are shown by black dots (mean value), solid lines (68% confidence) and dashed lines (90% confidence). Confidence intervals are also shown for 1,000 iterations of white noise (blue) and red noise (orange).

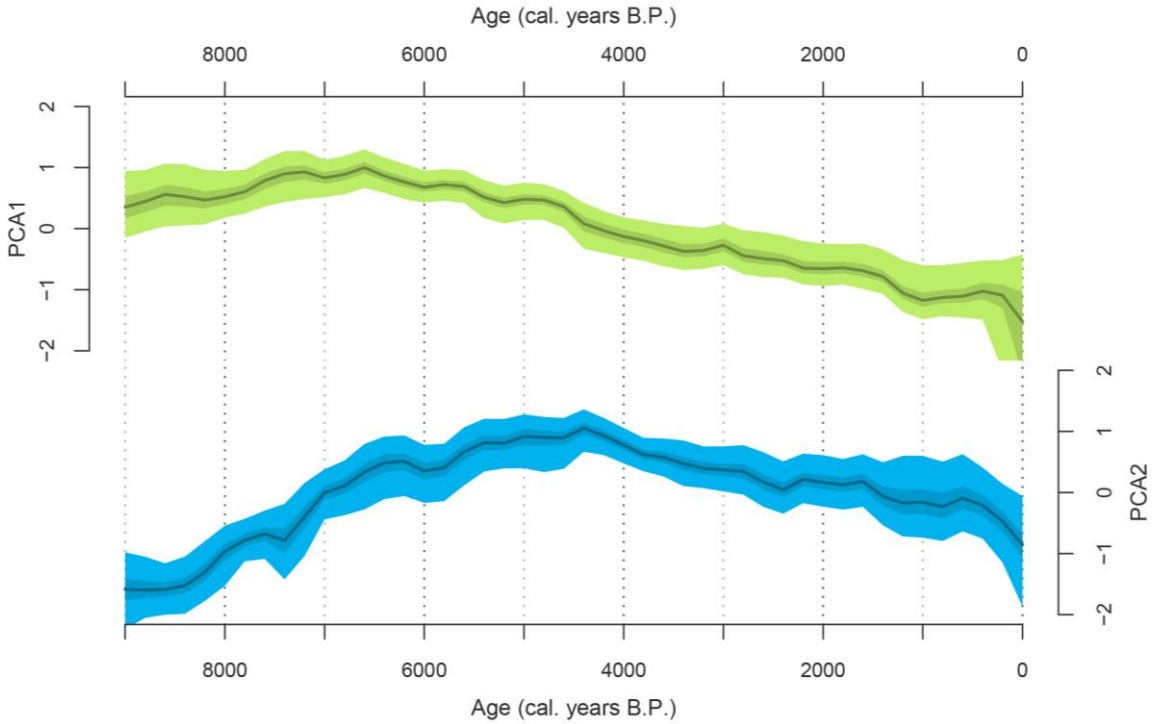

Figure 8: Time-series expansions of the first (PCA1) and second (PCA2) principal components extracted from an MCEOF analysis of 18 East Asian Summer Monsoon records. Confidence intervals are shown by solid lines (mean), dark bands (68%) and light bands (90%). Axes are orientated so that wetter conditions plot upwards.

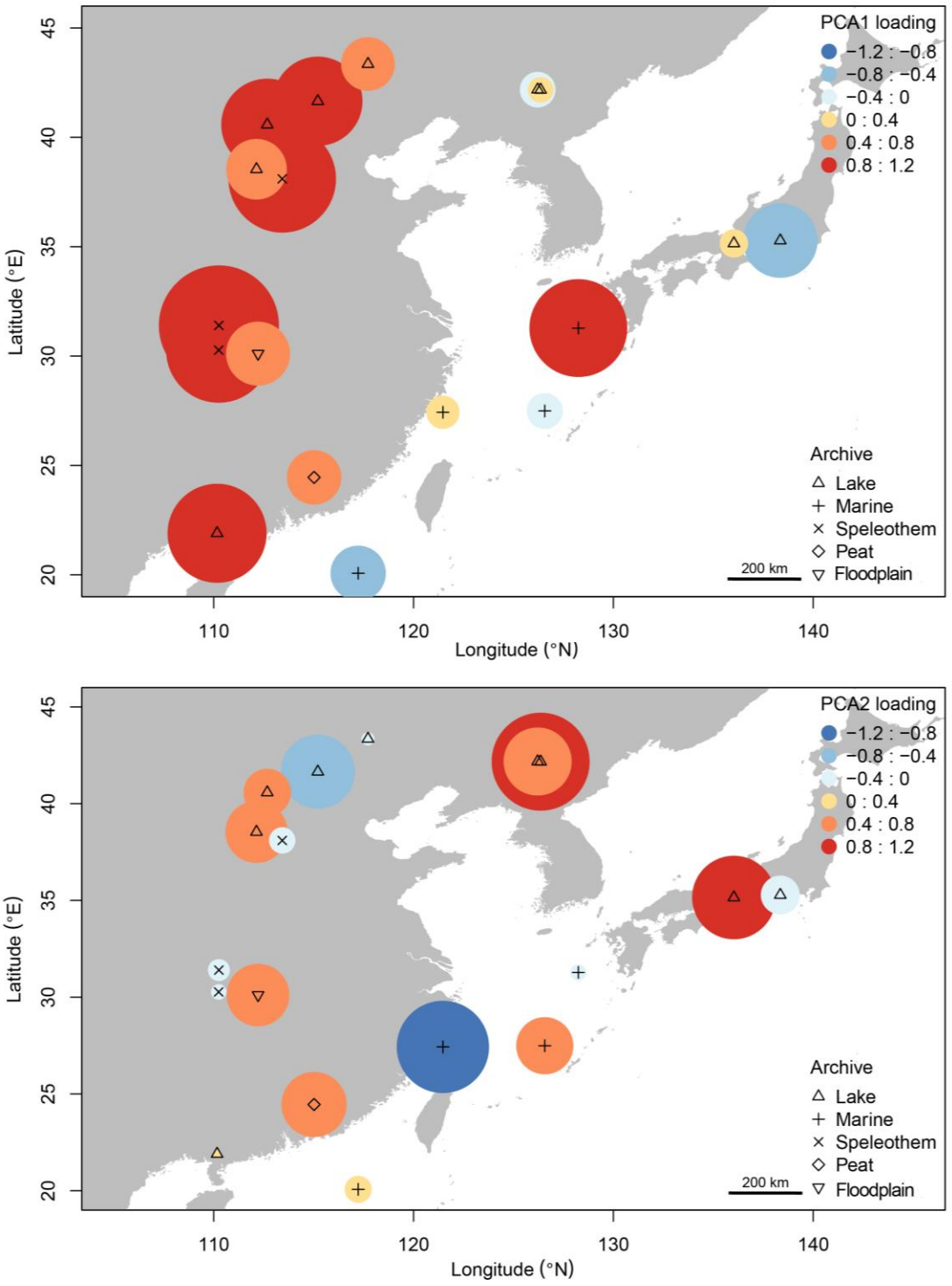

Figure 9: Map of the study region showing the principal component loadings for each site for the first principal component (PCA1; top) and second principal component (PCA2; bottom) of an MCEOF analysis of 18 East Asian Summer Monsoon records. Warm colours (positive loadings) represent sites with patterns which strongly (larger dots) reflect the regional trend. Cool colours (negative loadings) represent sites with patterns which strongly (larger dots) reflect the inverse of the regional trend. Symbols represent archive type.

DISCUSSION

Palaeohydrology of Lake Motosu

SOURCES OF ORGANIC MATTER

Although the organic matter composition of lake sediments is inextricably linked to climate, sedimentation can also be influenced by non-climatic processes, including the reworking of existing material (Monecke et al., 2004; Schnellmann et al., 2002). This is particularly the case in Japan, where steep topography, heavy rainfall and seismic activity contribute to frequent slope failure and sediment mass transport (Oguchi et al., 2001). Treated linescan images suggest a high proportion of re-worked terrestrial material in the Lake Motosu sediment core (Appendix F; Lamair et al., 2018). In some cases, these turbidite deposits were associated with anomalously high C/N or $\delta^{15}N$ (Appendix L). These samples were thus confidently interpreted as turbidites and are not included in the subsequent numerical analysis and plots. However, in most cases, whilst terrestrial material typically has a higher C/N ratio than aquatic material, the proposed turbidite sequences were geochemically indistinguishable from background sedimentation (Figure 5). The classification of turbidites from optical images is not always conclusive, as changes in sediment colour can also be driven by internal lake processes such as algal blooms or changes in sediment oxidation state. Consequently, whilst the exclusion all turbidite sequences prior to interpretation is preferable, given that their geochemistry is indistinguishable, the majority of proposed turbidites are included in the present record. However, it should be noted that the inclusion of these turbidite sequences may influence the interpretation of the record. Whilst beyond the scope of this thesis, future work should consider complementary techniques, such as

micro-facies analysis, which may better constrain the location of these deposits and the impact they have on the sedimentary, and hence palaeoclimate record, of Lake Motosu.

Accurately interpreting bulk organic proxies requires knowledge of the source of sedimented organic material. C/N ratios are a general indicator of the relative contributions of aquatic (C/N <10) and terrestrial (C/N >20) material to lake sediments (Leng & Marshall, 2004; Meyers & Terances, 2002). C/N ratios in Lake Motosu are consistent with a sub-equal mixture of aquatic and terrestrial material (Figure 10). However, sedimentary inorganic carbon, nitrogen limitation and preferential loss of nitrogen during diagenesis can also increase C/N ratios (Lehmann et al., 2002; Meyers & Terances, 2002; Talbot & Lærdal, 2000). The effect of inorganic carbon in Lake Motosu is minimal, as the sediments are devoid of calcium carbonate (Figure 6; Obrochta et al., 2018). However, Lake Motosu is nutrient-limited, deep, and oxic throughout the water column (Hamada et al., 2012). Both nitrogen limitation and diagenesis may thus act to increase the sediment C/N ratio in the absence of terrestrial material. Given that the sediments are composed primarily of diatom silica with few terrestrial macrofossils, it is reasonable to infer that organic matter in Lake Motosu is primarily aquatic with varying minor inputs of terrestrial material.

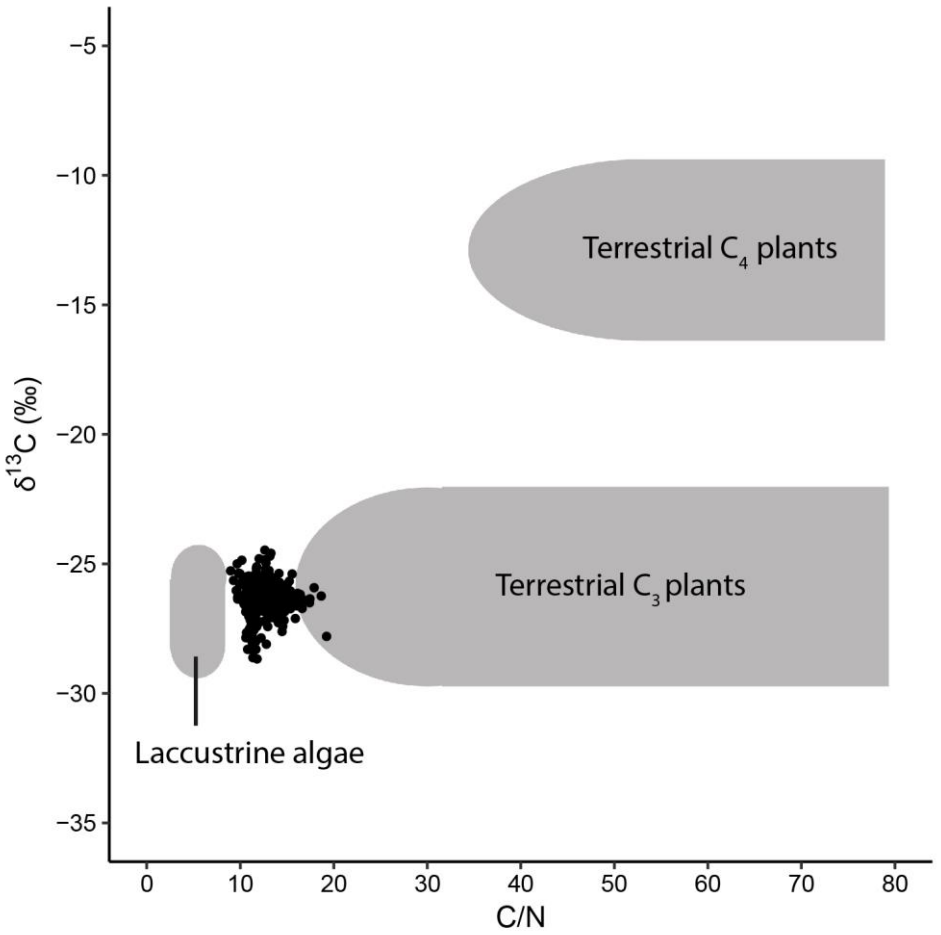

Figure 10: Source of organic matter to the Lake Motosu sediments. Shading represents regions associated with major sources of organic carbon to lake sediments. Figure adapted from Meyers & Lallier-Vergés (1999).

ENVIRONMENTAL INFLUENCE ON LAKE MOTOSU

Compared to terrestrial plants, algae have a higher protein content and are thus relatively nitrogen-rich (Meyers & Terances, 2002; Talbot, 2002). The increase in TN and the related decrease in C/N in the Lake Motosu sediments from 8-6 ka thus suggests a moderate increase in algal productivity within the lake (Figure 4). In lake systems, enhanced algal productivity is favoured by warmer water temperatures, increased nutrient influx in response to increased precipitation and run-off, and/or increased nutrient availability due to lake mixing (Adhikari et al., 2002; Ishiwatari et al., 2009;

Leng et al., 2006). Warmer water temperature, increased precipitation, and increased mixing could all reflect a strengthening of the EASM, culminating in peak conditions at 6-4 ka. Consequently, trends in the organic composition of sediments from Lake Motosu could be interpreted to reflect increasing monsoon strength and lake productivity from 8-6 ka, peak monsoon conditions between 6-4 ka, and a subsequent decline in monsoon strength towards 3 ka.

An alternative pattern is suggested by a subtle increase in $\delta^{18}O$ and TC through the Holocene (Figure 4). In East Asia, $\delta^{18}O$ is inversely correlated to monsoon strength through variations in either precipitation amount (Sakashita et al., 2016; Wang et al., 2005) or precipitation source (Kurita et al., 2015; Pausata et al., 2011). The possible minor increase in $\delta^{18}O$ could, therefore, be interpreted to reflect a drying trend in response to a weakening monsoon. In this context, the increase in TC could reflect a decrease in lithogenic input from a reduction in runoff. However, an increase in TC may also reflect an increase in organic deposition and productivity within Lake Motosu or an increase in the preservation of organic material within the sediments. In addition, the increasing trend in the $\delta^{18}O$ of cellulose is inferred from a much lower resolution dataset than the trends in TN and C/N. Consequently, the mid-Holocene peak in monsoon strength suggested by TN and C/N is favoured over the drying trend which could be inferred from $\delta^{18}O$ and TC. Additional proxies, including diatom productivity, $\delta^{18}O$ of biogenic silica and compound-specific isotopes, could be used to further constrain the relationship between sediment composition in Lake Motosu and EASM strength, and hence distinguish between a mid-Holocene monsoon peak or a gradual drying trend through the Holocene.

There are several possible reasons why the cellulose $\delta^{18}O$ from Lake Motosu may not reflect variations in monsoon strength, despite the well-established relationship between $\delta^{18}O$ and hydroclimate (Leng et al., 2006). Terrestrial organic matter contains abundant cellulose which is resistant to degradation. Interpretations of sedimentary cellulose isotopes can thus be affected by even small amounts of terrestrial contamination (Sauer et al., 2001). Whilst low C/N ratios in Lake Motosu suggest a predominance of algal material, there is likely to be some terrestrial input. Additionally, although FTIRS spectra show no contamination of the extracted cellulose (Figure 6), the cellulose oxygen content is lower than expected for pure cellulose (Appendix E). This may be due to minor impurities in the cellulose which may affect the isotopic composition through the release of traces of inorganically-bound oxygen during pyrolysis (Wissel et al., 2008). The link between precipitation $\delta^{18}O$ and the EASM in maritime Japan is less pronounced than in continental Asia due to a limited amount effect and proximity to the moisture source (Kurita et al., 2015; Mori et al., 2018). A subtle increasing trend in the $\delta^{18}O$ of lake water in response to declining monsoon strength may thus be overridden by variability introduced through contamination of sedimentary cellulose, either by terrestrial cellulose during deposition or by minor impurities which were not removed during the extraction process.

Maximum lake productivity in Lake Motosu, as inferred from TN and C/N, is coincident with marked low but variable $\delta^{13}C$. Low $\delta^{13}C$ in aquatic organic matter can reflect decreased productivity (Leng & Marshall, 2004; Meyers & Ishiwatari, 1993). However, this would contradict with TN and C/N in Lake Motosu, suggesting that either TN or $\delta^{13}C$ are not sensitive to lake productivity and monsoon strength. The $\delta^{13}C$ is generally stable throughout the record aside from the high-frequency oscillations

between 5.5-4.5 ka. This stability suggests that $\delta^{13}C$ responds to rapid, local shifts in lake ecosystem dynamics, whilst C/N is more sensitive to long-term changes in productivity and climate.

Where productivity may not be the main control of $\delta^{13}C$, influxes of isotopically light carbon into lake water, either from the surrounding catchment or from the oxidation of methane in lake sediments, can also contribute to low $\delta^{13}C$ (Herczeg, 1987, 1988; Rau, 1978). Recycling of isotopically light terrestrial carbon typically produces distinctly low isotopic values, significantly lower than those of the Lake Motosu record, and is associated increased C/N ratios due to an influx of terrestrial organic matter (Rau, 1978; Street-Perrott et al., 2018). This is opposite to the trend observed Lake Motosu. Methane remobilisation from lake sediments can decrease the $\delta^{13}C$ of dissolved inorganic carbon in the water column without the requirement for large changes in organic matter source (Hammarlund et al., 2005; Herczeg, 1988). Episodes of low $\delta^{13}C$ in Lake Motosu are preceded by periods of higher $\delta^{13}C$ associated with proposed turbidites (Figure 3; Lamair et al., 2018). Turbidite deposition may have disturbed existing sediments, reintroducing stored carbon to the water column. The introduction of stored carbon with low $\delta^{13}C$ to the water column through turbidite deposition may subsequently have been utilised by algae and incorporated into sedimented material. Episodes of low $\delta^{13}C$ are thus interpreted to reflect the release of methane from lake sediments in response to turbidite deposition.

$\delta^{15}N$ is not correlated with any other proxy and shows no distinct long-term trends (Figures 3, 4). Consequently, it appears that nitrogen cycling in Lake Motosu did not undergo major changes through the Holocene in response to climate. In nutrient-limited

lakes, variations in $\delta^{15}N$ reflect shifts in the relative dominance of nitrogen assimilation and nitrogen fixation (Leng et al., 2006; Talbot, 2002). The shorter-term oscillations in $\delta^{15}N$ in Lake Motosu are thus possibly due to subtle shifts in the major phytoplankton and nitrogen assimilation preferences. The relative importance of nitrogen fixation over assimilation could be further constrained by the analysis of pigments (Cadd et al., 2018) or chlorin-specific isotopes in the sediments (Tyler et al., 2010).

VOLCANIC INFLUENCE ON LAKE MOTOSU

Following a moderate decline in lake productivity between 4-3 ka, the inferred coupling between sediment composition in Lake Motosu, lake productivity, and regional climate deteriorated (Appendix K). Between 3.5-2.3 ka, Mt Fuji entered a period of explosive volcanism that caused major changes in the Lake Motosu catchment. Eruptions deposited scoria across the catchment, with five scoria deposits identified in Lake Motosu (Obrochta et al., 2018). The deposition of the Omuro scoria cone (3260-3056 cal. year B.P) reduced the Lake Motosu catchment area (Lamair et al., 2018). Modern-day Lake Motosu was subsequently formed by the division of an existing larger lake (Senoumi Lake) by the Aokigahara Lava Flow (868-854 CE; Hamada et al., 2012). These changes impacted soil stability, sedimentation patterns and local vegetation in the Mt Fuji area (Lamair et al., 2018; Yamamoto et al., 2018). Fluctuations in soil stability and vegetation, or reduced buffering due to a smaller lake volume, may account for the increased sedimentation rate and variability observed in the Lake Motosu record after 3 ka. Anthropogenic influences have also been recognised in nearby Lake Yamanaka since 1 ka (Yamamoto et al., 2018). This is possibly reflected in Lake Motosu by a rapid increase in TN at ~0.6 ka (Figure 3). These local changes mask regional climate signals, and thus the period from 3 ka to present in Lake Motosu is interpreted to represent local

catchment changes driven by volcanic activity and anthropogenic impacts, rather than variations in climate.

HOLOCENE PALAEOCLIMATE OF LAKE MOTOSU

Given the upper sediments of Lake Motosu (3-0 ka) are interpreted to reflect catchment disturbance by volcanism and anthropogenic impacts, all subsequent palaeoclimate interpretation will focus on the period between 8-3 ka. The evidence from these sediments suggests that the timing of peak monsoon strength occurred slightly later in Lake Motosu (6-4 ka) than suggested by existing studies in Japan (Figure 11). The Holocene warm and wet period in Japan is generally dated to between 8-6 ka (Grossman, 2001), with estimates ranging from 7.25-6.15 ka (Adhikari et al., 2002), 6.12-5.59 ka (Schöne et al., 2004), 7.3-3.6 ka (Shu et al., 2013), 6-8 ka (Mori et al., 2018) and 8-2 ka (Ishiwatari et al., 2009). The discrepancy between these records and the Lake Motosu record may be partly attributed to chronological uncertainties associated with each record. In most cases, the timing of peak warm and wet conditions recorded in these records is constrained by a low-resolution age model. In comparison, Lake Motosu benefits from a high-resolution Bayesian age model, which allows tighter constraints on the timing of climatic events (Obrochta et al., 2018). The interpretation of lake sediment records is also entirely qualitative and based on non-linear palaeoclimate proxies with complex responses to climate variability. This can also introduce uncertainty into the timing of palaeoclimate events. For example, in Lake Aoki and Ohtaki Cave, events of a similar magnitude to the proposed mid-Holocene climate optimum occurred

coincidently or slightly after the wettest period in the Lake Motosu record (Figure 11). These peaks may equally reflect warm and wet conditions, which would be consistent with the timing observed in Lake Motosu. The timing of peak moisture conditions in Lake Motosu is also supported by a correlation with peak regional moisture conditions extracted from a synthesis of EASM records (Appendix K). Strong monsoon conditions are therefore interpreted to have occurred in central Japan between ~6-4 ka.

Understanding the causes of climate change in the past is important for modelling how climate systems may respond in the future. Variations in Pacific Ocean conditions and solar insolation are proposed as major drivers of the monsoon in Japan and East Asia (Park, 2017; Sakashita et al., 2016; Wang et al., 2005; Zhao & Wang, 2014). However, there is no visual similarity between these drivers and the Lake Motosu record (Figure 11). Whilst a possible 1000-year periodicity, reminiscent of solar variability, is present in TC, TN, $\delta^{13}C$ and $\delta^{15}N$ prior to 3 ka, cross-wavelet analysis failed to identify any commonalities with total solar insolation (Steinhilber et al., 2012) or sea surface temperature in the West Pacific Warm Pool (Appendix I; Stott et al., 2004). As outlined above, the Lake Motosu record is sensitive to both the strength of the monsoon and local catchment changes. Furthermore, whilst the classification of turbidite sequences in Lake Motosu is unclear, the impact of sediment recycling associated with seismic events is not insignificant. Consequently, the absence of major climate drivers in our record may reflect the confounding influence of climatic and non-climatic factors, rather than an insensitivity to changes in insolation and Pacific Ocean conditions.

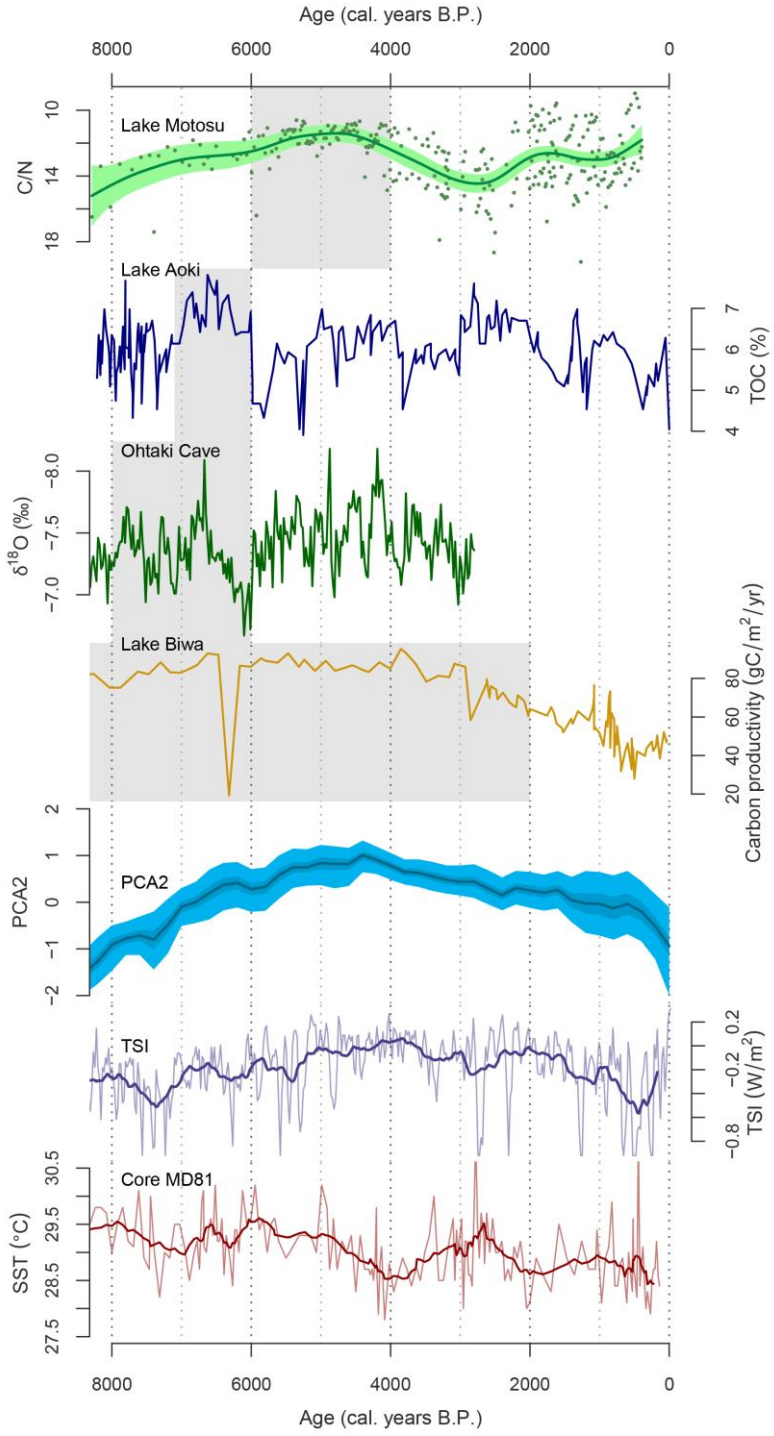

Figure 11: Comparison plot of selected Japanese palaeoclimate records and possible climate drivers. From top: C/N ratio of bulk organic matter in Lake Motosu (this study); total organic carbon in Lake Aoki, Japan (Adhikari et al., 2002); speleothem $\delta^{18}O$ from Ohtaki Cave, Japan (Mori et al., 2018); carbon productivity in Lake Biwa (Ishiwatari et al., 2009); the second principal component (PCA2) of climate in the East Asian Monsoon region (this study); total solar insolation (pale purple) fitted with a 20-point running mean (dark purple; Steinhilber et al., 2012); reconstructed sea surface temperatures in the West Pacific Warm Pool (light red) from core MD81 fitted with a 10-point running mean (dark red; Stott et al., 2004). Axes are oriented such that wet/strong monsoon conditions plot upwards. Grey shading indicates maximum warm and/or wet conditions inferred from each record.

Regional monsoon variability

Statistical analysis of numerous climate records from a region can be used to isolate climate trends, even when individual records are influenced by both climatic and non-climatic signals (Falster et al., 2018; Field et al., 2018; Tyler et al., 2015). Given the large non-climatic influences on sedimentation, to evaluate possible drivers of Holocene monsoon variability, Lake Motosu was included in a statistical analysis of 18 EASM records. This synthesis identified two coherent climate trends reflecting early-Holocene and mid-Holocene peaks in monsoon strength (Figure 8). A similar analysis of 92 records from the EASM and Indian Monsoon regions was conducted by Wang et al. (2010). Although Wang et al. (2010) included a much larger number of records in their synthesis and covered a wider geographic region, they noted that their synthesis was impacted by differing temporal-resolutions and age-controls between records. By factoring in this time uncertainty in the present analysis, the identification of similar trends reinforces the analysis of Wang et al. (2010). The present synthesis also identified spatial heterogeneity in moisture patterns, with the four sites located in northeast Asia and Japan differing to those in continental Asia (Figure 9). This pattern is supported by several studies which note the differences in Holocene moisture patterns between coastal and continental Asia (Chu et al., 2014; Mori et al., 2018; Park et al., 2018; Stebich et al., 2015).

The first significant hydroclimate trend is strongly reminiscent of the reduction in Northern Hemisphere summer insolation through the Holocene in response to a decline in precession-driven orbital forcing (Figure 12; Berger & Loutre, 1991). Orbital forcing has been identified as a major driver of Holocene monsoon variability in previous studies of Chinese speleothems in both the Indian Monsoon and EASM regions (Dong

et al., 2010; Rao et al., 2016; Wang et al., 2008, 2001, 2005). Declining summer insolation reduced spring heating over continental Asia, reducing the land-ocean thermal contrast and weakening onshore monsoon winds. This resulted in a decline in the strength of the Indian Monsoon and a contraction of the Indian Monsoon rain belt away from the EASM region. This is consistent with the absence of a decline in monsoon strength in northeast China and Japan, as these regions sit outside the geographic region influenced by the expansion and contraction of the Indian Monsoon rain belt (Schöne et al., 2004).

The second significant hydroclimate trend is consistent with a mid-Holocene optimum identified in numerous records from the EASM region (Hong et al., 2005; Ishiwatari et al., 2009; Stebich et al., 2015; Xu et al., 2010; Zhang et al., 2011; Zhong et al., 2011). Apart from Lake Motosu, this trend is more strongly expressed in northeast China and Japan than continental Asia. Whilst a mid-Holocene peak was identified in Lake Motosu, the record is strongly influenced by non-climatic factors, which may have affected the expression of this record within the analysis. Prior to the influence of volcanic activity on the Lake Motosu record from 3-0 ka, C/N in Lake Motosu was strongly correlated with PCA2 (Appendix K), suggesting that despite not loading strongly on PCA2, Lake Motosu does reflect a similar pattern to the other coastal East Asian sites.

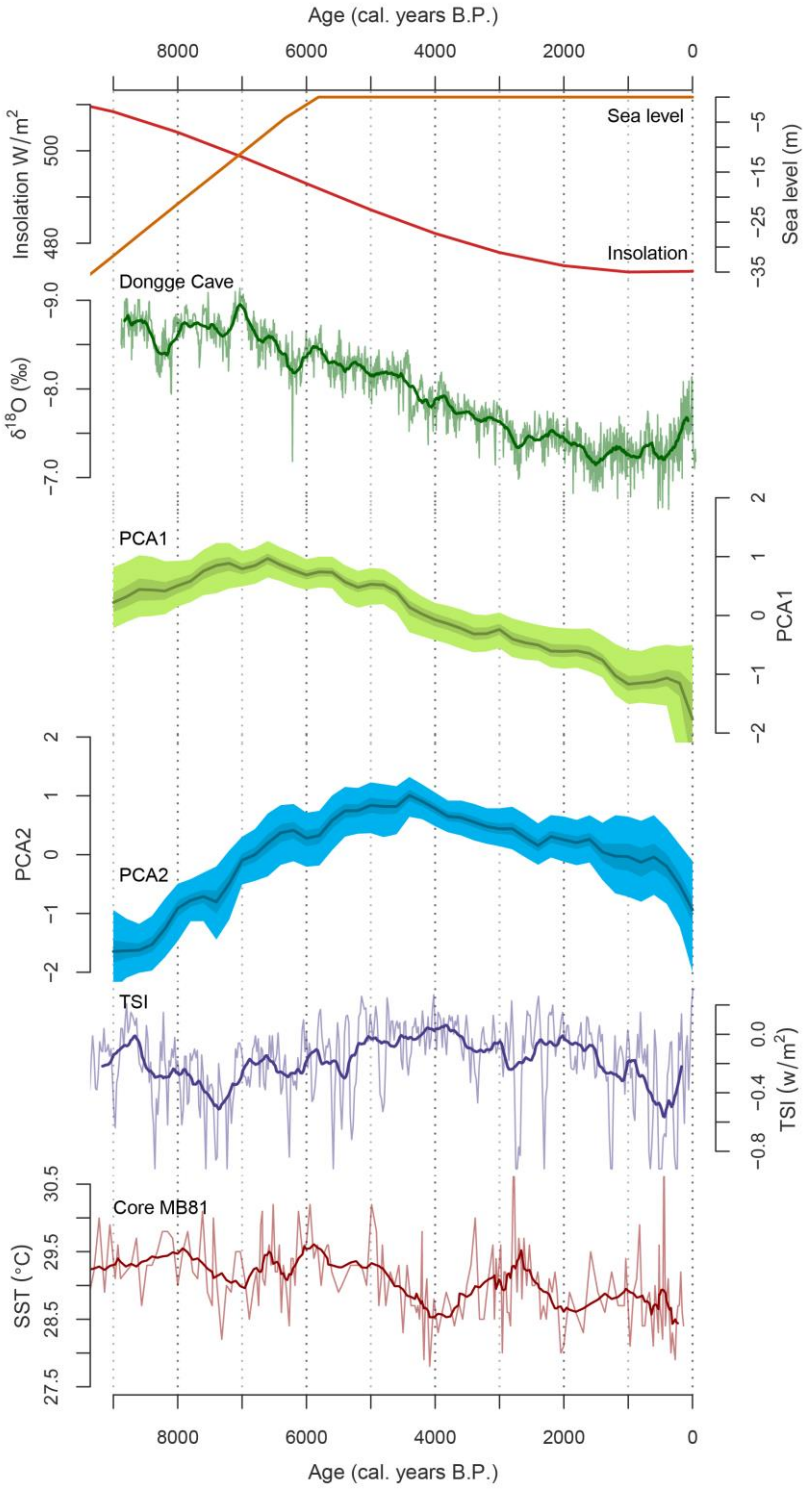

Figure 12: Comparison plot of selected regional trends in the East Asian Summer Monsoon and possible climate drivers. From top: global sea level (yellow; Yokoyama et al., 2007); orbital insolation (red; Berger & Loutre, 1991); $\delta^{18}O$ in Dongge Cave as a proxy for Indian Monsoon intensity (light green) fitted with a 20-point running mean (dark green; Wang et al., 2005); two major trends in East Asian monsoon climate (PCA1; PCA2; this study), total solar insolation (light purple) fitted with a 20-point running mean (dark purple; Steinhilber et al., 2012); reconstructed sea surface temperatures in the West Pacific Warm Pool (light red) from core MB81 fitted with a 10-point running mean (dark red; Stott et al., 2004).

After eliminating a Pacific Ocean control on the basis of stable Holocene sea surface temperatures, Wang et al. (2010) attributed a strong EASM in the mid-Holocene to interactions between the Indian Monsoon and the EASM, related to the decline in the strength of the Hadley Circulation. They proposed that as the Hadley Circulation weakened, atmospheric convection, and hence precipitation, was likely enhanced across East Asia. However, whilst sea surface temperatures in the West Pacific Warm Pool were stable to declining during the Holocene (Figure 12; Stott et al., 2004), major ocean currents in the North Pacific Ocean were variable. In particular, the Kuroshio Warm Current is inferred to have re-entered the Okinawa Trough at ~7 ka in response to deglacial sea level rise (Jian et al., 2000). The Kuroshio Warm Current plays an important role in transporting heat from the West Pacific Warm Pool north to Japan. An increase in the amount of warmth transported to the oceans surrounding Japan may have increased moisture evaporation and subsequent precipitation amounts over northeast China and Japan. The role of deglacial variations in ocean currents in the Pacific Ocean in driving increased EASM precipitation towards the mid-Holocene is supported by the visual similarity between PCA2 and global deglacial sea level rise (Figure 12). In contrast to Wang et al. (2010), this would imply a predominant, rather than absent, Pacific Ocean control on Holocene EASM climate.

A Pacific Ocean control on EASM variability is supported by the well-documented link between El Niño–Southern Oscillation (ENSO) variability and EASM precipitation (An et al., 2015; Park et al., 2018; Sakashita et al., 2016; Webster et al., 1998). ENSO is the dominant mode of climate variability in the Pacific Ocean region and is associated with centennial-scale variability in sea surface temperatures and subsequent changes in precipitation across the Pacific Ocean region. The strong expression of a mid-Holocene

optimum in coastal East Asian sites, compared to those in continental Asia, is also suggestive of a Pacific Ocean control, as a smaller land to ocean ratio and proximity to the moisture source makes this region more sensitive to Pacific Ocean variability (Chu et al., 2014; Mori et al., 2018; Park et al., 2018; Stebich et al., 2015). The present synthesis, combined with existing knowledge of monsoon mechanisms, thus suggests that the climate of coastal Asia is more susceptible to variations in Pacific Ocean conditions than continental Asia, which is more sensitive to orbital forcing through variations in the land-ocean thermal contrast.

Implications for the East Asian Monsoon

This thesis confirms that EASM variability through the Holocene is more spatially and temporally complex than suggested by highly-cited Chinese speleothem records (Wang et al., 2008, 2001, 2005). This complexity has implications for modelling future monsoon variability in response to anthropogenic warming. If, as the present synthesis suggests, coastal Asia is more sensitive to variations in Pacific Ocean conditions and associated atmospheric circulation systems than continental Asia, the future response of this region may differ to that of the rest of Asia. Modelling suggests that in response to future warming, tropical atmospheric circulation systems will weaken, with increased variability in Pacific Ocean sea surface conditions (Aldrian et al., 2013). In the context of the analysis presented here, this suggests possible drying in maritime Asia, but with increased variability and extreme rainfall events. In contrast, continental Asia, which is more sensitive to land-ocean thermal contrasts, may receive a greater amount of rainfall in response to increased temperatures over land.

However, the interpretation of a dominantly maritime control on the monsoon in northeast China and Japan is based on only four records. This includes Lake Motosu, where the climate signal is strongly influenced by volcanic activity and possible turbidite deposition. Assessing whether this pattern is unique to these records or consistent across the entire region will require a greater number of highly resolved, well-dated palaeoclimate records from coastal Asia, particularly records which can be unambiguously linked to hydroclimate. At present, records in Japan are predominantly based on bulk sediment proxies (Adhikari et al., 2002; Ishiwatari et al., 2009; Yamada et al., 2010) which, as is the case for Lake Motosu, may be influenced by a number of different factors. This complicates their interpretation with respect to the EASM. Compound-specific isotopes, oxygen isotopes and pollen-based precipitation reconstructions are increasingly being used to reconstruct Japanese palaeoclimate (Mori et al., 2018; Nakagawa et al., 2002; van Soelen et al., 2016). There is scope for the wider application of these approaches to develop new records from coastal Asia which span the duration of the Holocene. More broadly, modelling future changes and unpicking spatially heterogeneous climate drivers will require climate models with a greater spatial resolution to isolate regional-scale responses to monsoon variability, rather modelling the EASM as a single, homogenous system.

CONCLUSIONS

This thesis presents a well-dated, multi-proxy climate record from Lake Motosu, central Japan, and then uses this new record to expand the spatial coverage of a Monte Carlo Empirical Orthogonal Function analysis of EASM records. The main conclusions are that;

1. Sedimentation in Lake Motosu, Japan, was controlled by climate between 8-3 ka. The period between 6-4 ka was warm and wet with strong monsoon conditions. Following 3 ka, volcanic and anthropogenic influences dominate sedimentation processes in Lake Motosu.
2. EASM variability is sensitive to both external forcing though variations in orbital isolation and subsequent changes in the land-ocean thermal contrast, and internal variability through changes in Pacific Ocean conditions and the subsequent evaporative potential of the moisture source regions for the EASM.
3. The spatial response of the EASM is complex, reflecting varying contributions of continental and maritime influences. The climate of coastal Asia, including Japan, is influenced primarily by Pacific Ocean conditions and thus records a different climate history to that of continental Asia.

This work demonstrates that the drivers of EASM variability vary spatially across East Asia, with coastal regions more sensitive to local changes in Pacific Ocean conditions. Future work to unravel these effects will improve our ability to forecast centennial-scale climate variability in East Asia and hence assess possible climate impacts in this socially and economically important region.

ACKNOWLEDGMENTS

Thank you first and foremost to my supervisor Jonathan Tyler for his endless support and guidance this year. Stephen Obrochta, Yusuke Yokoyama and Yosuke Miyairi provided access to samples, additional data and shared their knowledge of Lake Motosu. This thesis benefited greatly from discussions with Haidee Cadd, who also provided advice on age models and GAMs. Martin Ankor greatly improved the efficiency of the MCEOF analysis. Isotope analysis was carried out by Kristine Nielson and Mark Rollog at the University of Adelaide. Finally, thank you to Tiah Bampton, Priya, Alex Harland and members of Jon's lab group for advice, support and assistance in the lab this year. This work is funded by JSPS Kakenhi 16K05571, with additional support from the School of Physical Sciences, University of Adelaide. Samples were collected as part of the "QuakeRecNankai" project, funded by the Belgian Science Policy Office.

REFERENCES

ADHIKARI, D. P. (2014). Hydrogeological features of Mount Fuji and the surrounding area, central Japan: an overview. *Journal of Institute of Science and Technology*, *19*(1), 96–105.

ADHIKARI, D. P., KUMON, F., & KAWAJIRI, K. (2002). Holocene climate variability as deduced from the organic carbon and diatom records in the sediments of Lake Aoki, central Japan. *The Journal of the Geological Society of Japan*, *108*(4), 249–265. https://doi.org/10.5575/geosoc.108.249

ALDRIAN, E., AN, S.-I., CAVALCANTI, I. F. A., DE CASTRO, M., DONG, W., GOSWAMI, P., HALL, A., KANYANGA, J. K., KITOH, A., KOSSIN, J., LAU, N.-C., RENWICK, J., STEPHENSON, D. B., XIE, S.-P., & ZHOU, T. (2013). Climate phenomena and their relevance for future regional climate change. In *Climate Change 2013: The Physical Science Basis. Contribution of Working Group 1 to the Fifth Assessment Report of the Intergovernmental Panel on Climate Change* (pp. 1217–1308). Cambridge: Cambridge University Press.

AN, Z., GUOXIONG, W., JIANPING, L., YOUBIN, S., YIMIN, L., WEIJIAN, Z., YANJUN, C., ANMIN, D., LI, L., JIANGYU, M., HAI, C., ZHENGGUO, S., LIANGCHENG, T., HONG, Y., HONG, A., HONG, C., & JUAN, F. (2015). Global monsoon dynamics and climate change. *Annual Review of Earth and Planetary Sciences*, *43*(1), 29–77. https://doi.org/10.1146/annurev-earth-060313-054623

ANCHUKAITIS, K. J., & TIERNEY, J. E. (2013). Identifying coherent spatiotemporal modes in time-uncertain proxy paleoclimate records. *Climate Dynamics*, *41*(5–6), 1291–1306. https://doi.org/10.1007/s00382-012-1483-0

BATTARBEE, R. W. (2000). Palaeolimnological approaches to climate change, with special regard to the biological record. *Quaternary Science Reviews*, *19*(1–5), 107–124. https://doi.org/10.1016/S0277-3791(99)00057-8

BERGER, A., & LOUTRE, M. F. (1991). Insolation values for the climate of the last 10 million years. *Quaternary Science Reviews*, *10*, 297–317.

BLAAUW, M., & CHRISTEN, J. A. (2011). Flexible paleoclimate age-depth models using an autoregressive gamma process. *Bayesian Analysis*, *6*(3), 457–474.

CADD, H. R., TIBBY, J., BARR, C., TYLER, J., UNGER, L., LENG, M. J., MARSHALL, J. C., MCGREGOR, G., LEWIS, R., ARNOLD, L. J., LEWIS, T., BALDOCK, J., LEWIS, T., AU, J. B., & BALDOCK, (J. (2018). Development of a southern hemisphere subtropical wetland (Welsby Lagoon, south-east Queensland, Australia) through the last glacial cycle. https://doi.org/10.1016/j.quascirev.2018.09.010

CHANG, F., LI, T., XIONG, Z., & XU, Z. (2015). Evidence for sea level and monsoonally driven variations in terrigenous input to the northern East China Sea during the last 24.3 ka. *Paleoceanography*, *30*(6), 642–658. https://doi.org/10.1002/2014PA002733

CHEN, F., XU, Q., CHEN, J., BIRKS, H. J. B., LIU, J., ZHANG, S., JIN, L., AN, C., TELFORD, R. J., CAO, X., WANG, Z., ZHANG, X., SELVARAJ, K., LU, H., LI, Y., ZHENG, Z., WANG, H., … RAO, Z. (2015). East Asian summer monsoon precipitation variability since the last deglaciation. *Scientific Reports*, *5*(1), 11186. https://doi.org/10.1038/srep11186

CHEN, F., YU, Z., YANG, M., ITO, E., WANG, S., MADSEN, D. B., HUANG, X., ZHAO, Y., SATO, T., BIRKS, J. B., BOOMER, I., CHEN, J., AN, C., & WU¨NNEMANN, B. W. (2008). Holocene moisture evolution in arid central Asia and its out-of-phase relationship with Asian monsoon history. *Quaternary Science Reviews*, *27*, 351–364. https://doi.org/10.1016/j.quascirev.2007.10.017

CHENG, J., EDWARDS, H., HE, R. L., KONG, Y. Q., & AN, X. G. (2007). Quantification of Holocene Asian monsoon rainfall from spatially separated cave records. https://doi.org/10.1016/j.epsl.2007.10.015

CHU, G., SUN, Q., XIE, M., LIN, Y., SHANG, W., ZHU, Q., SHAN, Y., XU, D., RIOUAL, P., WANG, L., & LIU, J. (2014). Holocene cyclic climatic variations and the role of the Pacific Ocean as recorded in varved sediments from northeastern China. *Quaternary Science Reviews*, *102*, 85–95. https://doi.org/10.1016/j.quascirev.2014.08.008

CLEMENS, S. C., PRELL, W. L., & SUN, Y. (2010). Orbital-scale timing and mechanisms driving Late Pleistocene Indo-Asian summer monsoons: Reinterpreting cave speleothem δ18O. *Paleoceanography*, *25*(4), 1–19. https://doi.org/10.1029/2010PA001926

CORLETT, R. T., CUI, X., INSAROV, G., LASCO, R., LINDGREN, E., & SURIJAN, A. (2014). Asia. In *Climate Change 2014: Impacts, Adaption, and Vulnerability. Part B: Regional Aspects. Contribution of Working Group II to the Fifth Assessment Report of the Intergovernmental Panel on Climate Change* (pp. 1327–1370). Cambridge: Cambridge University Press. Retrieved from http://www.ipcc.ch/pdf/assessment-report/ar5/wg2/WGIIAR5-Chap24_FINAL.pdf

DONG, J., SHEN, C.-C., KONG, X., WANG, H.-C., & JIANG, X. (2015). Reconciliation of hydroclimate sequences from the Chinese Loess Plateau and low-latitude East Asian Summer Monsoon regions over the past 14,500years. *Palaeogeography, Palaeoclimatology, Palaeoecology*, *435*, 127–135. https://doi.org/10.1016/j.palaeo.2015.06.013

DONG, J., WANG, Y., CHENG, H., HARDT, B., EDWARDS, R. L., KONG, X., WU, J., CHEN, S., LIU, D., JIANG, X., & ZHAO, K. (2010). A high-resolution stalagmite record of the Holocene East Asian monsoon from Mt Shennongjia, central China. *The Holocene*, *20*(2), 257–264. https://doi.org/10.1177/0959683609350393

DYKOSKI, C. A., EDWARDS, R. L., CHENG, H., YUAN, D., CAI, Y., ZHANG, M., LIN, Y., QING, J., AN, Z., & REVENAUGH, J. (2005). A high-resolution, absolute-dated Holocene and deglacial Asian monsoon record from Dongge Cave, China. *Earth and Planetary Science Letters*, *233*(1–2), 71–86. https://doi.org/10.1016/J.EPSL.2005.01.036

FALSTER, G., TYLER, J., GRANT, K., TIBBY, J., TURNEY, C., LÖHR, S., JACOBSEN, G., & KERSHAW, A. P. (2018). Millennial-scale variability in south-east Australian hydroclimate between 30,000 and 10,000 years ago. *Quaternary Science Reviews*, *192*, 106–122. https://doi.org/10.1016/j.quascirev.2018.05.031

FIELD, E., TYLER, J., GADD, P. S., MOSS, P., MCGOWAN, H., & MARX, S. (2018). Coherent patterns of environmental change at multiple organic spring sites in northwest Australia: Evidence of Indonesian-Australian summer monsoon variability over the last 14,500 years. *Quaternary Science Reviews*. https://doi.org/10.1016/J.QUASCIREV.2018.07.018

GOUHIER, T. C., GRINSTED, A., & SIMKO, V. (2018). R package biwavelet: conduct univariate and bivariate wavelet analyses.

GROSSMAN, M. J. (2001). Large floods and climatic change during the Holocene on the Ara River, Central Japan. *Geomorphology*, *39*(1–2), 21–37. https://doi.org/10.1016/S0169-555X(01)00049-6

HAMADA, H., KATSUMATA, D., & OYAGI, H. (2012). Investigation of seasonal change of water temperature and water quality and water balance on Lake Motosu-ko. *Bulletin of the Faculty of Education, Chiba University*, *60*, 459–468.

HAMMARLUND, D., BJORCK, S., BUCHARDT, B., & THOMSEN, C. T. (2005). Limnic responses to increased effective humidity during the 8200 cal. yr BP cooling event in southern Sweden. *Journal of Paleolimnology*, *34*(43), 471–480. https://doi.org/10.1007/s10933-005-5614-z

HAMMER, Ø., HARPER, D. A. T., & RYAN, P. D. (2001). Paleontological statistics software packages for education and data analysis. *Palaeontologia Electronica*, *4*(1). Retrieved from http://palaeo-electronic.org/2001_1/past/issue1_01.htm

HERCZEG, A. L. (1987). *A stable carbon isotope study of dissolved inorganic carbon cycling in a softwater lake*. *Biogeochemistry* (Vol. 4).

HERCZEG, A. L. (1988). Early diagenesis of organic matter in lake sediments: a stable carbon isotope study of pore waters. *Chemical Geology*, *72*, 199–209.

HERZSCHUH, U. (2006). Palaeo-moisture evolution in monsoonal Central Asia during the last 50,000 years. *Quaternary Science Reviews*, *25*(1–2), 163–178. https://doi.org/10.1016/J.QUASCIREV.2005.02.006

HEYNG, A. M., MAYR, C., LÜCKE, A., MOSCHEN, R., WISSEL, H., STRIEWSKI, B., & BAUERSACHS, T. (2015). Middle and Late Holocene paleotemperatures reconstructed from oxygen isotopes and GDGTs of sediments from Lake Pupuke, New Zealand. *Quaternary International*, *374*, 3–14. https://doi.org/10.1016/J.QUAINT.2014.12.040

HONG, Y. T., HONG, B., LIN, Q. H., SHIBATA, Y., HIROTA, M., ZHU, Y. X., LENG, X. T., WANG, Y., WANG, H., & YI, L. (2005). Inverse phase oscillations between the East Asian and Indian Ocean summer monsoons during the last 12 000 years and paleo-El Niño. *Earth and Planetary Science Letters*, *231*(3–4), 337–346. https://doi.org/10.1016/J.EPSL.2004.12.025

ISHIWATARI, R., NEGISHI, K., YOSHIKAWA, H., & YAMAMOTO, S. (2009). Glacial–interglacial productivity and environmental changes in Lake Biwa, Japan: A sediment core study of organic carbon, chlorins and biomarkers. *Organic Geochemistry*, *40*(4), 520–530. https://doi.org/10.1016/J.ORGGEOCHEM.2009.01.002

JAPAN METEOROLOGICAL AGENCY. (2018). Table of monthly climate statistics. Retrieved May 6, 2018, from http://www.data.jma.go.jp/obd/stats/etrn/view/monthly_s3_en.php?block_no=47640&view=13

JIA, G., BAI, Y., YANG, X., XIE, L., WEI, G., OUYANG, T., CHU, G., LIU, Z., & AN PENG, P. '. (2015). Biogeochemical evidence of Holocene East Asian summer and winter monsoon variability from a tropical maar lake in southern China. *Quaternary Science Reviews*, *111*, 51–61. https://doi.org/10.1016/j.quascirev.2015.01.002

JIAN, Z., WANG, P., SAITO, Y., WANG, J., PFLAUMANN, U., OBA, T., & CHENG, X. (2000). Holocene variability of the Kuroshio Current in the Okinawa Trough, northwestern Pacific Ocean. *Earth and Planetary Science Letters*, *184*(1), 305–319. https://doi.org/10.1016/S0012-821X(00)00321-6

JIANG, W., GUO, Z., SUN, X., WU, H., CHU, G., YUAN, B., HATTÉ, C., & EL GUIOT, J. (2006). Reconstruction of climate and vegetation changes of Lake Bayanchagan (Inner Mongolia): Holocene variability of the East Asian monsoon. https://doi.org/10.1016/j.yqres.2005.10.007

KOSHIMIZU, S., & TOMURA, K. (2000). Geochemical behaviour of trace vanadium in the spring, grounwater and lake water at the foot of Mt. Fuji, Central Japan. In K. Sato (Ed.), *Groundwater Updates* (pp. 171–176). Tokyo: Springer.

KURITA, N., FUJIYOSHI, Y., NAKAYAMA, T., MATSUMI, Y., & KITAGAWA, H. (2015). East Asian Monsoon controls on the inter-annual variability in precipitation isotope ratio in Japan. *Climate of the Past*, *11*(2), 339–353. https://doi.org/10.5194/cp-11-339-2015

LAMAIR, L., HUBERT-FERRARI, A., YAMAMOTO, S., EL OUAHABI, M., VANDER AUWERA, J., OBROCHTA, S., BOES, E., NAKAMURA, A., FUJIWARA, O., SHISHIKURA, M., SCHMIDT, S., SIANI, G., MIYAIRI, Y., YOKOYAMA, Y., DE BATIST, M., & HEYVAERT, V. M. A. (2018). Volcanic influence of Mt. Fuji on the watershed of Lake Motosu and its impact on the lacustrine sedimentary record. *Sedimentary Geology*, *363*, 200–220. https://doi.org/10.1016/J.SEDGEO.2017.11.010

LARKIN, P. (2011). *Infrared and Raman Spectroscopy: Principles and Spectral Interpretation*. Elsevier. https://doi.org/10.1016/B978-0-12-386984-5.10008-4

LEHMANN, M. F., BERNASCONI, S. M., BARBIERI, A., & MCKENZIE, J. A. (2002). Preservation of organic matter and alteration of its carbon and nitrogen isotope composition during simulated and in situ early sedimentary diagenesis. *Geochimica et Cosmochimica Acta*, *66*(20), 3573–3584. https://doi.org/10.1016/S0016-7037(02)00968-7

LENG, M. J., LAMB, A. L., HEATON, T. H. H., MARSHALL, J. D., WOLFE, B. B., JONES, M. D., HOLMES, J. A., & ARROWSMITH, C. (2006). Isotopes in lake sediments. In M. J. Leng (Ed.), *Isotopes in Palaeoenvironmental Research* (pp. 147–184). Dordrecht: Kluwer Academic Publishers. https://doi.org/10.1007/1-4020-2504-1_04

LENG, M. J., & MARSHALL, J. D. (2004). Palaeoclimate interpretation of stable isotope data from lake sediment archives. *Quaternary Science Reviews*, *23*(7–8), 811–831. https://doi.org/10.1016/J.QUASCIREV.2003.06.012

LI, F., ZHU, C., WU, L., SUN, W., LIU, H., CHYI, S.-J., KUNG, C.-L., ZHU, G., & WANG, X. (2014). Environmental humidity changes inferred from multi-indicators in the Jianghan Plain, Central China during the last 12,700 years. https://doi.org/10.1016/j.quaint.2013.09.040

LIU, J., CHEN, J., ZHANG, X., LI, Y., RAO, Z., & CHEN, F. (2015). Holocene East Asian summer monsoon records in northern China and their inconsistency with Chinese stalagmite δ18O records. *Earth-Science Reviews*, *148*, 194–208. https://doi.org/10.1016/J.EARSCIREV.2015.06.004

LIU, Y.-H., HENDERSON, G. M., HU, C.-Y., MASON, A. J., CHARNLEY, N., JOHNSON, K. R., & XIE, S.-C. (2013). Links between the East Asian monsoon and North Atlantic climate during the 8,200 year event. *Nature Geoscience*, *6*(2), 117–120. https://doi.org/10.1038/ngeo1708

MAHER, B. A. (2008). Holocene variability of the East Asian summer monsoon from Chinese cave records: a re-assessment. *Holocene*, *18*(6), 861–866.

MEYERS, P. A., & ISHIWATARI, R. (1993). *Lacustrine organic geochemistry - an overview of indicators of organic matter sources and diagenesis in lake sediments*. *Organic Geochemistry* (Vol. 20). Retrieved from https://ac-els-cdn-com.proxy.library.adelaide.edu.au/014663809390100P/1-s2.0-014663809390100P-main.pdf?_tid=a999c601-ff9c-4ecc-8191-79272381a464&acdnat=1536988499_31fdd6b2576957938a29051c3a0ee54d

MEYERS, P. A., & LALLIER-VERGÉS, E. (1999). Lacustrine Sedimentary Organic Matter Records of Late Quaternary Paleoclimates. *Journal of Paleolimnology*, *21*(3), 345–372. https://doi.org/10.1023/A:1008073732192

MEYERS, P. A., & TERANCES, J. L. (2002). Sediment organic matter. In W. M. Last & J. P. Smol (Eds.), *Tracking Environmental Change Using Lake Sediments. Volume 2* (pp. 239–270). Springer. Retrieved from https://ebookcentral.proquest.com/lib/adelaide/reader.action?docID=197244&ppg=264

MONECKE, K., ANSELMETTI, F. S., BECKER, A., STURM, M., & GIARDINI, D. (2004). The record of historic earthquakes in lake sediments of Central Switzerland. *Tectonophysics*, *394*, 21–40. https://doi.org/10.1016/j.tecto.2004.07.053

MORI, T., KASHIWAGI, K., AMEKAWA, S., KATO, H., OKUMURA, T., TAKASHIMA, C., WU, C.-C., SHEN, C.-C., QUADE, J., & KANO, A. (2018). Temperature and seawater isotopic controls on two stalagmite records since 83 ka from maritime Japan. *Quaternary Science Reviews*, *192*, 47–58. https://doi.org/10.1016/J.QUASCIREV.2018.05.024

MOSCHEN, R., LÜCKE, A., PARPLIES, J., & SCHLESER, G. H. (2009). Controls on the seasonal and interannual dynamics of organic matter stable carbon isotopes in mesotrophic Lake Holzmaar, Germany. *Limnology and Oceanography*, *54*(1), 194–209. https://doi.org/10.4319/lo.2009.54.1.0194

NAKAGAWA, T., TARASOV, P. E., NISHIDA, K., GOTANDA, K., & YASUDA, Y. (2002). Quantitative pollen-based climate reconstruction in central Japan: application to surface and Late Quaternary spectra. *Quaternary Science Reviews*, *21*, 2099–2113.

OBROCHTA, S. P., YOKOYAMA, Y., YOSHIMOTO, M., YAMAMOTO, S., MIYAIRI, Y., NAGANO, G., NAKAMURA, A., TSUNEMATSU, K., LAMAIR, L., HUBERT-FERRARI, A., LOUGHEED, B. C., HOKANISHI, A., YASUDA, A., HEYVAERT, V. M. A., DE BATIST, M., FUJIWARA, O., & THE QUAKERECNANKAI TEAM. (2018). Mt. Fuji Holocene eruption history reconstructed from proximal lake sediments and high-density radiocarbon dating. *Quaternary Science Reviews*. https://doi.org/10.1016/j.quascirev.2018.09.001

OGUCHI, T., SAITO, K., KADOMURA, H., & GROSSMAN, M. (2001). *Fluvial geomorphology and paleohydrology in Japan*. *Geomorphology* (Vol. 39). Retrieved from www.elsevier.nlrlocatergeomorph

OKSANEN, J., BLANCHET, G., FRIENDLY, M., KINDT, R., LEGENDRE, P., MCGLINN, D., MINCHIN, P. R., O'HARA, R. B., SIMPSON, G. L., SOLYMOS, P., STEVENS, M. H. H., SZOECS, E., & WAGNER, H. (2018). vegan: community ecology package. Retrieved from https://cran.r-project.org/package=vegan

OLDFIELD, F., BARNOSKY, C., LEOPOLD, E. B., & SMITH, J. P. (1983). Mineral magnetic studies of lake sediments. *Hydrobiologia*, *103*(1), 37–44. https://doi.org/10.1007/BF00028425

PARK, J. (2017). Solar and tropical ocean forcing of late-Holocene climate change in coastal East Asia. *Palaeogeography, Palaeoclimatology, Palaeoecology*, *469*, 74–83. https://doi.org/10.1016/J.PALAEO.2017.01.005

PARK, J., PARK, J., YI, S., KIM, J. C., LEE, E., & JIN, Q. (2018). The 8.2 ka cooling event in coastal East Asia: High-resolution pollen evidence from southwestern Korea. *Scientific Reports*, *8*(1), 12423. https://doi.org/10.1038/s41598-018-31002-7

PAUSATA, F. S. R., BATTISTI, D. S., NISANCIOGLU, K. H., & BITZ, C. M. (2011). Chinese stalagmite δ18O controlled by changes in the Indian monsoon during a simulated Heinrich event. *Nature Geoscience*, *4*(7), 474–480. https://doi.org/10.1038/ngeo1169

RAO, Z., JIA, G., LI, Y., CHEN, J., XU, Q., & CHEN, F. (2016). Asynchronous evolution of the isotopic composition and amount of precipitation in north China during the Holocene revealed by a record of compound-specific carbon and hydrogen isotopes of long-chain n-alkanes from an alpine lake. *Earth and Planetary Science Letters*, *446*, 68–76. https://doi.org/10.1016/J.EPSL.2016.04.027

RAU, G. (1978). Carbon-13 depletion in a subalpine lake: carbon flow implications. *Science*, *201*(4359), 901–902. Retrieved from https://www-jstor-

org.proxy.library.adelaide.edu.au/stable/pdf/1746907.pdf?refreqid=excelsior%3Ac31b7e1471e0662ecd8e9078ce880adc

REIMER, P. J., BARD, E., BAYLISS, A., BECK, J. W., BLACKWELL, P. G., RAMSEY, C. B., BUCK, C. E., CHENG, H., EDWARDS, R. L., FRIEDRICH, M., GROOTES, P. M., GUILDERSON, T. P., HAFLIDASON, H., HAJDAS, I., HATTÉ, C., HEATON, T. J., HOFFMANN, D. L., … VAN DER PLICHT, J. (2013). IntCal13 and Marine13 radiocarbon age calibration curves 0–50,000 years cal BP. *Radiocarbon*, *55*(04), 1869–1887. https://doi.org/10.2458/azu_js_rc.55.16947

ROSÉN, P., VOGEL, H., CUNNINGHAM, L., HAHN, A., HAUSMANN, S., PIENITZ, R., ZOLITSCHKA, B., WAGNER, B., & PERSSON, P. (2011). Universally Applicable Model for the Quantitative Determination of Lake Sediment Composition Using Fourier Transform Infrared Spectroscopy. *Environmental Science & Technology*, *45*(20), 8858–8865. https://doi.org/10.1021/es200203z

SAKASHITA, W., MIYAHARA, H., AZE, T., NAKATSUKA, T., HOSHINO, Y., OHYAMA, M., YONENOBU, H., & TAKEMURA, K. (2017). Hydroclimate reconstruction in central Japan over the past four centuries from tree-ring cellulose δ18O. *Quaternary International*, *455*, 1–7. https://doi.org/10.1016/J.QUAINT.2017.06.020

SAKASHITA, W., MIYAHARA, H., YAMAGUCHI, Y. T., AZE, T., OBROCHTA, S. P., & NAKATSUKA, T. (2016). Relationship between early summer precipitation in Japan and the El Niño-Southern and Pacific Decadal Oscillations over the past 400 years. *Quaternary International*, *397*, 300–306. https://doi.org/10.1016/J.QUAINT.2015.05.054

SAUER, P. E., MILLER, G. H., & OVERPECK, J. T. (2001). Oxygen isotope ratios of organic matter in arctic lakes as a paleoclimate proxy: field and laboratory investigations. *Journal of Paleolimnology*, *25*(1), 43–64. https://doi.org/10.1023/A:1008133523139

SCHNELLMANN, M., ANSELMETTI, F. S., GIARDINI, D., MCKENZIE, J. A., & WARD, S. N. (2002). Prehistoric earthquake history revealed by lacustrine slump deposits. *Geology*, *30*(12), 1131. https://doi.org/10.1130/0091-7613(2002)030<1131:PEHRBL>2.0.CO;2

SCHÖNE, B. R., OSCHMANN, W., TANABE, K., DETTMAN, D., FIEBIG, J., HOUK, S. D., & KANIE, Y. (2004). Holocene seasonal environmental trends at Tokyo Bay, Japan, reconstructed from bivalve mollusk shells—implications for changes in the East Asian monsoon and latitudinal shifts of the Polar Front. *Quaternary Science Reviews*, *23*(9–10), 1137–1150. https://doi.org/10.1016/J.QUASCIREV.2003.10.013

SHEN, C.-C., KANO, A., HORI, M., LIN, K., CHIU, T.-C., & BURR, G. S. (2010). East Asian monsoon evolution and reconciliation of climate records from Japan and Greenland during the last deglaciation. *Quaternary Science Reviews*, *29*(23–24), 3327–3335. https://doi.org/10.1016/J.QUASCIREV.2010.08.012

SHU, J.-W., SASAKI, N., TAKAHARA, H., & HASE, Y. (2013). Vegetation and fire history with their implication for climatic change and fire events since the last deglacial in the Aso Valley, central Kyushu, southwestern Japan: new pollen and charcoal data. *Vegetation History and Archaeobotany*, *22*(4), 285–298. https://doi.org/10.1007/s00334-012-0375-x

SONE, T., KANO, A., OKUMURA, T., KASHIWAGI, K., HORI, M., JIANG, X., & SHEN, C.-C. (2013). Holocene stalagmite oxygen isotopic record from the Japan Sea side of the Japanese Islands, as a new proxy of the East Asian winter monsoon. *Quaternary Science Reviews*, *75*, 150–160. https://doi.org/10.1016/J.QUASCIREV.2013.06.019

STEBICH, M., REHFELD, K., SCHLÜTZ, F., TARASOV, P. E., LIU, J., & MINGRAM, J. (2015). Holocene vegetation and climate dynamics of NE China based on the pollen record from Sihailongwan Maar Lake. *Quaternary Science Reviews*, *124*, 275–289. https://doi.org/10.1016/j.quascirev.2015.07.021

STEINHILBER, F., ABREU, J. A., BEER, J., BRUNNER, I., CHRISTL, M., FISCHER, H., HEIKKILÄ, U., KUBIK, P. W., MANN, M., MCCRACKEN, K. G., MILLER, H., MIYAHARA, H., OERTER, H., & WILHELMS, F. (2012). 9,400 years of cosmic radiation and solar activity from ice cores and tree rings. *Proceedings of the National Academy of Sciences of the United States of America*, *109*(16), 5967–5971. https://doi.org/10.1073/pnas.1118965109

STOTT, L., CANNARIATO, K., THUNELL, R., HAUG, G. H., KOUTAVAS, A., & LUND, S. (2004). Decline of surface temperature and salinity in the western tropical Pacific Ocean in the Holocene epoch. *Nature*, *431*(7004), 56–59. https://doi.org/10.1038/nature02903

STREET-PERROTT, F. A., HOLMES, J. A., ROBERTSON, I., FICKEN, K. J., KOFF, T., LOADER, N. J., MARSHALL, J. D., & MARTMA, T. (2018). The Holocene isotopic record of aquatic cellulose from Lake Äntu Sinijärv, Estonia: Influence of changing climate and organic-matter sources. *Quaternary Science Reviews*, *193*, 68–83. https://doi.org/10.1016/J.QUASCIREV.2018.05.010

SUN, Y., OPPO, D. W., XIANG, R., LIU, W., & GAO, S. (2005). Last deglaciation in the Okinawa Trough:

Subtropical northwest Pacific link to Northern Hemisphere and tropical climate. *Paleoceanography*, *20*(4), n/a-n/a. https://doi.org/10.1029/2004PA001061

TAKEUCHI, K., KIRIISHI, F., & IMAMURA, H. (1995). The water balance analyses of the five lakes of Mt. Fuji. *Annual Journal of Hydraulic Engineering*, *39*, 31–36.

TALBOT, M. R. (2002). Nitrogen Isotopes in palaeolimnology. In W. M. Last & J. P. Smol (Eds.), *Tracking Environmental Change Using Lake Sediments. Volume 2* (pp. 401–439). Dordrecht: Kluwer Academic Publishers. https://doi.org/10.1007/0-306-47670-3_15

TALBOT, M. R., & LÆRDAL, T. (2000). The Late Pleistocene-Holocene palaeolimnology of Lake Victoria, East Africa, based upon elemental and isotopic analyses of sedimentary organic matter. *Journal of Paleolimnology*, *23*, 141–164.

THOMAS, E. K., CLEMENS, S. C., SUN, Y., PRELL, W. L., HUANG, Y., GAO, L., LOOMIS, S., CHEN, G., & LIU, Z. (2016). Heterodynes dominate precipitation isotopes in the East Asian monsoon region, reflecting interaction of multiple climate factors. *Earth and Planetary Science Letters*, *455*, 196–206. https://doi.org/10.1016/J.EPSL.2016.09.044

TYLER, J. J., MILLS, K., BARR, C., SNIDERMAN, J. M. K., GELL, P. A., & KAROLY, D. J. (2015). Identifying coherent patterns of environmental change between multiple, multivariate records: an application to four 1000-year diatom records from Victoria, Australia. *Quaternary Science Reviews*, *119*, 94–105. https://doi.org/10.1016/J.QUASCIREV.2015.04.010

TYLER, J., KASHIYAMA, Y., OHKOUCHI, N., OGAWA, N., YOKOYAMA, Y., CHIKARAISHI, Y., STAFF, R. A., IKEHARA, M., BRONK RAMSEY, C., BRYANT, C., BROCK, F., GOTANDA, K., HARAGUCHI, T., YONENOBU, H., & NAKAGAWA, T. (2010). Tracking aquatic change using chlorine-specific carbon and nitrogen isotopes: The last glacial-interglacial transition at Lake Suigetsu, Japan. *Geochemistry Geophysics Geosystems*, *11*(9), Q09010. https://doi.org/10.1029/2010GC003186

VAN SOELEN, E. E., OHKOUCHI, N., SUGA, H., DAMSTÉ, J. S. S., & REICHART, G.-J. (2016). A late Holocene molecular hydrogen isotope record of the East Asian Summer Monsoon in Southwest Japan. *Quaternary Research*, *86*(03), 287–294. https://doi.org/10.1016/j.yqres.2016.07.005

WANG, B. (2006). *The Asian Monsoon*. (B. Wan, Ed.). Chichester: Praxis Publishing.

WANG, K., ZHENG, H., TADA, R., IRINO, T., ZHENG, Y., SAITO, K., & KARASUDA, A. (2014). Millennial-scale East Asian Summer Monsoon variability recorded in grain size and provenance of mud belt sediments on the inner shelf of the East China Sea during mid-to late Holocene. *Quaternary International*, *349*, 79–89. https://doi.org/10.1016/j.quaint.2014.09.014

WANG, L., SARNTHEIN, M., GROOTES, P. M., & ERLENKEUSER, H. (1999). Millennial reoccurrence of century-scale abrupt events of East Asian Monsoon: A possible heat conveyor for the global deglaciation. *Paleoceanography*, *14*(6), 725–731. https://doi.org/10.1029/1999PA900028

WANG, Y., CHENG, H., EDWARDS, R. L., HE, Y., KONG, X., AN, Z., WU, J., KELLY, M. J., DYKOSKI, C. A., & LI, X. (2005). The Holocene Asian monsoon: links to solar changes and North Atlantic climate. *Science*, *308*(5723), 854–857. https://doi.org/10.1126/science.1106296

WANG, Y., CHENG, H., EDWARDS, R. L., KONG, X., SHAO, X., CHEN, S., WU, J., JIANG, X., WANG, X., & AN, Z. (2008). Millennial- and orbital-scale changes in the East Asian monsoon over the past 224,000 years. *Nature*, *451*(7182), 1090–1093. https://doi.org/10.1038/nature06692

WANG, Y. J., CHENG, H., EDWARDS, R. L., AN, Z. S., WU, J. Y., SHEN, C. C., & DORALE, J. A. (2001). A high-resolution absolute-dated late Pleistocene Monsoon record from Hulu Cave, China. *Science*, *294*(5550), 2345–2348. https://doi.org/10.1126/science.1064618

WANG, Y., LIU, X., & HERZSCHUH, U. (2010). Asynchronous evolution of the Indian and East Asian Summer Monsoon indicated by Holocene moisture patterns in monsoonal central Asia. *Earth-Science Reviews*, *103*(3–4), 135–153. https://doi.org/10.1016/J.EARSCIREV.2010.09.004

WEBSTER, P. J., MAGAÑA, V. O., PALMER, T. N., SHUKLA, J., TOMAS, R. A., YANAI, M., & YASUNARI, T. (1998). Monsoons: Processes, predictability, and the prospects for prediction. *Journal of Geophysical Research: Oceans*, *103*(C7), 14451–14510. https://doi.org/10.1029/97JC02719

WISSEL, H., MAYR, C., & LÜCKE, A. (2008). A new approach for the isolation of cellulose from aquatic plant tissue and freshwater sediments for stable isotope analysis. *Organic Geochemistry*, *39*(11), 1545–1561. https://doi.org/10.1016/J.ORGGEOCHEM.2008.07.014

WOLFE, B. B., EDWARDS, T. W. D., ELGOOD, R. J., & BEUNING, K. R. M. (2001). Carbon and oxygen isotope analysis of lake sediment cellulose: methods and applications. In W. M. Last & J. P. Smol (Eds.), *Tracking Environmental Change Using Lake Sediments. Volume 2* (pp. 373–400). Dordrecht: Kluwer Academic Publishers.

WOLFE, B. B., FALCONE, M. D., CLOGG-WRIGHT, K. P., MONGEON, C. L., YI, Y., BROCK, B. E., AMOUR, N. A. ST., MARK, W. A., & EDWARDS, T. W. D. (2007). Progress in isotope paleohydrology using

lake sediment cellulose. *Journal of Paleolimnology*, *37*(2), 221–231. https://doi.org/10.1007/s10933-006-9015-8

WOOD, S. N. (2017). *Generalized Additive Models: an introduction with R* (2nd ed.). Chapman and Hall/CRC.

WU, D., CHEN, X., LV, F., BRENNER, M., CURTIS, J., ZHOU, A., CHEN, J., ABBOTT, M., YU, J., & CHEN, F. (2018). Decoupled early Holocene summer temperature and monsoon precipitation in southwest China. *Quaternary Science Reviews*, *193*, 54–67. https://doi.org/10.1016/J.QUASCIREV.2018.05.038

XIAO, J., SI, B., ZHAI, D., ITOH, S., & LOMTATIDZE, Z. (2008). Hydrology of Dali Lake in central-eastern Inner Mongolia and Holocene East Asian monsoon variability. *Journal of Paleolimnology*, *40*(1), 519–528. https://doi.org/10.1007/s10933-007-9179-x

XU, Q., XIAO, J., LI, Y., TIAN, F., & NAKAGAWA, T. (2010). Pollen-Based Quantitative Reconstruction of Holocene Climate Changes in the Daihai Lake Area, Inner Mongolia, China. *Journal of Climate*, *23*(11), 2856–2868. https://doi.org/10.1175/2009JCLI3155.1

YAMADA, K., KAMITE, M., SAITO-KATO, M., OKUNO, M., SHINOZUKA, Y., & YASUDA, Y. (2010). Late Holocene monsoonal-climate change inferred from Lakes Ni-no-Megata and San-no-Megata, northeastern Japan. *Quaternary International*, *220*(1–2), 122–132. https://doi.org/10.1016/J.QUAINT.2009.09.006

YAMAMOTO, S., UCHIYAMA, T., MIYAIRI, Y., & YOKOYAMA, Y. (2018). Volcanic and environmental influences of Mt. Fuji on the δ13C of terrestrially-derived n-alkanoic acids in sediment from Lake Yamanaka, central Japan. *Organic Geochemistry*, *119*, 50–58. https://doi.org/10.1016/J.ORGGEOCHEM.2018.02.002

YASUHARA, M., KAZAHAYA, K., & MARUI, A. (2007). An isotopic study on where, when and how groundwater is recharged in Fuji Volcano, Central Japan. In *Mount Fuji Volcano* (pp. 389–405). Yamanashi Prefectural Environmental Science Research Center.

YIHUI, D., & CHAN, J. C. L. (2005). The East Asian summer monsoon: an overview. *Meteorology and Atmospheric Physics*, *89*(1–4), 117–142. https://doi.org/10.1007/s00703-005-0125-z

YOKOYAMA, Y., KIDO, Y., MINAMI, I., FINKEL, R. C., & MATSUZAKI, H. (2007). Japan Sea oxygen isotope stratigraphy and global sea-level changes for the last 50,000 years recorded in sediment cores from the Oki Ridge. *Palaeogeography, Palaeoclimatology, Palaeoecology*, *247*(1–2), 5–17. https://doi.org/10.1016/J.PALAEO.2006.11.018

YOSHIZAWA, K. (2009). Trends in the concentration of dissolved COD in Fuji Five Lakes. *Annual Report of the Yamanashi Research Institute*, *53*, 61–66.

ZHANG, J., CHEN, F., HOLMES, J. A., LI, H., GUO, X., WANG, J., LI, S., LÜ, Y., ZHAO, Y., & QIANG, M. (2011). Holocene monsoon climate documented by oxygen and carbon isotopes from lake sediments and peat bogs in China: a review and synthesis. *Quaternary Science Reviews*, *30*(15–16), 1973–1987. https://doi.org/10.1016/J.QUASCIREV.2011.04.023

ZHAO, L., & WANG, J.-S. (2014). Robust Response of the East Asian Monsoon Rainband to Solar Variability. *Journal of Climate*, *27*(8), 3043–3051. https://doi.org/10.1175/JCLI-D-13-00482.1

ZHENG, X., LI, A., WAN, S., JIANG, F., KAO, S. J., & JOHNSON, C. (2014). ITCZ and ENSO pacing on East Asian winter monsoon variation during the Holocene: Sedimentological evidence from the Okinawa Trough. *Journal of Geophysical Research: Oceans*, *119*(7), 4410–4429. https://doi.org/10.1002/2013JC009603

ZHONG, W., MA, Q., XUE, J., ZHENG, Y., CAI, Y., OUYANG, Y., & YU, X. (2011). Humification degree as a proxy climatic record since the last deglaciation derived from a limnological sequence in South China. *Geochemistry International*, *49*(4), 407–414. https://doi.org/10.1134/S0016702911040094

APPENDIX A: MODERN CLIMATOLOGY

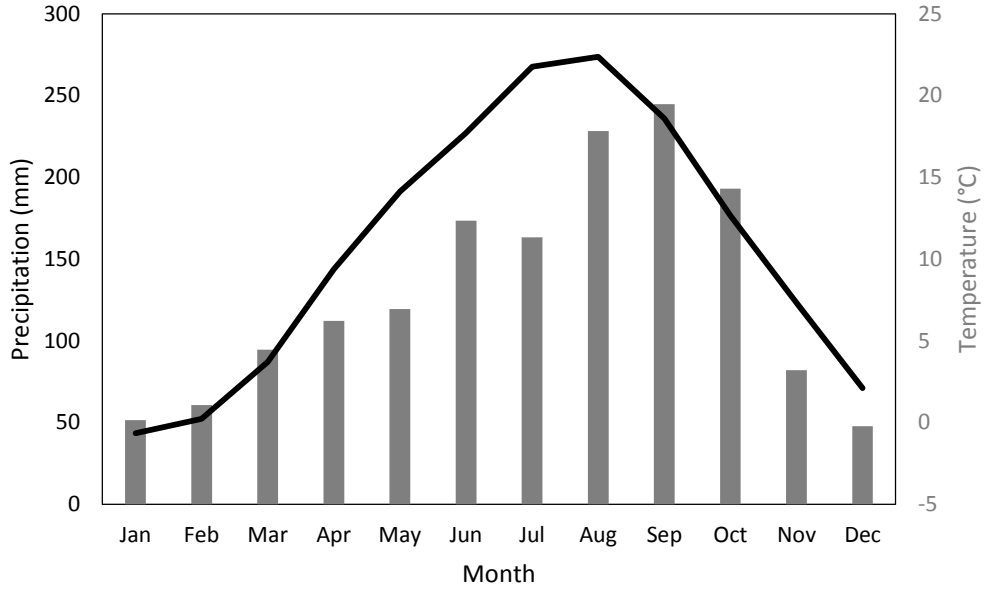

Figure A1: Modern climatology of the Mt Fuji region. Data represent mean monthly temperature and precipitation amounts for the period 1933-2017 at Kawaguchiko (35°30.0' N, 138°45.6'E). Data from the Japan Meteorological Agency (2018).

APPENDIX B: AGE MODEL

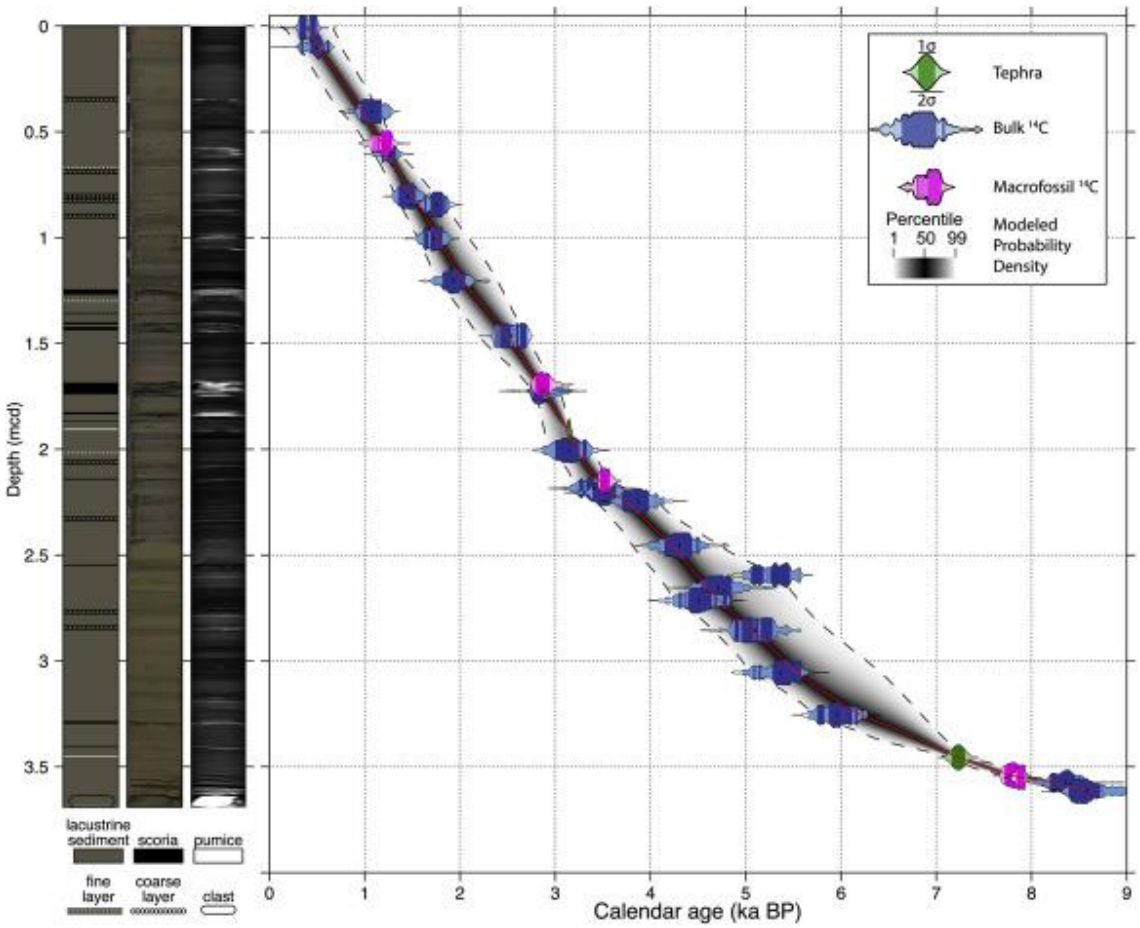

Figure A2: Core MOT15-2 age model with, from left to right, stratigraphic column, composite core image, and CT scan. Figure from Obrochta et al. (2018).

APPENDIX C: CELLULOSE EXTRACTION METHOD

1. Prepare cuprammonium solution in advance. Into a 1 L amber glass bottle, add 15 g copper hydroxide, 750 ml ammonium hydroxide solution (30%) and 250 ml deionised water. Stir at room temperature overnight. Filter.
2. Sieve sediment at 250 µm, transferring fine fraction to a clean 50 ml centrifuge tube.
3. Allow fine sediment to settle overnight and decant supernatant water.
4. Fill centrifuge tube to 40 ml with 7% $NaClO_2$ acidified to pH 4-5 with concentrated acetic acid. Heat to 60ºC for 10 hours on a hotplate.
5. Heat 1 L of deionised water on a hotplate to 70ºC.
6. Centrifuge the sediment and $NaClO_2$ at 4000 rpm for 5 minutes. Check that the supernatant is obviously clear and free of suspended particles – if not, repeat the centrifugation and take note of the required time for future reference. Once the supernatant is clear, decant supernatant liquid for disposal.
7. Fill the centrifuge with hot deionised water to ~30-40 ml. Shake to disturb the pellet and repeat centrifugation.
8. Repeat the process of centrifugation and decanting 5 x to remove all $NaClO_2$.
9. Freeze, and freeze dry the sediment.
10. Add 30 ml cuprammonium solution to dry sediment and close the lid. Stir at room temperature for 6 hours using an end-on-end shaker, then leave for 10 hours to completely dissolve the cellulose.
11. Centrifuge for 5 minutes and decant supernatant copper complex cellulose solution to a separate centrifuge tube.

12. Centrifuge at 4000 rpm for 25 min and decant supernatant to another centrifuge tube.
13. Add 3 ml H_2SO_4 (20%) and fill to 50 ml with DI water. Carefully cap the tube and carefully shake. Leave to stand for 20 min at room temperature.
14. Centrifuge at 4000 rpm for 25 min. Decant supernatant to waste.
15. Add 1 ml DI water and 1 ml H_2SO_4 (20%) to dissolve the blue pellet. Allow to sit for 1-5 min until precipitate becomes completely decopperised – i.e. it turns from blue to white.
16. Fill with cold DI water, centrifuge at 4000 rpm for 25 min, decant water. Repeat x 3.
17. After final centrifugation, add 1 ml DI water to suspend the cellulose, and transfer to a 2 ml 'eppendorf' tube'. Centrifuge this down using microcentrifuge and decant water.
18. Freeze dry resultant cellulose.

APPENDIX D: CARBON AND NITROGEN ISOTOPE DATA

Table A1: Bulk organic composition data for Lake Motosu. Shaded samples were excluded from analysis.

Depth (c.m.c.d.)	Age (cal. year B.P.)	$\delta^{15}N$ (‰)	$\delta^{15}N$ error (‰)	$\delta^{13}C$ (‰)	$\delta^{13}C$ error (‰)	TN (%)	TN error (%)	TC (%)	TC error (%)	C/N (atomic)
0	379	3.41	0.05	-25.64	0.11	0.36	0.09	2.95	0.29	8.79
1	394	2.77	0.27	-27.86	0.21	0.31	0.027	3.22	0.19	12.23
2	402	2.73	0.05	-26.24	0.11	0.48	0.12	4.16	0.40	9.19
3	402	2.96	0.27	-27.1	0.21	0.3	0.026	3.33	0.19	12.91
4	434	2.93	0.05	-25.36	0.11	0.45	0.11	4.20	0.41	9.82
5	449	2.65	0.27	-27.09	0.21	0.33	0.028	3.78	0.22	13.69
6	463	2.76	0.05	-25.64	0.11	0.51	0.13	4.48	0.44	9.28
7	478	5.38	0.27	-27.53	0.21	0.3	0.026	3.75	0.21	14.53
8	492	2.88	0.05	-25.27	0.11	0.52	0.13	4.40	0.43	8.97
9	506	3.25	0.27	-27.08	0.21	0.33	0.028	3.61	0.21	13.22
10	520	3.15	0.05	-25.78	0.11	0.50	0.13	5.23	0.51	10.98
11	535	2.37	0.27	-26.5	0.21	0.33	0.028	3.79	0.22	13.54
12	551	3.11	0.05	-25.00	0.11	0.45	0.11	4.14	0.40	9.67
13	566	2.84	0.27	-26.23	0.21	0.34	0.029	4.01	0.23	14.2
14	582	2.99	0.05	-25.38	0.11	0.50	0.13	4.68	0.46	9.97
15	597	6.52	0.27	-26.87	0.21	0.38	0.032	4.52	0.26	14.48
16	613	2.52	0.05	-24.86	0.11	0.50	0.13	4.80	0.47	10.17
17	628	2.92	0.27	-25.96	0.21	0.34	0.03	4.17	0.24	14.56
18	644	2.88	0.03	-24.59	0.06	0.36	0.03	4.12	0.12	13.28
19	659	2.94	0.27	-27.35	0.21	0.34	0.029	3.68	0.21	13.03

20	675	2.99	0.03	-24.80	0.06	0.36	0.03	3.66	0.10	12.02
21	691	3.29	0.27	-25.91	0.21	0.34	0.029	3.97	0.23	14.2
22	706	3.01	0.03	-25.43	0.06	0.37	0.03	3.65	0.10	11.52
23	721	4.04	0.27	-26.79	0.21	0.33	0.028	3.67	0.21	13.55
24	737	2.65	0.03	-25.35	0.06	0.36	0.03	3.99	0.11	12.80
25	752	3.65	0.27	-26.57	0.21	0.3	0.026	3.73	0.22	14.83
26	767	2.73	0.03	-24.70	0.06	0.36	0.03	4.01	0.11	13.17
27	783	3.2	0.27	-26.77	0.21	0.32	0.027	3.68	0.21	13.85
28	798	2.77	0.03	-24.47	0.06	0.37	0.03	3.99	0.11	12.63
29	814	3.16	0.27	-26.93	0.21	0.31	0.027	3.71	0.22	14.36
30	830	2.62	0.03	-24.85	0.06	0.38	0.04	4.12	0.12	12.58
31	845	2.91	0.27	-26.79	0.21	0.34	0.029	4.1	0.24	14.55
32	861	2.54	0.03	-24.96	0.06	0.38	0.04	4.19	0.12	12.75
33	876	3.12	0.27	-27.18	0.21	0.32	0.028	3.94	0.23	14.69
34	892	2.52	0.03	-25.17	0.06	0.34	0.03	4.01	0.11	13.90
35	907	2.89	0.27	-26.31	0.21	0.31	0.026	4.31	0.24	15.89
36	923	2.71	0.03	-25.63	0.06	0.26	0.02	3.06	0.09	13.76
37	938	2.66	0.27	-26.36	0.21	0.29	0.025	3.48	0.2	14.19
38	953	2.30	0.03	-25.18	0.06	0.41	0.04	4.16	0.12	11.72
39	969	2.14	0.27	-26.82	0.21	0.34	0.029	4.1	0.24	14.26
40	984	2.45	0.03	-25.11	0.06	0.32	0.03	3.24	0.09	11.76
41	997	4.24	0.27	-27.25	0.21	0.17	0.015	2.2	0.13	14.83
42	1010	2.59	0.03	-25.57	0.06	0.39	0.04	4.19	0.12	12.44
43	1022	2.63	0.27	-27.41	0.21	0.35	0.03	4.27	0.25	14.54
44	1034	2.28	0.03	-25.28	0.06	0.38	0.04	4.17	0.12	12.86
45	1046	2.17	0.1	-26.56	0.12	0.32	0.09	3.24	0.14	10.42
46	1058	1.98	0.03	-26.20	0.06	0.38	0.04	4.55	0.13	14.08

47	1069	2.08	0.1	-26.69	0.12	0.32	0.09	3.26	0.14	10.64
48	1080	1.82	0.03	-26.31	0.06	0.42	0.04	4.78	0.13	13.44
49	1092	1.9	0.1	-26.08	0.12	0.34	0.09	3.52	0.15	10.72
50	1104	2.37	0.03	-26.53	0.06	0.37	0.03	3.93	0.11	12.54
51	1116	1.67	0.1	-26.44	0.12	0.34	0.09	3.39	0.14	10.26
52	1129	2.62	0.03	-25.37	0.06	0.35	0.03	4.22	0.12	14.14
53	1142	2.73	0.1	-25.49	0.12	0.28	0.08	2.95	0.12	10.75
54	1156	2.51	0.03	-25.72	0.06	0.38	0.03	4.58	0.13	14.21
55	1169	2.88	0.1	-25.33	0.12	0.28	0.08	3.04	0.13	11.11
56	1183	2.37	0.03	-26.19	0.06	0.39	0.04	5.06	0.14	15.04
57	1199	2.8	0.1	-25.53	0.12	0.27	0.07	2.72	0.11	10.33
58	1217	2.55	0.03	-25.60	0.06	0.34	0.03	4.02	0.11	13.72
59	1235	2.77	0.1	-25.83	0.12	0.3	0.08	3.38	0.14	11.63
60	1254	2.68	0.03	-25.82	0.06	0.37	0.03	4.35	0.12	13.69
61	1269	2.43	0.1	-27.8	0.12	0.3	0.08	5.5	0.23	19.23
62	1282	2.55	0.03	-25.93	0.06	0.40	0.04	4.51	0.13	13.01
63	1293	2.3	0.1	-25.56	0.12	0.31	0.08	3.65	0.15	12.12
64	1305	2.03	0.03	-25.39	0.06	0.41	0.04	5.51	0.15	15.55
65	1316	2.04	0.1	-25.26	0.12	0.38	0.1	4.72	0.2	13.08
66	1327	1.84	0.03	-26.11	0.06	0.40	0.04	5.28	0.15	15.38
67	1339	2.78	0.1	-26.31	0.12	0.3	0.08	3.04	0.13	10.35
68	1350	3.07	0.03	-26.12	0.06	0.38	0.03	4.91	0.14	15.20
69	1361	2.99	0.1	-26.07	0.12	0.19	0.05	1.75	0.07	9.67
70	1372	2.34	0.03	-26.21	0.06	0.36	0.03	4.82	0.13	15.76
71	1383	2.72	0.1	-25.83	0.12	0.26	0.07	2.79	0.12	10.92
72	1394	2.22	0.03	-25.76	0.06	0.38	0.03	4.15	0.12	12.89
73	1406	2.34	0.1	-25.85	0.12	0.29	0.08	3.14	0.13	11.16

74	1418	2.34	0.03	-25.88	0.06	0.36	0.03	4.30	0.12	13.94
75	1430	2.54	0.1	-25.88	0.12	0.27	0.07	3.06	0.13	11.55
76	1443	2.48	0.03	-25.90	0.06	0.38	0.04	4.59	0.13	14.15
77	1457	2.6	0.1	-26.02	0.12	0.29	0.08	3.22	0.14	11.67
78	1470	2.21	0.03	-25.93	0.06	0.38	0.04	4.68	0.13	14.42
79	1484	2.53	0.1	-25.92	0.12	0.28	0.08	3.18	0.13	11.82
80.5	1498	1.27	0.03	-27.75	0.06	0.39	0.04	7.84	0.22	23.72
81	1518	2.8	0.1	-26	0.12	0.16	0.04	1.92	0.08	12.29
82	1546	2.39	0.03	-25.73	0.06	0.36	0.03	4.17	0.12	13.45
83	1573	2.28	0.1	-26.14	0.12	0.31	0.08	3.12	0.13	10.5
84	1600	2.04	0.03	-26.00	0.06	0.41	0.04	4.44	0.12	12.75
85	1618	2.21	0.1	-26.03	0.12	0.33	0.09	3.01	0.13	9.57
86	1627	1.74	0.03	-26.13	0.06	0.40	0.04	4.25	0.12	12.48
87	1635	2.9	0.1	-26.29	0.12	0.3	0.08	2.76	0.12	9.72
88	1644	0.77	0.03	-26.38	0.06	0.37	0.03	3.62	0.10	11.39
89	1652	2.73	0.1	-26.28	0.12	0.31	0.08	3.15	0.13	10.63
90	1661	2.04	0.03	-26.27	0.06	0.38	0.04	4.38	0.12	13.49
91	1670	2.17	0.1	-26.53	0.12	0.27	0.07	3.21	0.13	12.1
92	1679	1.93	0.03	-26.50	0.06	0.41	0.04	5.15	0.14	14.64
93	1688	2.12	0.1	-26.06	0.12	0.35	0.09	3.98	0.17	11.96
94	1697	2.12	0.03	-26.65	0.06	0.38	0.04	4.64	0.13	14.09
95	1707	2.15	0.1	-26.3	0.12	0.36	0.1	3.71	0.16	10.75
96	1717	1.64	0.03	-26.23	0.06	0.42	0.04	4.99	0.14	13.76
97	1726	2.14	0.1	-25.71	0.12	0.32	0.09	3.16	0.13	10.19
98	1736	1.94	0.03	-25.82	0.06	0.39	0.04	4.37	0.12	13.14
99	1746	1.89	0.1	-26.31	0.12	0.25	0.07	3.13	0.13	12.71
100.5	1756	1.71	0.03	-26.39	0.06	0.38	0.04	5.51	0.15	16.77

101	1767	1.34	0.1	-26.14	0.12	0.33	0.09	4.61	0.19	14.47
102	1779	2.27	0.03	-25.97	0.06	0.35	0.03	4.35	0.12	14.65
103	1791	2.41	0.1	-25.95	0.12	0.21	0.06	2.05	0.09	9.87
104	1803	2.29	0.03	-25.79	0.06	0.35	0.03	4.05	0.11	13.54
105	1815	2.38	0.1	-25.82	0.12	0.21	0.06	2.07	0.09	9.95
106	1827	1.99	0.03	-26.83	0.06	0.40	0.04	4.68	0.13	13.83
107	1839	2.14	0.1	-25.86	0.12	0.34	0.09	3.54	0.15	10.92
108	1851	2.09	0.03	-26.87	0.06	0.36	0.03	4.23	0.12	13.74
109	1863	1.93	0.1	-25.96	0.12	0.32	0.08	3.4	0.14	11.22
110	1875	1.88	0.03	-26.44	0.06	0.38	0.04	4.72	0.13	14.51
111	1887	2.36	0.1	-25.78	0.12	0.31	0.08	3.09	0.13	10.34
112	1899	2.60	0.03	-26.61	0.06	0.32	0.03	3.27	0.09	11.89
113	1911	2.75	0.1	-25.63	0.12	0.26	0.07	2.56	0.11	10.28
114	1924	3.29	0.12	-26.22	0.15	0.36	0.04	4.07	0.18	14.05
115	1937	3.23	0.1	-26.39	0.12	0.3	0.08	3.2	0.13	10.97
116	1950	2.31	0.12	-26.57	0.15	0.40	0.04	4.75	0.21	14.54
117	1963	2.02	0.1	-26.85	0.12	0.36	0.1	3.62	0.15	10.59
118	1976	2.42	0.12	-26.20	0.15	0.37	0.04	3.87	0.17	13.08
119	1989	2.34	0.1	-26.36	0.12	0.27	0.07	2.54	0.11	9.73
120	2003	2.85	0.12	-25.83	0.15	0.33	0.03	3.90	0.17	14.77
121	2019	2.76	0.1	-26.35	0.12	0.12	0.03	1.33	0.06	11.32
122	2037	2.46	0.12	-26.56	0.15	0.38	0.04	4.39	0.20	14.16
123	*2055*	*2.88*	*0.1*	*-25.96*	*0.12*	*0.18*	*0.05*	*1.97*	*0.08*	*11.05*
124	2074	3.03	0.12	-25.60	0.15	0.06	0.01	0.60	0.03	12.75
125	2093	2.75	0.1	-26.34	0.12	0.04	0.01	0.46	0.02	12.44
126	2112	2.75	0.12	-26.04	0.15	0.05	0.01	0.47	0.02	11.61
127	2132	2.41	0.1	-26.43	0.12	0.29	0.08	2.88	0.12	10.16

128	2151	3.08	0.12	-25.90	0.15	0.35	0.04	3.92	0.18	13.96
129	2171	2.86	0.1	-26.59	0.12	0.28	0.08	3.06	0.13	11.24
130	2190	2.16	0.12	-26.07	0.15	0.37	0.04	4.19	0.19	14.17
131	2209	2.06	0.1	-25.95	0.12	0.3	0.08	3.07	0.13	10.74
132	2228	2.67	0.12	-25.79	0.15	0.34	0.04	4.13	0.18	15.02
133	2246	2.59	0.1	-26.01	0.12	0.26	0.07	2.89	0.12	11.31
134	2264	2.77	0.12	-26.21	0.15	0.34	0.04	4.40	0.20	15.81
135	2282	2.69	0.1	-26.14	0.12	0.17	0.05	1.92	0.08	11.55
136	2301	2.45	0.12	-25.88	0.15	0.29	0.03	2.97	0.13	12.62
137	2319	2.49	0.1	-26.02	0.12	0.29	0.08	2.73	0.11	9.73
138	2338	2.86	0.12	-25.88	0.15	0.36	0.04	3.91	0.17	13.31
139	2357	2.4	0.1	-26.34	0.12	0.31	0.08	2.84	0.12	9.44
140	2375	2.77	0.12	-25.58	0.15	0.30	0.03	3.41	0.15	13.86
141	2394	2.22	0.1	-26.09	0.12	0.27	0.07	2.5	0.11	9.53
142	2413	2.90	0.12	-25.73	0.15	0.11	0.01	1.13	0.05	12.76
143	2431	2.09	0.07	-26.71	0.09	0.22	0.01	2.98	0.07	16.58
144	2449	2.47	0.12	-25.90	0.15	0.23	0.02	2.51	0.11	13.19
145	2467	2.31	0.07	-26.21	0.09	0.34	0.02	4.10	0.10	14.43
146	2484	2.74	0.12	-26.20	0.15	0.38	0.04	4.07	0.18	13.26
147	2500	2.51	0.07	-26.35	0.09	0.31	0.01	4.43	0.11	17.45
148	2516	1.98	0.12	-25.46	0.15	0.40	0.04	5.62	0.25	17.46
149	2532	2.49	0.07	-26.01	0.09	0.29	0.01	3.55	0.09	14.87
150	2547	2.77	0.12	-25.82	0.15	0.39	0.04	4.12	0.18	12.97
151	2563	2.48	0.07	-26.72	0.09	0.31	0.01	4.20	0.10	16.62
152	2579	2.97	0.12	-26.09	0.15	0.40	0.04	4.67	0.21	14.57
153	2595	2.55	0.07	-26.55	0.09	0.31	0.01	4.73	0.12	18.51
154	2611	2.22	0.12	-26.06	0.15	0.25	0.03	2.76	0.12	13.57

155	2626	2.18	0.07	-26.14	0.09	0.30	0.01	4.01	0.10	16.14
156	2641	2.87	0.12	-26.01	0.15	0.36	0.04	3.88	0.17	13.28
157	2655	2.29	0.07	-26.77	0.09	0.34	0.02	4.12	0.10	14.77
158	2669	2.58	0.12	-25.92	0.15	0.29	0.03	2.89	0.13	12.36
159	2683	2.80	0.07	-26.23	0.09	0.29	0.01	3.44	0.09	14.22
160	2697	2.53	0.12	-25.86	0.15	0.35	0.04	3.56	0.16	12.51
161	2711	3.02	0.07	-26.73	0.09	0.24	0.01	3.08	0.08	15.37
162	2725	3.11	0.12	-25.99	0.15	0.34	0.04	3.70	0.17	13.58
163	2738	3.15	0.07	-26.33	0.09	0.27	0.01	3.48	0.09	15.82
164	2752	3.44	0.12	-26.45	0.15	0.33	0.03	3.61	0.16	13.64
165	2766	3.14	0.07	-26.35	0.09	0.26	0.01	3.50	0.09	16.21
166	2779	3.20	0.12	-25.72	0.15	0.33	0.03	3.63	0.16	13.63
167	2794	3.15	0.07	-26.28	0.09	0.21	0.01	2.90	0.07	16.90
168	2809	3.07	0.12	-26.03	0.15	0.26	0.03	2.73	0.12	13.00
169	2824	3.40	0.07	-26.44	0.09	0.22	0.01	3.01	0.07	16.09
170	2842	3.04	0.12	-27.36	0.15	0.06	0.01	0.59	0.03	12.17
171	2861	3.18	0.07	-25.96	0.09	-0.03	0.00	0.43	0.01	-14.60
172	2877	3.65	0.12	-26.07	0.15	0.06	0.01	0.55	0.02	11.99
173	2891	2.82	0.07	-26.64	0.09	0.24	0.01	3.07	0.08	15.37
174	2904	2.74	0.12	-26.19	0.15	0.35	0.04	3.50	0.16	12.51
175	2916	2.81	0.07	-26.52	0.09	0.14	0.01	2.13	0.05	17.48
176	2929	2.87	0.12	-26.83	0.15	0.37	0.04	3.73	0.17	12.52
177	2942	2.71	0.07	-26.26	0.09	0.27	0.01	3.47	0.09	15.21
178	2955	2.69	0.12	-26.27	0.15	0.41	0.04	4.36	0.19	13.12
179	2967	2.96	0.07	-26.05	0.09	0.31	0.01	3.58	0.09	14.05
180	2980	NA	0.12	-26.74	0.15	1.41	0.15	8.59	0.37	7.19
181	2992	3.46	0.07	-26.62	0.09	0.30	0.01	3.99	0.10	16.03

182	3005	3.66	0.12	-27.27	0.15	0.17	0.02	1.91	0.08	13.58
183	3018	2.04	0.07	-26.80	0.09	0.03	0.00	1.04	0.02	43.27
184	3032	2.32	0.12	-25.62	0.15	0.03	0.00	0.35	0.01	12.53
185	3046	2.87	0.07	-27.43	0.09	0.34	0.02	4.14	0.10	14.52
186	3061	2.73	0.12	-25.80	0.15	0.33	0.03	3.33	0.15	12.40
187	3076	2.67	0.07	-26.73	0.09	0.27	0.01	3.34	0.08	14.99
188	3091	3.10	0.12	-26.67	0.15	0.27	0.03	2.72	0.12	12.33
189	3106	2.34	0.07	-26.62	0.09	-0.04	0.00	0.40	0.01	-12.21
190	3121	3.08	0.12	-26.06	0.15	0.22	0.02	2.15	0.10	12.22
190.5	3136	3.28	0.07	-26.13	0.09	0.18	0.01	2.51	0.06	17.02
192	3148	3.05	0.12	-27.27	0.15	0.42	0.04	4.26	0.19	12.68
193	3158	2.60	0.07	-26.91	0.09	0.34	0.02	3.98	0.10	14.13
194	3166	2.88	0.12	-25.98	0.15	0.40	0.04	4.03	0.18	12.62
195	3173	3.55	0.07	-26.14	0.09	0.29	0.01	3.50	0.09	14.78
196	3180	3.39	0.12	-25.80	0.15	0.38	0.04	4.15	0.19	13.64
197	3188	3.26	0.07	-26.50	0.09	0.29	0.01	3.63	0.09	15.28
198	3195	2.80	0.12	-25.98	0.15	0.38	0.04	4.03	0.18	13.04
199	3202	2.71	0.07	-27.61	0.09	0.36	0.02	4.27	0.11	14.47
200	3210	2.54	0.12	-26.00	0.15	0.43	0.05	4.68	0.21	13.46
201	3219	3.50	0.07	-26.05	0.09	0.24	0.01	3.11	0.08	15.37
202	3229	2.65	0.12	-26.56	0.15	0.34	0.04	3.49	0.16	12.54
203	3241	3.12	0.07	-25.67	0.09	0.27	0.01	3.42	0.09	15.24
204	3254	2.77	0.12	-26.07	0.15	0.34	0.04	3.47	0.15	12.49
205	3268	2.76	0.07	-26.71	0.09	0.29	0.01	3.69	0.09	15.14
207	3299	2.73	0.07	-25.92	0.09	0.20	0.01	3.02	0.07	17.90
208	3315	2.31	0.12	-26.41	0.15	0.41	0.04	4.08	0.18	12.24
209	3331	2.47	0.07	-26.73	0.09	0.32	0.02	3.88	0.10	14.69

210	3349	2.65	0.12	-25.47	0.15	0.41	0.04	4.20	0.19	12.57
211	3368	2.34	0.07	-26.98	0.09	0.35	0.02	4.09	0.10	14.00
212	3385	2.41	0.04	-26.89	0.10	0.37	0.02	3.53	0.10	11.38
213	3403	2.48	0.07	-27.24	0.09	0.08	0.00	1.59	0.04	22.48
214	3428	2.29	0.04	-27.36	0.10	0.39	0.02	3.78	0.11	11.60
215	3451	2.22	0.07	-27.07	0.09	0.35	0.02	4.28	0.11	14.61
216	3459	2.50	0.04	-26.66	0.10	0.40	0.03	4.16	0.12	12.19
217	3465	2.75	0.07	-25.92	0.09	0.32	0.02	3.80	0.09	14.56
218	3471	2.37	0.04	-26.40	0.10	0.38	0.02	3.81	0.11	11.76
219	3494	2.19	0.07	-26.84	0.09	0.32	0.02	3.86	0.10	14.76
220	3542	2.16	0.04	-27.24	0.10	0.39	0.02	3.96	0.11	12.12
221	3592	2.54	0.07	-26.93	0.09	0.32	0.02	3.79	0.09	14.15
222	3641	2.73	0.04	-26.44	0.10	0.40	0.03	3.94	0.11	11.69
223	3690	2.60	0.07	-26.20	0.09	0.29	0.01	3.38	0.08	13.89
224	3734	2.68	0.04	-26.26	0.10	0.37	0.02	3.44	0.10	11.15
225	3768	2.76	0.07	-26.40	0.09	0.28	0.01	3.24	0.08	14.18
226	3795	2.47	0.04	-27.41	0.10	0.42	0.03	7.30	0.20	20.71
227	3821	2.99	0.07	-26.05	0.09	0.29	0.01	3.39	0.08	14.28
228	3846	3.21	0.04	-25.64	0.10	0.35	0.02	3.63	0.10	12.17
229	3871	2.86	0.07	-26.17	0.09	0.29	0.01	3.37	0.08	13.84
230	3896	3.12	0.04	-26.22	0.10	0.31	0.02	3.00	0.09	11.37
231	3919	2.92	0.07	-26.24	0.09	0.24	0.01	2.84	0.07	14.26
232	3942	2.77	0.04	-26.65	0.10	0.36	0.02	3.32	0.09	11.08
233	3963	2.52	0.07	-26.46	0.09	0.24	0.01	2.92	0.07	14.33
234	3984	2.55	0.04	-26.66	0.10	0.43	0.03	4.16	0.12	11.52
235	4006	2.63	0.07	-26.16	0.09	0.30	0.01	3.43	0.09	13.62
236	4027	2.95	0.04	-26.06	0.10	0.35	0.02	3.34	0.09	11.28

237	4048	2.75	0.07	-26.61	0.09	0.28	0.01	3.48	0.09	14.87
238	4071	2.67	0.04	-27.03	0.10	0.36	0.02	3.32	0.09	10.92
239	4092	2.90	0.07	-27.12	0.09	0.31	0.02	3.61	0.09	13.99
240	4115	2.69	0.04	-27.00	0.10	0.40	0.03	3.72	0.11	10.93
241	4137	3.03	0.13	-26.62	0.11	0.38	0.05	3.31	0.24	10.84
242	4159	3.13	0.04	-26.92	0.10	0.37	0.02	3.47	0.10	11.08
243	4181	3.12	0.13	-25.79	0.11	0.35	0.04	3.27	0.24	11.88
244	4203	3.25	0.04	-26.08	0.10	0.35	0.02	3.41	0.10	11.48
245	4225	3.18	0.13	-25.63	0.11	0.37	0.05	3.41	0.25	11.77
246	4245	3.33	0.04	-25.96	0.10	0.35	0.02	3.58	0.10	12.07
247	4264	3.14	0.13	-25.61	0.11	0.35	0.04	3.42	0.25	12.21
248	4283	3.17	0.04	-25.82	0.10	0.35	0.02	3.42	0.10	11.53
249	4301	3.26	0.13	-25.45	0.11	0.35	0.04	3.41	0.25	12.16
250	4318	3.20	0.04	-25.63	0.10	0.35	0.02	3.65	0.10	12.26
251	4335	3.36	0.13	-25.48	0.11	0.31	0.04	3.13	0.23	12.6
252	4352	3.95	0.04	-26.47	0.10	0.41	0.03	4.26	0.12	12.23
253	4368	2.14	0.13	-27.27	0.11	0.45	0.06	5.18	0.37	14.07
254	4384	2.49	0.04	-27.27	0.10	0.42	0.03	4.08	0.12	11.48
255	4399	NA	0.13	-26.88	0.11	0.13	0.02	1.21	0.08	10.73
256	4414	2.62	0.04	-26.81	0.10	0.41	0.03	3.96	0.11	11.57
257	4428	2.61	0.13	-25.99	0.11	0.43	0.05	4.01	0.29	11.77
258	4444	2.65	0.04	-25.89	0.10	0.38	0.02	3.46	0.10	10.67
259	4460	2.74	0.13	-25.56	0.11	0.39	0.05	3.62	0.26	11.81
260	4477	2.92	0.04	-26.03	0.10	0.35	0.02	3.36	0.10	11.34
261	4494	2.5	0.13	-25.47	0.11	0.36	0.05	3.12	0.23	10.9
262	4511	2.46	0.04	-25.89	0.10	0.36	0.02	3.28	0.09	10.79
263	4528	2.52	0.13	-25.71	0.11	0.38	0.05	3.38	0.25	11.22

264	4545	2.63	0.04	-26.28	0.10	0.36	0.02	3.31	0.09	10.87
265	4562	2.47	0.13	-26.07	0.11	0.35	0.04	3	0.22	10.86
266	4581	2.43	0.04	-27.10	0.10	0.39	0.02	3.70	0.10	11.30
267	4600	2.25	0.13	-27.12	0.11	0.4	0.05	3.55	0.26	11.27
268	4620	2.51	0.04	-27.70	0.10	0.36	0.02	3.28	0.09	10.85
269	4640	2.41	0.13	-27.46	0.11	0.37	0.05	3.22	0.23	11.07
270	4660	2.40	0.04	-28.07	0.10	0.38	0.02	3.64	0.10	11.31
271	4679	2.41	0.13	-27.78	0.11	0.39	0.05	3.49	0.25	11.25
272	4701	2.33	0.04	-28.62	0.10	0.37	0.02	3.53	0.10	11.35
273	4724	2.33	0.13	-28.34	0.11	0.36	0.05	3.24	0.24	11.39
274	4749	2.05	0.04	-28.67	0.10	0.36	0.02	3.58	0.10	11.80
275	4774	2.36	0.13	-28.3	0.11	0.33	0.04	3.06	0.22	11.68
276.5	4800	2.52	0.04	-28.29	0.10	0.36	0.02	3.33	0.09	10.98
277	4825	2.57	0.13	-27.76	0.11	0.37	0.05	3.28	0.24	11.14
278	4849	2.94	0.04	-27.60	0.10	0.33	0.02	3.14	0.09	11.26
279	4873	3.41	0.13	-26.27	0.11	0.28	0.04	2.7	0.19	12.06
280	4899	3.29	0.04	-26.73	0.10	0.32	0.02	2.99	0.09	10.93
281	4925	2.92	0.13	-26.01	0.11	0.35	0.04	3.24	0.24	11.7
282	4953	3.36	0.04	-26.61	0.10	0.33	0.02	3.29	0.09	11.71
283	4980	2.92	0.13	-26.4	0.11	0.34	0.04	3.3	0.24	12.28
284	5006	2.92	0.04	-27.44	0.10	0.36	0.02	3.39	0.10	11.29
285	5031	NA	0.13	-27.91	0.11	0.16	0.02	1.54	0.11	11.51
286	5054	2.79	0.04	-28.10	0.10	0.39	0.03	4.21	0.12	12.79
287	5077	3.28	0.13	-26.91	0.11	0.38	0.05	3.53	0.26	11.76
288	5099	3.38	0.04	-26.27	0.10	0.34	0.02	3.33	0.09	11.64
289	5121	3.12	0.13	-25.69	0.11	0.37	0.05	3.49	0.25	11.96
290	5144	3.23	0.04	-26.12	0.10	0.35	0.02	3.55	0.10	11.92

291	5167	3.07	0.13	-25.79	0.11	0.37	0.05	3.53	0.26	12.05
292	5189	2.84	0.04	-26.48	0.10	0.37	0.02	3.72	0.11	11.87
293	5211	3	0.13	-26.03	0.11	0.37	0.05	3.55	0.26	12.01
294	5233	2.43	0.04	-28.30	0.10	0.35	0.02	3.19	0.09	10.79
295	5253	2.5	0.13	-27.66	0.11	0.34	0.04	2.89	0.21	10.67
296	5273	2.84	0.04	-27.54	0.10	0.35	0.02	3.25	0.09	10.94
297	5293	2.89	0.13	-26.33	0.11	0.35	0.04	3.08	0.22	11.2
298	5312	2.67	0.04	-26.06	0.10	0.35	0.02	3.58	0.10	12.03
299	5331	3	0.13	-26.14	0.11	0.33	0.04	3.17	0.23	12.05
300	5351	2.30	0.04	-27.85	0.10	0.38	0.02	3.37	0.10	10.60
301	5372	2.84	0.13	-27.31	0.11	0.38	0.05	3.55	0.26	11.68
302	5393	3.10	0.04	-27.50	0.10	0.39	0.03	3.73	0.11	11.30
303	5414	2.49	0.13	-27.48	0.11	0.38	0.05	3.33	0.24	11.18
304	5435	2.77	0.04	-28.00	0.10	0.37	0.02	3.60	0.10	11.66
305	5457	2.56	0.13	-27.49	0.11	0.35	0.04	3.1	0.22	11.17
306	5483	2.89	0.04	-27.98	0.10	0.36	0.02	3.44	0.10	11.24
307	5514	2.56	0.13	-27.56	0.11	0.38	0.05	3.48	0.25	11.46
308	5546	2.85	0.04	-27.74	0.10	0.40	0.03	3.78	0.11	11.27
309	5578	2.81	0.13	-27.42	0.11	0.4	0.05	3.77	0.27	11.77
310	5609	2.57	0.09	-26.88	0.09	0.35	0.01	3.86	0.04	12.84
311	5641	3	0.13	-25.78	0.11	0.33	0.04	3.19	0.23	12.33
312	5673	10.11	0.09	-25.43	0.09	0.27	0.01	3.16	0.03	13.53
313	5705	2.73	0.13	-25.61	0.11	0.33	0.04	3.25	0.24	12.51
314	5736	2.11	0.09	-25.62	0.09	0.26	0.01	3.07	0.03	13.57
315	5768	3.01	0.13	-27.18	0.11	0.35	0.04	3.04	0.22	11.08
316	5799	1.96	0.09	-27.2	0.09	0.23	0.01	2.44	0.03	12.61
317	5830	2.66	0.13	-27.02	0.11	0.4	0.05	3.67	0.27	11.53

318	5861	NA	0.09	-26.59	0.09	0.14	0	1.69	0.02	13.71
319	5893	2.9	0.13	-26.25	0.11	0.3	0.04	2.76	0.2	11.58
320	5926	2.81	0.09	-26.18	0.09	0.2	0.01	2.75	0.03	16.41
321	5959	3.2	0.13	-25.63	0.11	0.32	0.04	3.07	0.22	12.24
322	5994	2.59	0.09	-25.61	0.09	0.27	0.01	3.16	0.03	13.8
323	6029	2.9	0.13	-25.97	0.11	0.37	0.05	3.36	0.24	11.32
324	6065	1.72	0.09	-26	0.09	0.31	0.01	3.35	0.04	12.71
325	6102	2.87	0.13	-25.55	0.11	0.35	0.04	3.22	0.23	11.77
326	6148	2.55	0.09	-26.11	0.09	0.27	0.01	2.97	0.03	12.67
327	6202	2.97	0.13	-26.47	0.11	0.36	0.05	3.7	0.27	12.99
328	6259	2.6	0.09	-26.29	0.09	0.24	0.01	2.66	0.03	12.77
329	6319	NA	0.13	-26.47	0.11	0.14	0.02	1.41	0.1	12.09
330	6380	2.88	0.05	-26.87	0.13	-0.01	0.00	1.42	0.09	-183.99
331	6441	NA	0.09	-26.19	0.09	0.06	0	0.8	0.01	15.75
332	6504	3.12	0.13	-26.04	0.11	0.34	0.04	3.25	0.24	12.19
333	6565	2.47	0.09	-25.74	0.09	0.33	0.01	3.87	0.04	13.59
334	6624	2.89	0.13	-25.6	0.11	0.35	0.04	3.53	0.26	12.87
335	6680	2.83	0.09	-25.5	0.09	0.29	0.01	3.35	0.04	13.28
336	6733	2.94	0.13	-25.68	0.11	0.36	0.05	3.45	0.25	12.1
337	6785	-1.25	0.09	-25.59	0.09	0.3	0.01	3.39	0.04	13.21
338	6837	2.84	0.13	-25.67	0.11	0.36	0.05	3.38	0.25	11.82
339	6888	2.32	0.09	-25.53	0.09	0.29	0.01	3.35	0.04	13.35
340	6940	2.87	0.05	-25.89	0.13	0.27	0.01	3.57	0.26	16.59
341	6991	1.83	0.09	-25.8	0.09	0.31	0.01	3.45	0.04	13.15
342	7042	3.07	0.05	-26.40	0.13	0.16	0.00	2.68	0.19	20.49
343	7094	2.28	0.09	-26.42	0.09	0.3	0.01	3.16	0.03	12.44
344	7146	3.12	0.05	-26.16	0.13	0.27	0.01	3.32	0.24	15.07

345	7201	2.86	0.09	-25.78	0.09	0.28	0.01	2.96	0.03	12.23
346	7262	2.88	0.05	-26.40	0.13	0.09	0.00	1.97	0.13	23.85
347	7330	2.94	0.09	-26	0.09	0.27	0.01	2.92	0.03	12.77
348	7396	3.12	0.05	-26.50	0.13	0.25	0.00	3.51	0.25	17.41
349	7459	1.14	0.09	-26.68	0.09	0.29	0.01	3.18	0.03	12.74
350	7520	3.00	0.05	-27.21	0.13	0.25	0.00	3.61	0.26	17.96
351	7582	1.14	0.09	-26.76	0.09	0.24	0.01	2.68	0.03	12.86
352	7646	3.03	0.05	-26.35	0.13	0.25	0.00	3.65	0.26	17.97
353	7712	1.5	0.09	-26.45	0.09	0.32	0.01	3.7	0.04	13.62
354	7781	3.15	0.05	-26.89	0.13	0.21	0.00	3.58	0.26	20.66
355	7887	3.15	0.09	-26.55	0.09	0.3	0.01	3.44	0.04	13.28
356	8020	3.70	0.05	-27.11	0.13	0.20	0.00	2.66	0.19	15.89
357	8162	3.66	0.09	-26.07	0.09	0.26	0.01	2.94	0.03	13.41
358	8288	3.61	0.05	-26.46	0.13	0.18	0.00	2.52	0.18	16.49
359	8380	4.44	0.27	-27.82	0.21	0.14	0.012	1.46	0.08	11.78
360	8460	4.57	0.27	-28.36	0.21	0.09	0.008	0.85	0.05	10.73
361	8524	4.31	0.05	-27.13	0.13	0.00	0.00	1.09	0.07	429.22

APPENDIX E: SEDIMENTARY CELLULOSE OXYGEN ISOTOPE DATA

Table A2: Sedimentary cellulose oxygen isotope data from Lake Motosu.

Depth (c.m.c.d.)	Age (cal. year B.P.)	$\delta^{18}O$ (‰)	$\delta^{18}O$ error (‰)	TO (%)	TO error (%)
16.5	675	22.73	0.39	37.27	2.09
31.5	861	23.25	0.43	41.13	2.48
36	923	22.70	0.39	45.94	2.57
40.5	984	23.44	0.43	42.60	2.56
44	1034	22.18	0.39	43.27	2.42
60	1254	23.80	0.39	38.61	2.16
68	1350	23.40	0.39	45.06	2.52
84	1600	22.62	0.39	47.26	2.65
92	1679	24.11	0.39	43.02	2.41
108	1851	23.66	0.39	40.31	2.26
116	1950	23.71	0.39	38.24	2.14
132	2228	23.07	0.39	44.11	2.47
149	2532	23.73	0.43	37.96	2.29
156	2641	23.70	0.39	40.83	2.29
164	2752	22.29	0.39	43.18	2.42
165	2766	22.67	0.43	39.62	2.39
172	2877	22.33	0.39	45.42	2.54
174	2904	22.77	0.43	40.61	2.44
180	2980	23.34	0.43	33.45	2.01
183.5	3018	22.08	0.43	38.46	2.32
188	3091	23.34	0.43	33.45	2.01
212	3385	23.04	0.39	44.85	2.51
252	4352	22.10	0.39	46.90	2.63
260	4477	23.30	0.39	43.18	2.42
276	4800	23.91	0.39	29.71	1.66
284	5006	22.35	0.39	40.91	2.29
300	5351	20.05	0.43	35.98	2.17
308	5546	22.91	0.39	36.98	2.07
324	6065	23.14	0.39	38.11	2.13
332	6504	22.47	0.43	38.13	2.30
348	7396	22.22	0.39	43.33	2.43
356	8020	21.50	0.39	37.87	2.12

APPENDIX F: LOCATION OF PROPOSED TURBIDITES

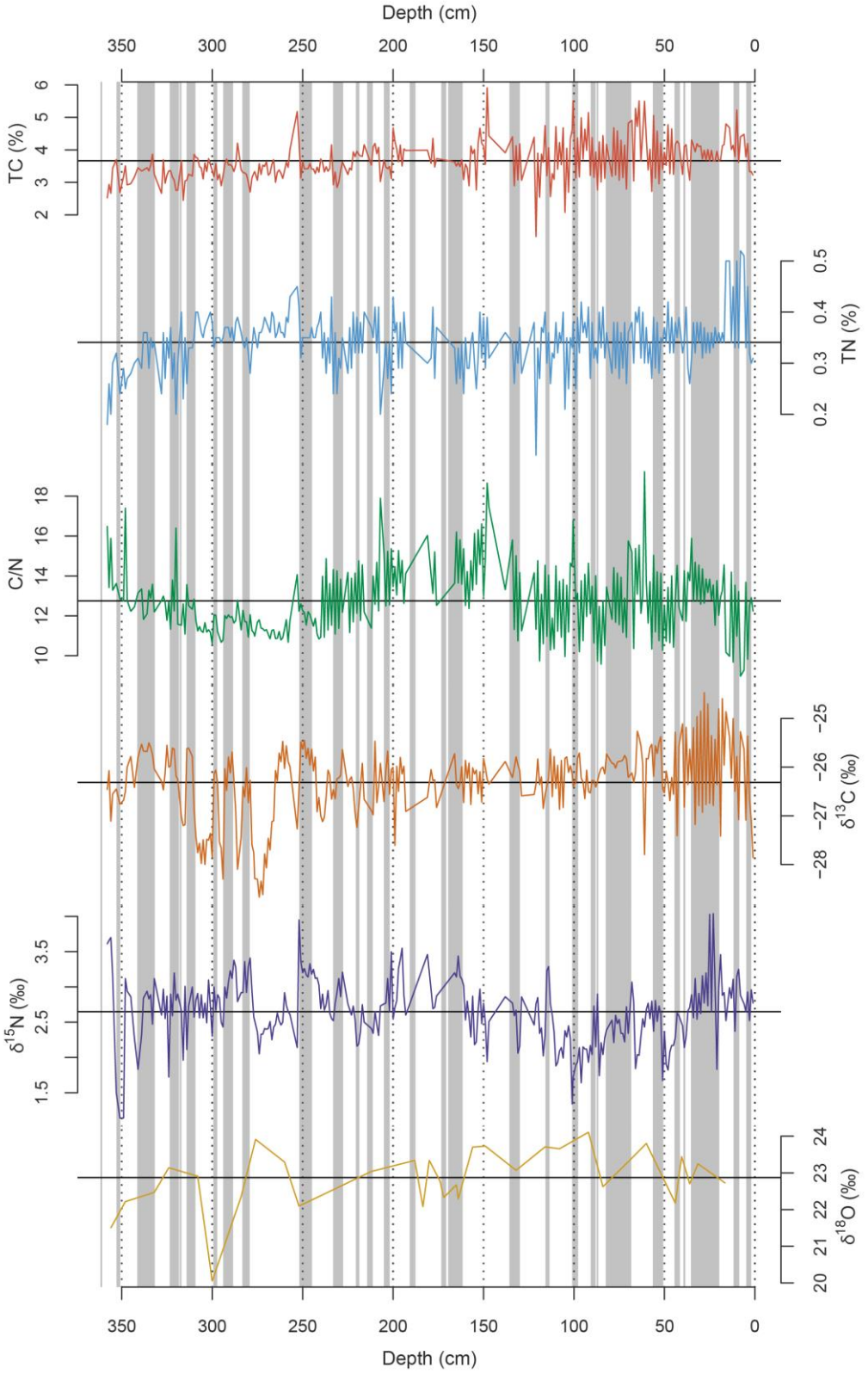

Figure A3: Lake Motosu elemental and isotopic data. Grey vertical lines indicate the location of proposed turbidites following Lamair et al. (2018).

APPENDIX G: SPECTRAL ANALYSIS

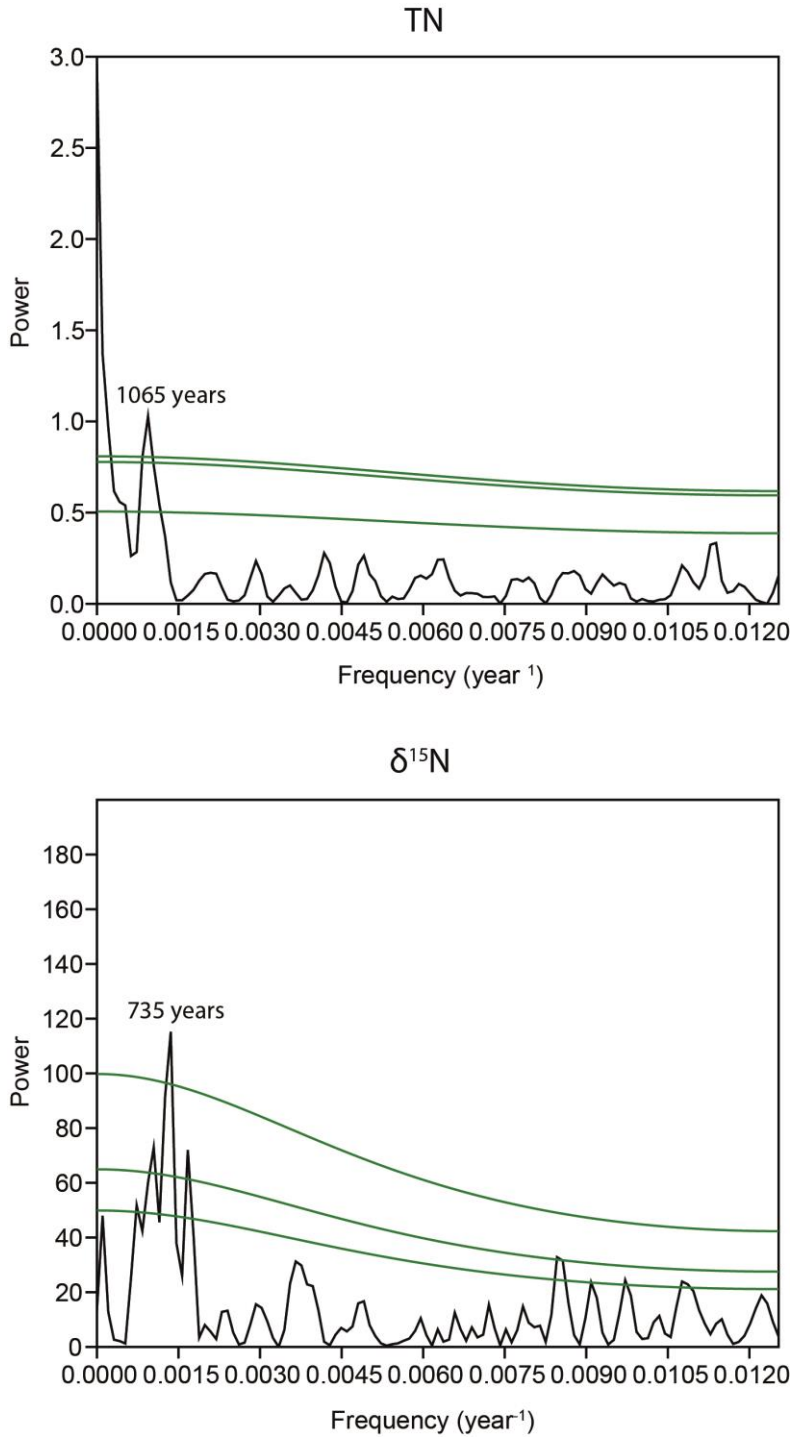

Figure A4: Spectral analysis of TN and $\delta^{15}N$ from Lake Motosu. Green lines show chi2 99% confidence (upper), 95% confidence (middle) and 90% confidence (lower) levels.

APPENDIX H: WAVELET ANALYSIS

TC

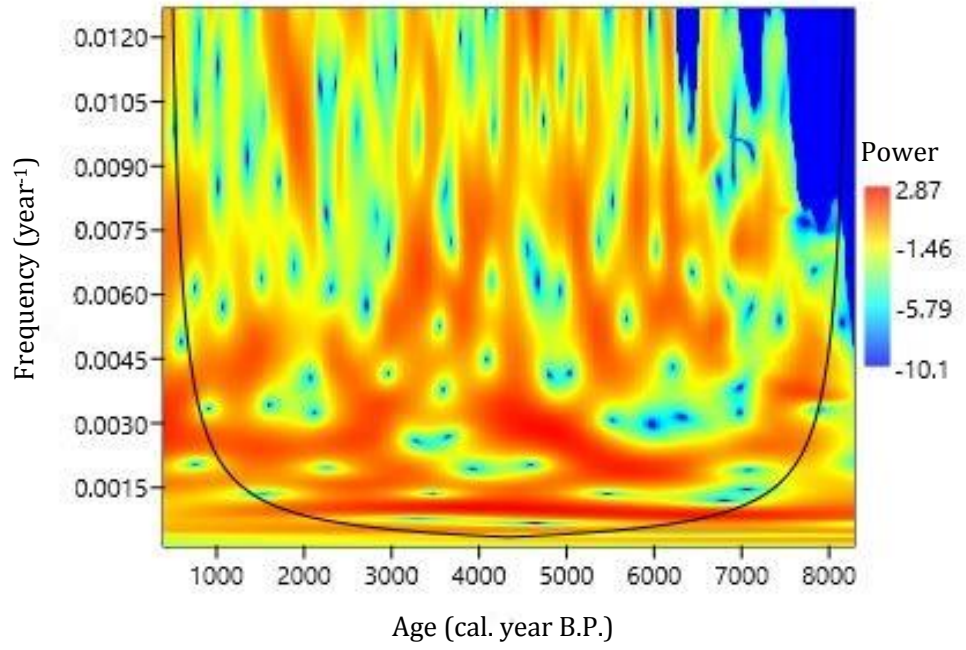

TN

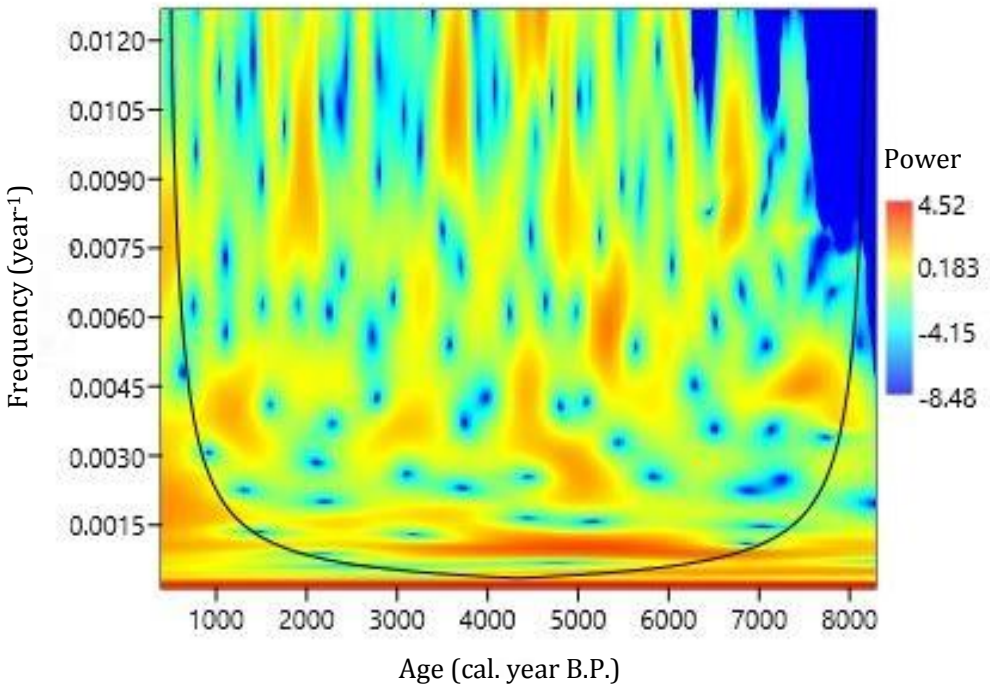

C/N

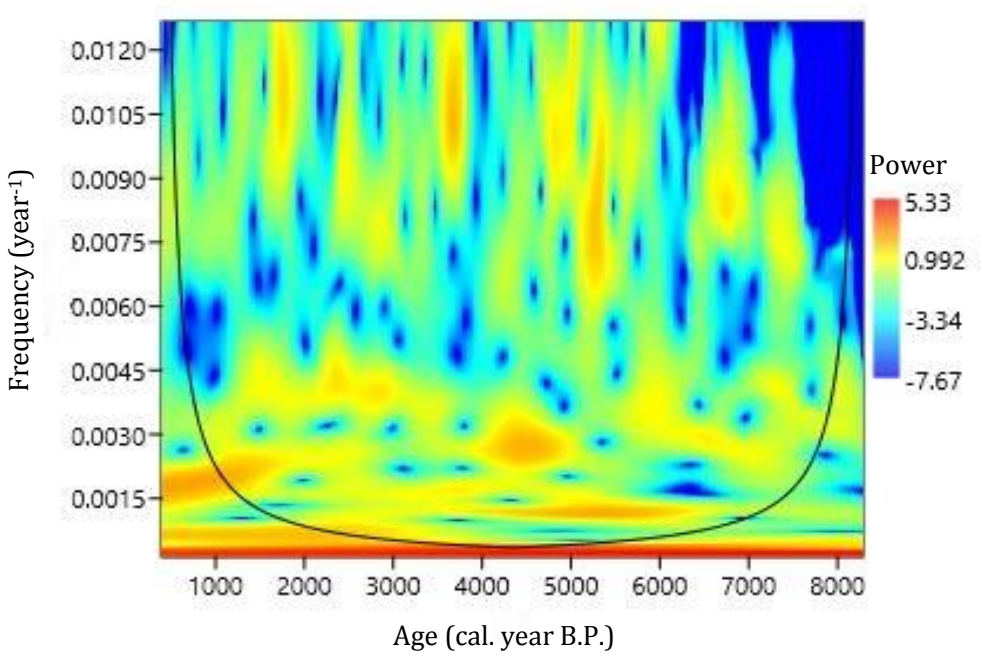
Frequency (year-1)
0.0120
0.0105
0.0090
0.0075
0.0060
0.0045
0.0030
0.0015
1000
2000
3000
4000
5000
6000
7000
8000
Age (cal. year B.P.)
Power
5.33
0.992
-3.34
-7.67

$\delta^{13}C$

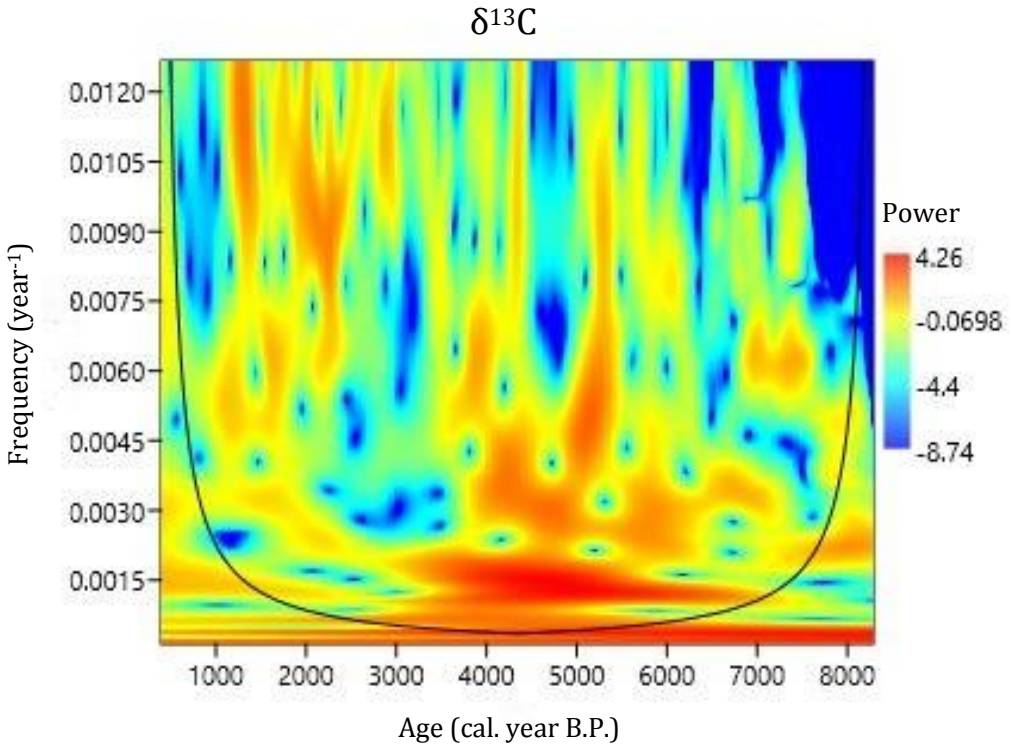
Frequency (year-1)
0.0120
0.0105
0.0090
0.0075
0.0060
0.0045
0.0030
0.0015
1000
2000
3000
4000
5000
6000
7000
8000
Age (cal. year B.P.)
Power
4.26
-0.0698
-4.4
-8.74

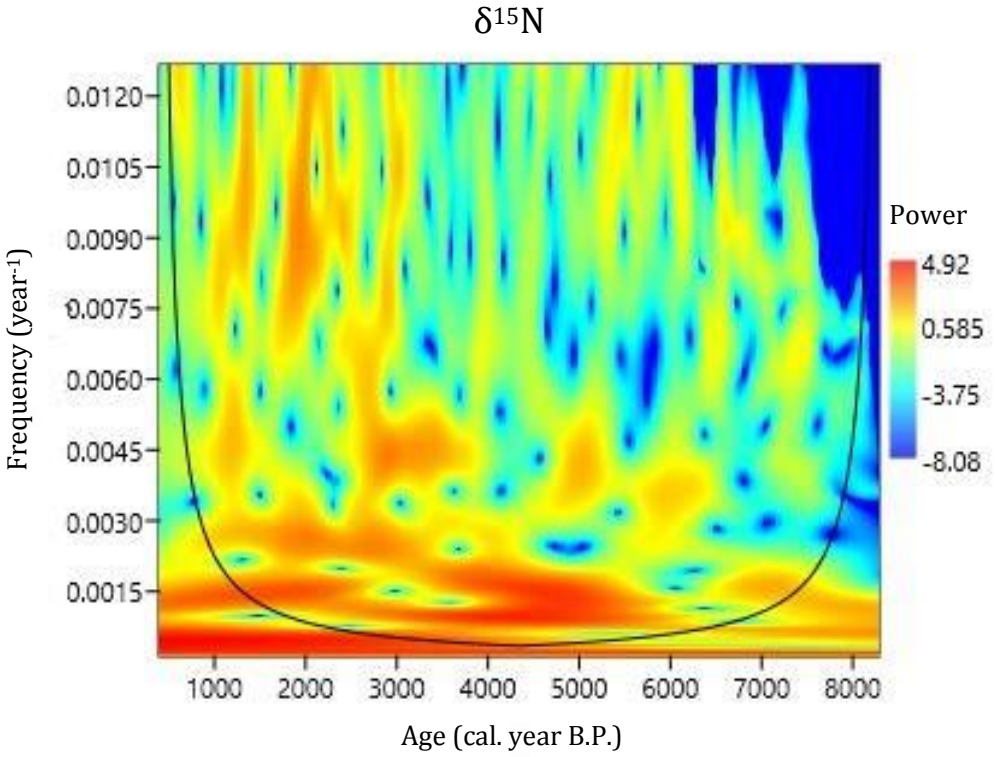

Figure A5: Wavelet analysis of palaeoclimate proxies from Lake Motosu. Higher powers occur at frequencies which are present in each record. Black line represents the cone of influence, within which the analysis is interpretable.

APPENDIX I: CROSS-WAVELET ANALYSIS

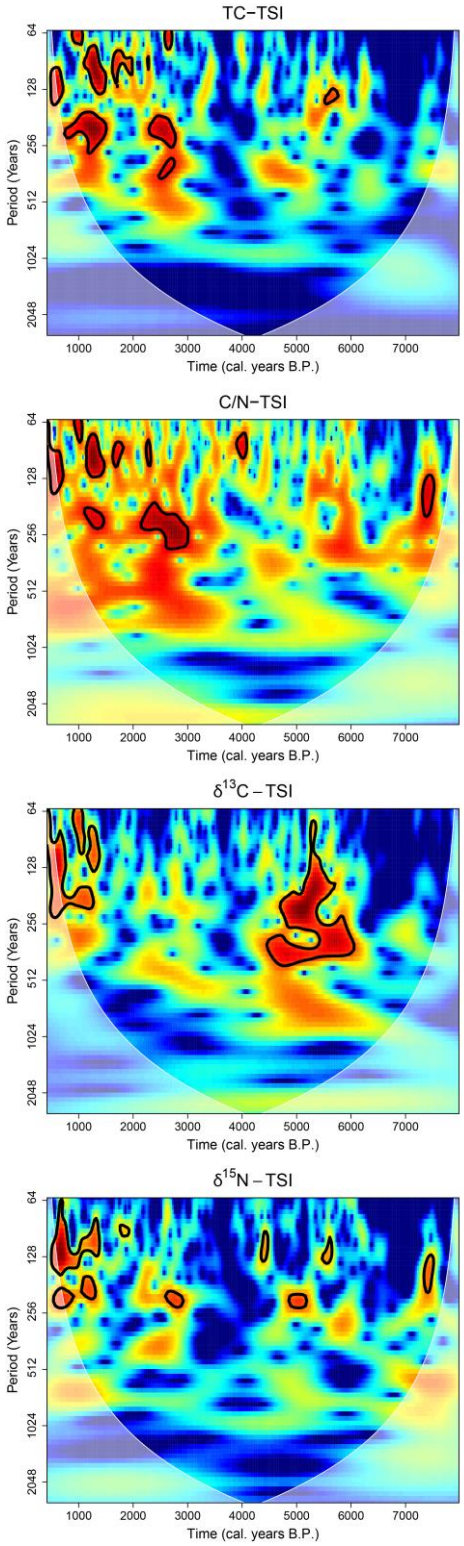

Figure A6: Cross-wavelet analysis of Lake Motosu geochemical data with total solar insolation (Steinhilber et al., 2012). Black lines indicate periodicities significant at the 95% confidence interval. White shading represents the cone of influence, within which the analysis is interpretable.

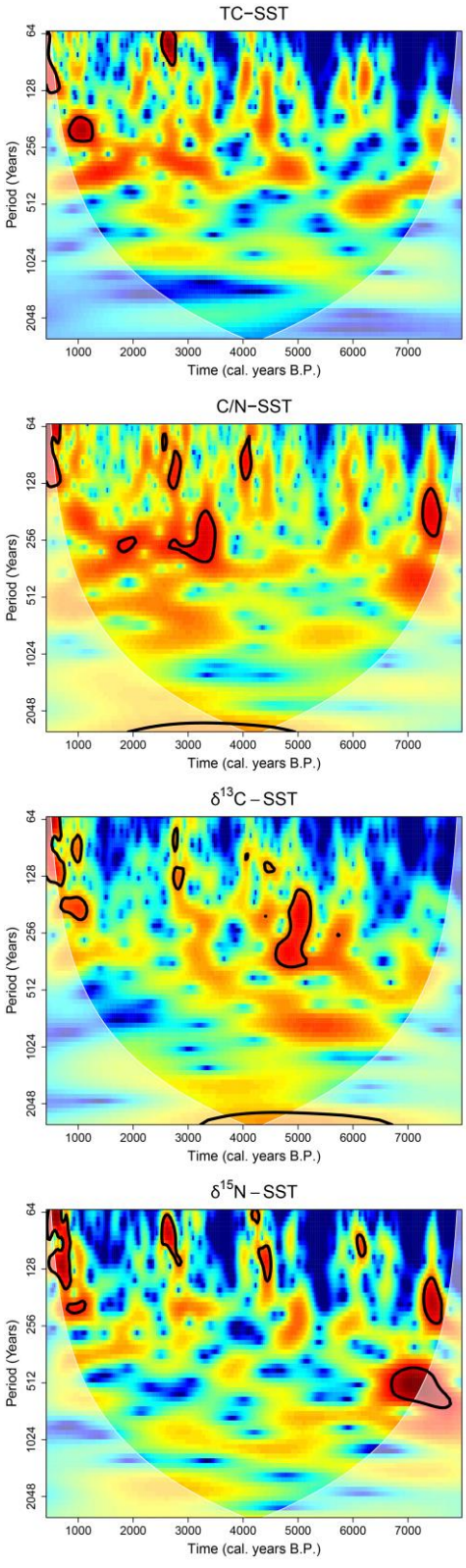

Figure A7: Cross-wavelet analysis of Lake Motosu geochemical data with West Pacific Warm Pool sea surface temperatures (Stott et al., 2004). Black lines indicate periodicities significant at the 95% confidence interval. White shading represents the cone of influence, within which the analysis is interpretable.

APPENDIX J: ORIGINAL DATASETS INCLUDED IN MULTI-PROXY SYNTHESIS

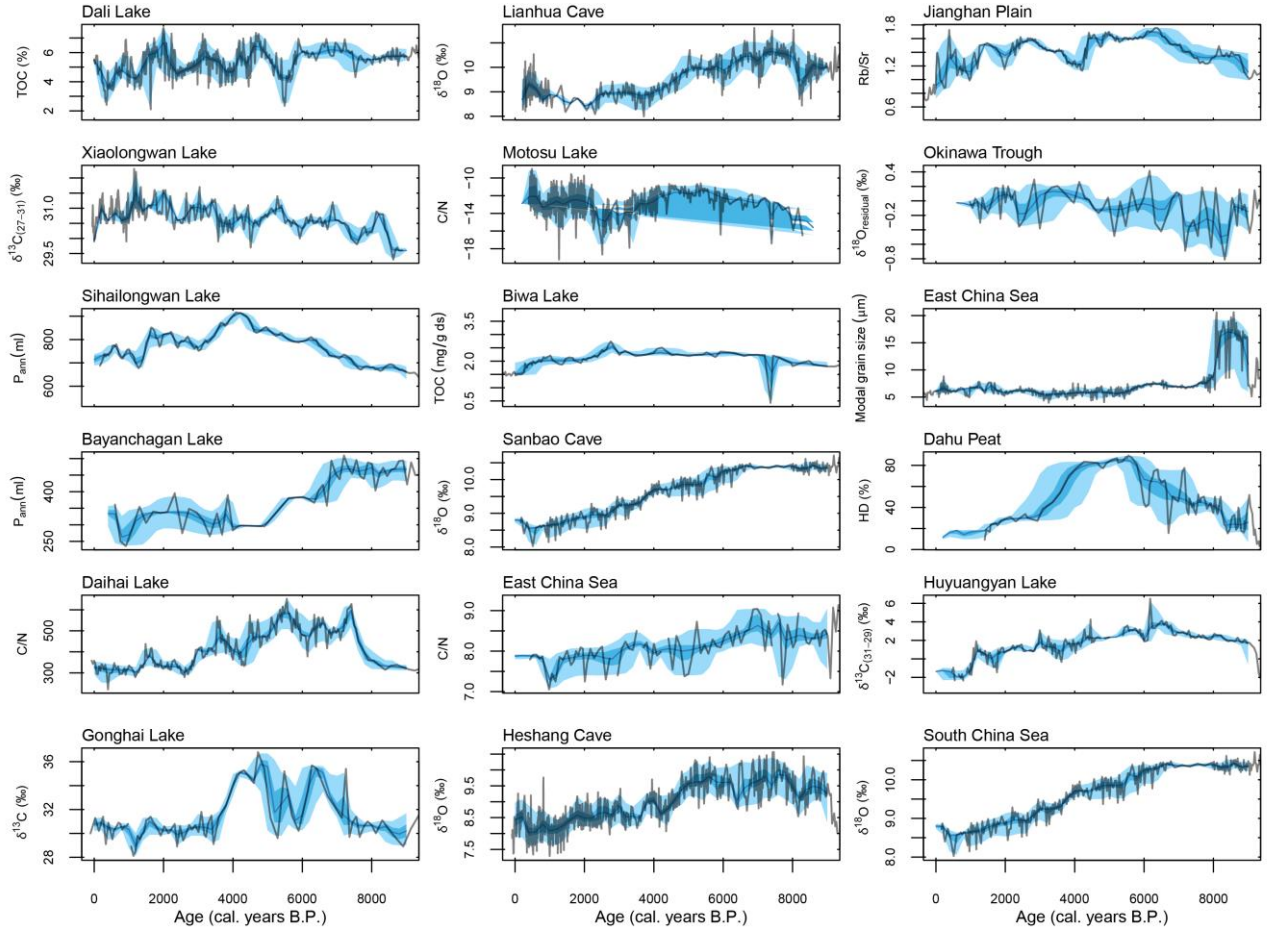

Figure A8: Original datasets included in multi-proxy synthesis arranged north to south. Grey lines represent original data. Shading represent chronological uncertainties calculated on 10,000 age model iterations (dark = 68%, light = 90%). Axes are orientated such that wetter conditions plot upwards.

APPENDIX K: CORRELATION BETWEEN LAKE MOTOSU AND REGIONAL CLIMATE

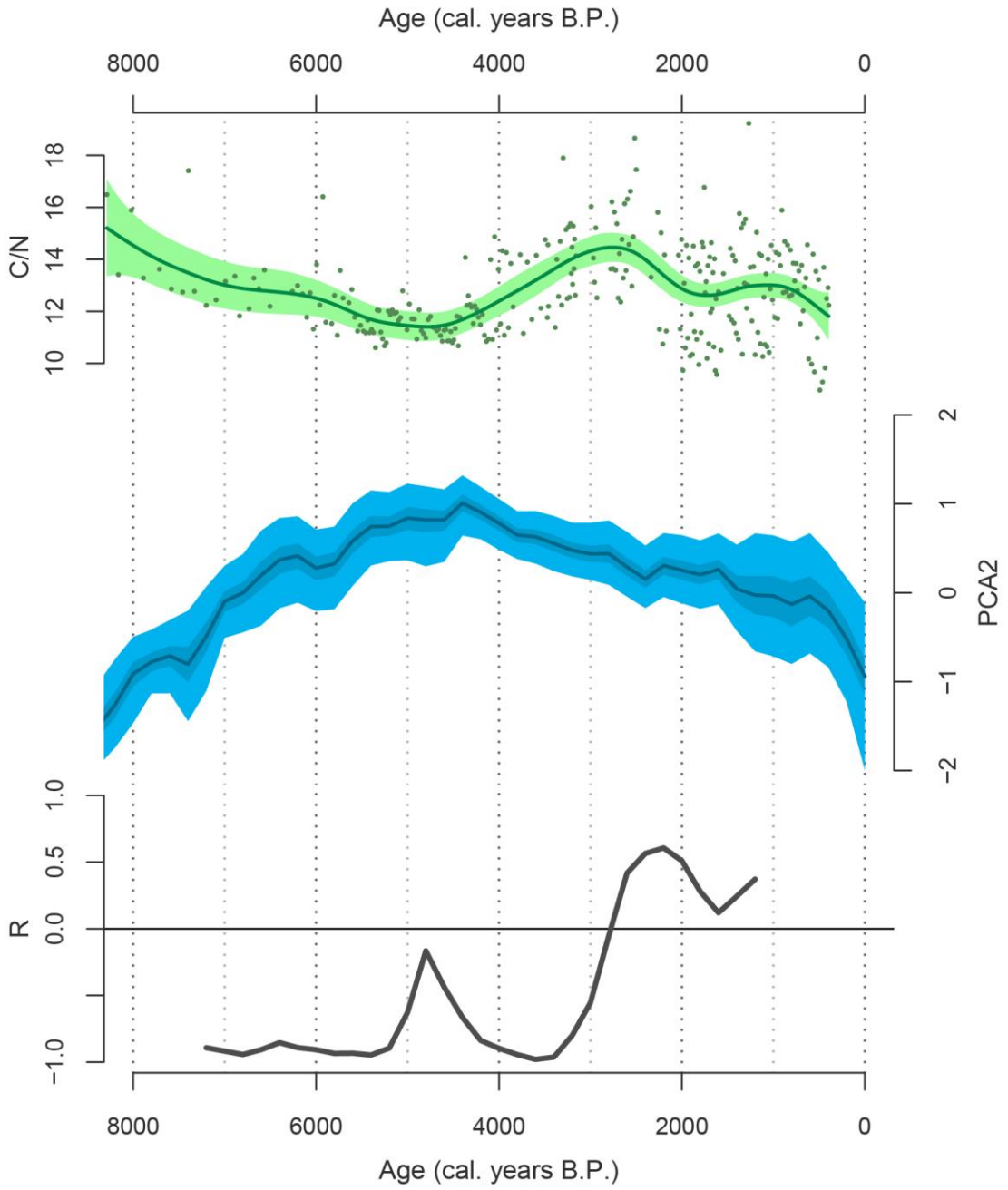

Figure A9: Rolling correlation between the C/N ratio in Lake Motosu and regional climate. Top: GAM fitted to Lake Motosu C/N data. Middle: Second principal component (PCA2) of East Asian climate. Bottom: rolling correlation between C/N and PCA2 calculated over 1.6 ka windows. An R value of -1 implies total negative correlation, a value of 0 implies no correlation and a value of 1 implies total positive correlation.

APPENDIX L: EXCLUDED TURBIDITES

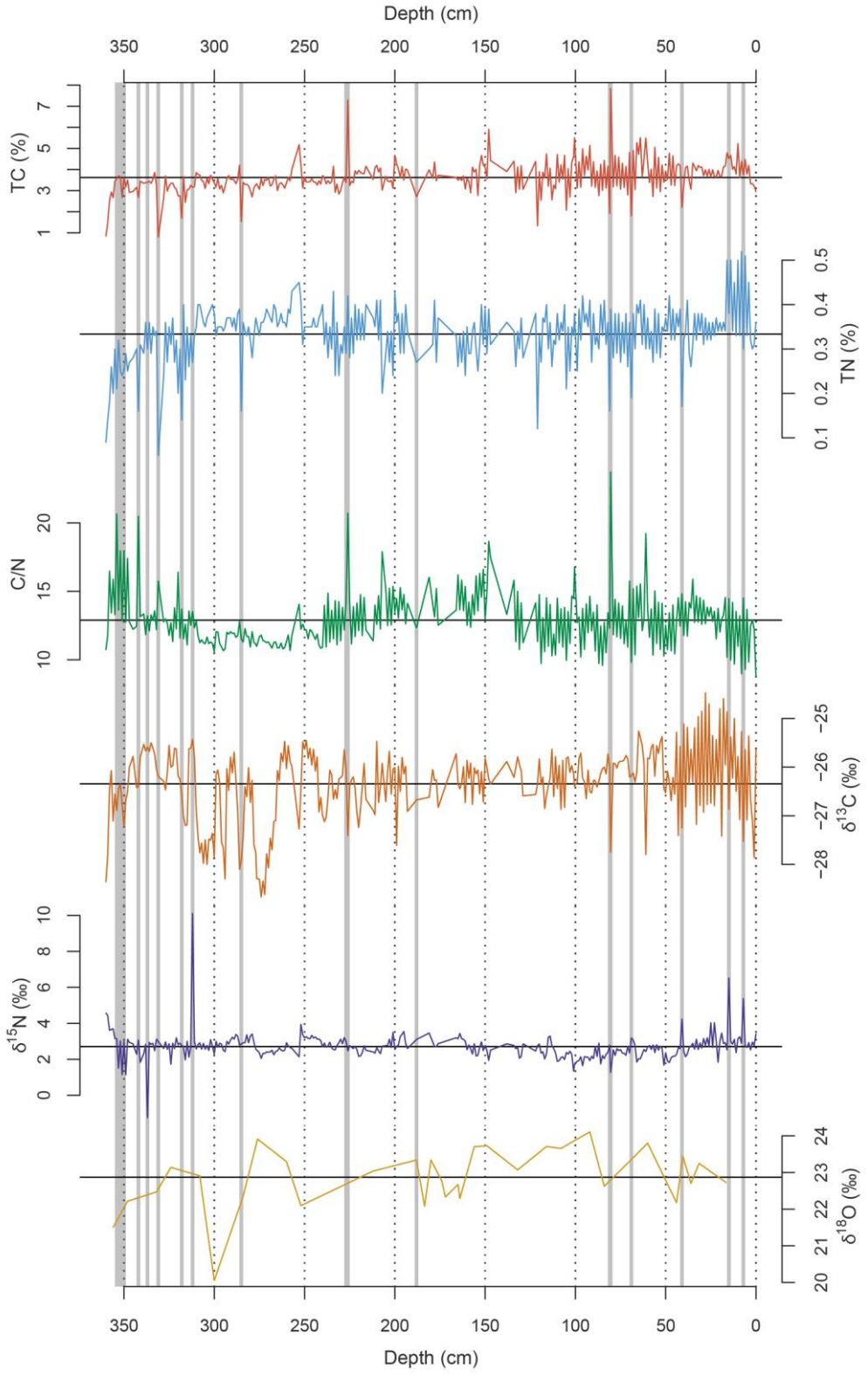

Figure 10: Lake Motosu elemental and isotopic data. Horizontal lines indicate mean values. Grey shading indicates proposed turbidite layers which were excluded from analysis